Reviewed Preprint
v1 • April 13, 2026
Not revised

Reviewed Preprint
v2 • August 21, 2026
Revised by authors

REM sleep prefrontal high-frequency oscillation chains mediate distinct cortical – hippocampal reactivation patterns compared to NREM sleep

Justin D Shin, Michael Satchell, Paul Miller, Shantanu P Jadhav

Neuroscience Program, Department of Psychology, and Volen National Center for Complex Systems, Brandeis University, Waltham, United States

For correspondence: shantanu@brandeis.edu

Competing interests: No competing interests declared

Funding: See page 45

Reviewing editor: Caleb Kemere, Rice University, United States

eLife Assessment

Shin et al present significant new observations highlighting a novel oscillatory window during REM sleep that impacts neuronal dynamics and cross-regional communication and could have implications for our understanding of sleep's role in memory consolidation. This **important** study identifies and characterizes high-frequency oscillations (HFOs) in the prefrontal cortex (PFC) during REM sleep, reporting their temporal dynamics and coordination with hippocampal area CA1, and an intriguing dissociation between activation of CA1 neurons during REM HFOs and non-REM ripples that may impact sleep-dependent firing rate decreases. The main claims are supported with **convincing** evidence including an impressive range of analyses.

https://doi.org/10.7554/eLife.110795.2.sa4

Abstract

REM (rapid eye movement) and non-REM (NREM) sleep stages contribute to systems memory consolidation in hippocampal-cortical circuits. However, the physiological mechanisms underlying REM memory processes remain relatively unclear compared to NREM memory reactivation. Here we report, in rodents, the existence of prefrontal cortical (PFC) high-frequency oscillation (HFO) chains in REM sleep during consolidation of recently acquired spatial memory. High-density tetrode recordings in hippocampal area CA1 and PFC reveal that REM cortical HFOs occur in characteristic chains that are phase modulated by theta oscillations, corresponding to increased CA1-PFC theta coherence and delineating periods of enhanced hippocampal-cortical communication. REM HFO chains sequentially organize sparse PFC ensemble reactivation of behavioral activity during periods of local suppression, distinct from widespread reactivation bursts during NREM ripple oscillations. REM HFO chains also preferentially engage CA1 neuronal populations that demonstrate a shift in their preferred theta-phase from behavior to REM sleep. CA1 neuronal activation during REM HFO chains was correlated with CA1 activity suppression during NREM PFC ripples, and linked to differential changes in CA1 firing rates in sleep, suggesting REM-driven regulation of hippocampal excitability. A cortical network model incorporating the effects of acetylcholine can reproduce the distinct REM and NREM activity patterns, providing a mechanistic basis for widespread coactivity during NREM cortical ripples, compared to sparse, temporally extended reactivation on a background of local suppression during REM HFO chains. Overall, these findings establish a role for PFC high-frequency oscillations in regulating distinct dual sleep stage reactivation patterns.

Introduction

Rapid eye movement (REM) sleep, often referred to as paradoxical sleep due to its electrophysiological similarities to wakefulness, is a relatively transient stage of sleep that occurs after NREM sleep stages in cycles, and plays a crucial role in a wide range of brain functions.[1,2] Although largely appreciated for its role in emotional processing, recent evidence has highlighted its role in the consolidation of spatial, declarative, and procedural memory, indicating a broader function of REM sleep in mnemonic processing.[3-5] Importantly, REM dysregulation is associated with memory deficits and is thought to contribute to the progression of neuropsychiatric disorders and neurodegenerative diseases such as depression and dementia, highlighting the critical need for a deeper understanding of this sleep state to benefit human health.[6]

Primary models of systems memory consolidation, including the standard two-stage theory of consolidation or trace transformation theory,[7-10] rest under the assumption of cooperative hippocampal-cortical reactivation during sleep to transform initially encoded episodic hippocampal representations into broadly distributed hippocampal-cortical representations for long-term storage and semantic memory formation. In support of this view, several rodent and human studies have confirmed that, in non-rapid eye movement (NREM) sleep, coordination of hippocampal sharp-wave ripples (SWRs) with cortical slow oscillations (1-4 Hz), spindles (12-16 Hz), and ripples (150-250 Hz) underlies the neurophysiological mechanism supporting consolidation.[11-14] While the role of offline memory reactivation in the hippocampus and prefrontal cortex (PFC) during NREM sleep has been extensively studied in relation to memory function, the precise mechanisms through which REM sleep contributes to these processes, particularly in the context of hippocampal-cortical interactions, is still unclear.

REM sleep is characterized by high theta-delta ratio,[15,16] and while hippocampal SWRs are primarily reported in NREM states with relatively low theta power, hippocampal theta rhythms during REM sleep have been shown to be important for memory consolidation.[17] Correspondingly, phasic theta activity bursts during REM are often coupled with elevated gamma and cortical high-frequency oscillation (HFO) power in hippocampal and cortical networks, potentially organizing neural activity in distributed circuits for mnemonic processing.[18-25] Furthermore, REM sleep is associated with a unique neuromodulatory landscape that is conducive for the induction of plasticity within and across circuits.[26] However, the role of REM sleep cortical oscillations, whether they are coordinated with hippocampal activity patterns or with cortical-hippocampal reactivation, and the relationship between REM and NREM activity for dual sleep state regulation of reactivation and excitability are all open questions.

Cortical ripples (high-frequency or fast oscillations, ~150-250 Hz) have been reported in NREM sleep,[27-29] and our recent study showed that independent PFC ripples that are dissociated from hippocampal SWRs are prevalent in NREM sleep and mediate suppression of hippocampal activity and reactivation, potentially facilitating the selection and consolidation of specific hippocampal memory ensembles, while facilitating local cortical reactivation.[28] A related study had similar findings, suggesting that these cortical ripples reflect intracortical processing that occurs independently of hippocampal input, allowing for interference-free consolidation of memory representations within cortical circuits.[30]

In REM sleep, previous studies have established cortical HFOs (in a similar frequency range to high-frequency NREM ripples) along with gamma oscillations – REM HFOs have been detected in different frequency ranges and sometimes reported with different nomenclature.[19,21,22,31] Since recent studies note the possibility of spurious spectral detection in high frequency ranges,[32] monitoring spiking activity simultaneously with LFP/EEG activity can therefore provide key confirmation about the existence and impact of high-frequency oscillations on neuronal activity via spiking modulation in local circuits.

Previous studies in rodents have reported a role of REM sleep in homeostatic regulation of firing rates, using recordings lasting from less than an hour to across the 24-hour cycle, but without the context of a behavioral task.[33-35] Studies have also reported prominent phenomena such as hippocampal REM-theta phase reversing cells[36] and hippocampal reactivation,[37] using behavioral

tasks and examining brief sleep periods in post-task rest sessions. Further, a recent study in mice reported PFC coding and activation of recent experiences and inferred knowledge in NREM and REM sleep using imaging methods, but did not examine any potential role of oscillations.[38]

Despite these results, an explicit examination of REM cortical HFO events, and how they impact cortical and hippocampal activity during consolidation of recent experiences is not known, despite the similarity of these high-frequency oscillations to cortical ripples in NREM. Furthermore, how NREM and REM sleep activity patterns may together complementarily shape the development and refinement of cortical-hippocampal ensembles to support learning is unclear. Therefore, we used high-density electrophysiological recordings in PFC and CA1 during learning and subsequent sleep to investigate whether and how coordinated activity during REM sleep may drive circuit changes underlying systems memory consolidation, and whether prefrontal and hippocampal dynamics differ during cortical ripple and HFO activity patterns in NREM and REM sleep, respectively.

Results

High-frequency events in PFC during REM sleep

We simultaneously recorded local field potential (LFP) and neuronal populations in CA1 (n = 1,468) and PFC (n = 1,151) from animals (n = 10 rats) during REM sleep (Figure S1A, Table S1, REM duration = 164.6 ± 10.8 s/epoch for the 36 epochs included in analysis) throughout the course of learning a spatial memory task that requires hippocampal-prefrontal interactions[39,40] (Figure S1B). Activity was continuously acquired across multiple run (8 epochs) and sleep (9 epochs) sessions during learning within a single day.[40] We separated NREM and REM sleep stages based on theta-to-delta (TD) ratio in CA1,[15,16] which revealed coherent shifts in TD ratio across CA1 and PFC at the onset and offset of REM sleep (Figures 1A-C). Waking periods showed higher movement and intracranial EMG compared to REM sleep, validating the behavioral state designations (Figures S1C-I).

To investigate the high-frequency component of phasic burst activity in PFC, cortical ripples during NREM sleep and HFOs during REM sleep were detected as transient events in the 150-250 Hz range, as previously described[28] (Figures 1D,E and S2A,B). Similar criteria were used to detect cortical high-frequency events in NREM and REM states; however, to avoid ambiguity and to conform to previous nomenclature,[21,22] we refer to cortical NREM events as ripples, cortical REM events as HFOs, and hippocampal sharp-wave ripples in NREM as SWRs throughout. Cortical event rates during REM were higher than NREM, and REM HFOs were associated with elevated theta and gamma power,[21,31] in contrast to spindle- and slow oscillation-coupled ripple events in NREM[28,41] (Figures 1F,G). Interestingly, examining the temporal structure of event occurrence, using both the event autocorrelation (the likelihood of finding another HFO at a given time lag) and the distribution of inter-event-intervals (IEIs, the time between consecutive HFOs), we find that REM HFOs often recur at intervals of ~130 ms (Figures 1H,I) as HFO “chains”, which is consistent with theta frequency modulation and elevated theta power during these events (Figure 1F).

REM HFOs are associated with fast, theta timescale fluctuations in PFC population/multiunit activity (MUA) during transient periods of locally reduced activity, as evidenced by the overall decrease in population activity during these events (Figure 2A). Furthermore, to isolate the spectral component driving this PFC population response, we re-detected HFOs using a broader 100–250 Hz passband and separated them by co-occurrence with the original 150–250 Hz HFOs (coordinated vs. non-coordinated). HFOs that occurred independently of 150–250 Hz detections elicited little to no phasic PFC spiking modulation, whereas those temporally coordinated with 150–250 Hz events reproduced the phasic theta-modulated response, indicating that this phasic PFC response is selectively associated with HFOs containing prominent 150–250 Hz activity (Figure 2B). This phenomenon was also present when using different parameters for HFO detection or REM sleep designation (Figures S2D-F). In contrast, NREM cortical ripples were associated with

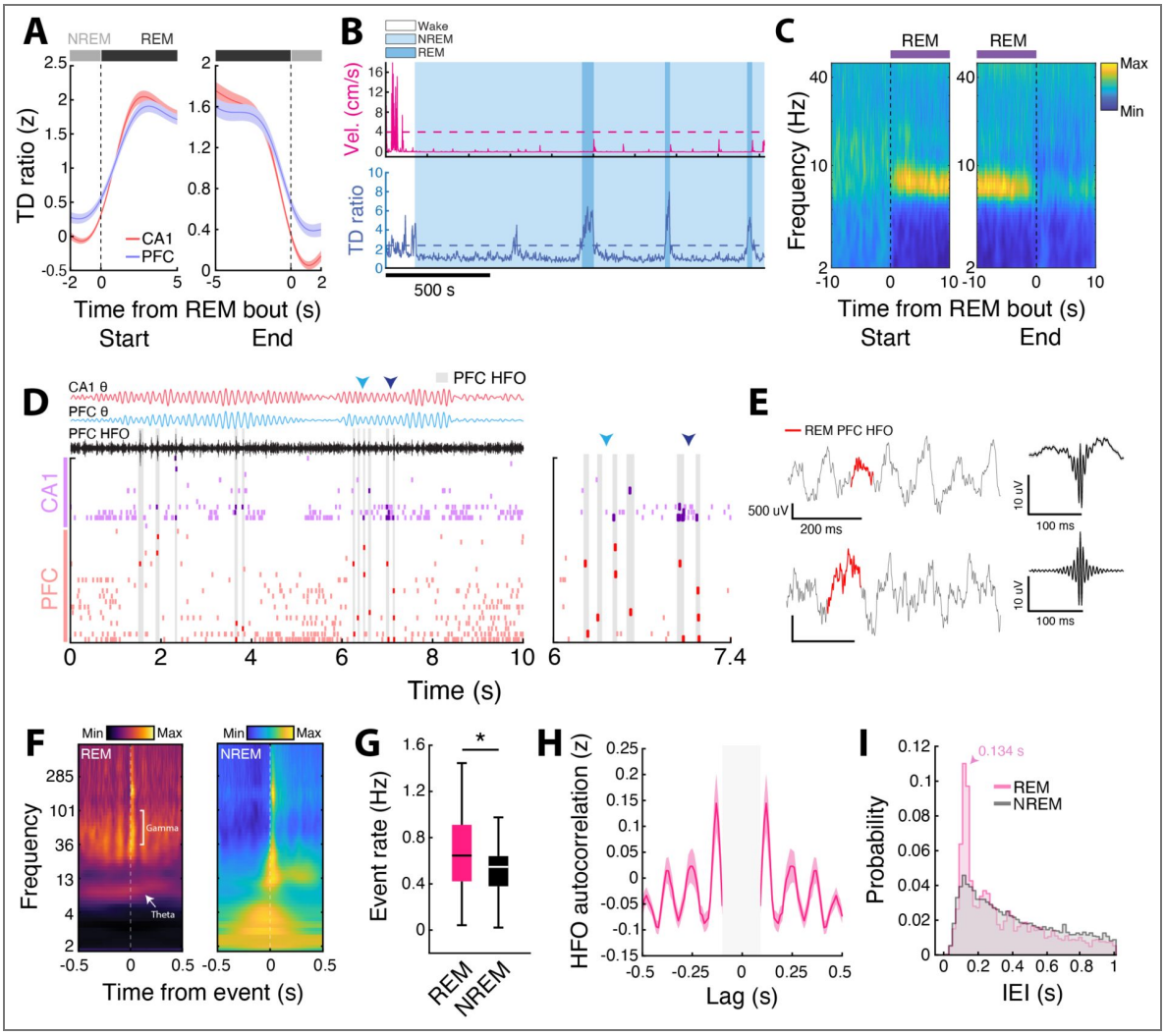

Figure 1. High-Frequency Oscillations (HFOs) in PFC during REM sleep.

(**A**) CA1 and PFC theta-delta (TD) ratio time locked to either the start or end of a detected REM sleep bout. Start and end times were determined using CA1 TD ratio. Note the similar increases and decreases in CA1 and PFC TD ratio surrounding REM bout starts and ends, respectively. (**B**) An example sleep session for an animal showing each behavioral state detected using the sleep state algorithm that utilizes theta-to-delta ratio (TD ratio) and animal velocity (cm/s). (**C**) Average spectrograms across all REM bouts centered on the start (left) and end (right) of each bout. Note the sharp increase and decrease in theta power at the start and end of REM sleep, respectively. (**D**) Raster plot of CA1 and PFC cells during REM sleep with PFC theta and HFO amplitude plotted above. Gray shaded areas indicate PFC HFOs, and arrows denote periods expanded on the right to show single unit spiking during HFO events. (**E**) (Left) Example PFC HFOs during REM sleep. Note the theta frequency fluctuations in the local field potential. (Right) Example grand average PFC HFO waveform (top) and amplitude (bottom) across all events in an example animal. (**F**) Example PFC event triggered spectrogram for REM HFOs and NREM ripples. Note the elevated gamma (40-100 Hz) and theta (6-12 Hz) band activity associated with REM HFOs, in contrast to the elevated slow oscillation (0.1-4 Hz) and spindle (12-16 Hz) band power in during NREM ripples. (**G**) PFC high-frequency event rates in REM (HFOs) and NREM (ripples) sleep (REM = 0.66 ± 0.06, NREM = 0.54 ± 0.05, *p = 0.013, WSR). (**H**) PFC HFO autocorrelation in REM sleep. Note the peaks in the autocorrelation that repeat approximately every 125 ms. (**I**) Distribution of inter-event intervals (IEIs) for NREM ripples and REM HFOs. Note the prevalence of IEIs less than 200 ms for REM HFOs (Mode = 0.134 s). Only IEIs up to 1 s are shown for visualization purposes.

a singular burst of activity spanning several hundred milliseconds[28] (Figures 2C and S2C). Thus, these findings establish distinct high-frequency event-associated activity profiles in PFC that may underlie differential processing of memory related information during NREM and REM sleep.

Coupling of theta, gamma, and prefrontal HFOs in REM sleep

Theta-gamma phase-amplitude coupling (PAC) is one of the most widely studied cross-frequency coupled phenomena in the brain and involves the coupling of distributed, lower frequency theta oscillations and local higher frequency bursts.[42] Thus, cross-frequency PAC is considered to be a physiological marker that links distributed brain regions during bouts of coherent activity to integrate information across different spatiotemporal scales.[42] Furthermore, previous work has proposed that phasic REM sleep may support cortical-hippocampal dialogue through this theta frequency-based coordination.[43]

Phasic REM is characterized by higher theta power and frequency as compared to tonic REM in both the neocortex and hippocampus.[18,19] Thus, we detected putative bouts of phasic REM as periods of elevated theta power (Figure S3). We further quantified the inter-peak-intervals of the filtered CA1 theta signal during low and high theta power bouts to determine whether they may correspond to putative tonic and phasic substages, respectively. Inter-peak intervals were significantly shorter during high theta power bouts than low power bouts, consistent with these periods reflecting putative phasic REM (Figures S3A-C). The rate of REM HFOs, as well as chaining of events, was significantly elevated during periods of high theta power (Figures S3D-G), indicating that the prevalence of REM HFO chains is elevated during bouts of putative phasic REM sleep. Consistent with this, we found that theta cycles were more likely to contain embedded HFOs during putative phasic REM than during tonic REM (Figure 3A). Thus, we restricted further analyses for quantifying gamma and HFO coupling to theta oscillations to these phasic bouts of high theta power (Figures 3B,C and S4A-F). To further validate the coupling of theta, gamma, and HFOs (illustrated in Figure 1F), we quantified PAC, which is a measure of how strongly the amplitude of fast oscillations vary as a function of the phase of a slower one, between theta phase and gamma to HFO frequency (40-250 Hz) amplitudes (Figure 3B). Examining the modulation indices at two discrete frequency bands, gamma (40-100 Hz) and HFO (150-250 Hz), revealed a higher frequency, HFO component that is also modulated by theta phase (Figures S4A-F). The modulation index summarizes this coupling as a single number, with higher values indicating tighter phase-locked amplitude modulation.

To further verify that gamma and HFO are separable rhythms, we examined theta nesting of both oscillations, which quantifies the oscillatory components of the average raw LFP waveform centered on peaks of gamma or HFO power within the preferred theta phase bin (see **Methods**). This revealed two distinct fast oscillatory components embedded within the theta cycle that are tightly coupled, with gamma events leading HFOs (Figures 3C and S4C,D). Since the coupling metrics used here quantify relationships across theta cycles in aggregate rather than on a cycle-by-cycle basis, analyses of theta coupling for gamma and HFO activity were restricted to periods of high theta power (putative phasic REM), as mentioned above. Including periods of relatively low HFO occurrence could obscure genuine coupling dynamics. Focusing on epochs with robust theta oscillations, where HFOs are more prevalent, therefore provides a stronger basis for distinguishing gamma from HFOs and yields a more faithful representation of theta, gamma, and HFO cross-frequency coupling.

Furthermore, the phase locking preferences of PFC neurons to these two oscillatory components differ (Figures 3D and S4G), confirming gamma and HFO separation, and potentially reflecting distinct modes of local ensemble memory related processing. Importantly, we observed elevated CA1-PFC theta coherence during these REM HFOs as compared to baseline (Figure 3E), suggesting that increased theta coherence is associated with HFO generation in PFC during REM sleep.

Since we observed short-latency HFO recurrence during REM (Figures 1H,I), we reasoned that these HFO “chains” may be functionally different than HFOs that occur in isolation. Indeed, previous studies have characterized oscillatory events in multiple brain areas that occur in

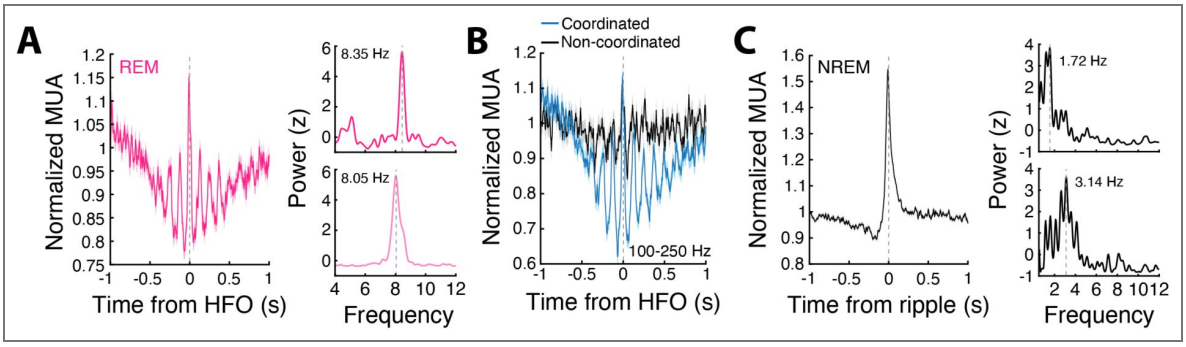

Figure 2. HFOs in PFC during REM sleep are associated with theta-modulated population activity and transient suppression.

(**A**) (Left) REM HFO aligned multiunit activity (MUA) in PFC (n = 10 animals, 36 epochs), and (Right) the power spectral density (PSD) calculated for two example animals. The vertical dashed gray lines indicate the peak theta frequency of the population activity fluctuations surrounding HFO events. (**B**) PFC multiunit activity aligned to REM HFO events extracted from a wider frequency range (100-250 Hz). The separation into coordinated and non-coordinated events (Coordinated = 48.75 ± 2.6%) was determined by the overlap of these HFOs with HFOs extracted using the standard frequency range (150-250 Hz). This analysis was performed to demonstrate that the HFOs extracted from the 150-250 Hz range primarily drives the theta frequency multiunit activity and transient suppression in PFC. (**C**) Same as in (**A**) but for NREM ripples. Note the synchronous activity burst time-locked to NREM ripples, in contrast to the distinctive activity pattern during REM HFOs in (**A**). Top and bottom PSDs are from the same animals as in (**A**).

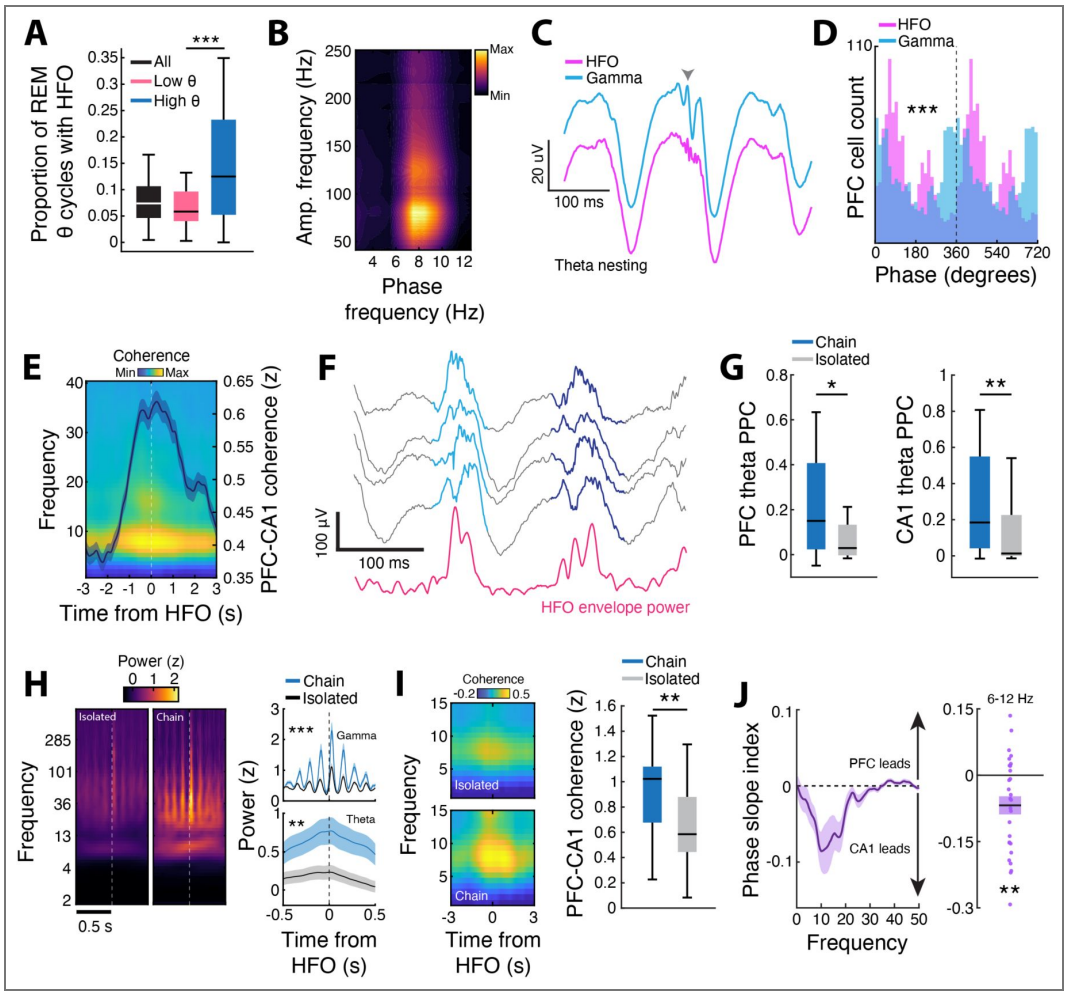

Figure 3. Theta, gamma, HFO coupling underlies distinct REM modulation states in PFC.

(**A**) Proportion of theta cycles with HFOs across all, low theta power (putative tonic), and high theta power (putative phasic) cycles (All = 0.075 ± 0.007, Low = 0.065 ± 0.006, High = 0.140 ± 0.018, ***p = 4.90×10^{-5}, WSR). (**B**) Phase-amplitude coupling (PAC). Averaged modulation across phase-amplitude pair occurrences during high theta power REM periods. The phase of the theta oscillation at a peak frequency of 7-8 Hz strongly modulates the amplitude of higher frequency oscillations. (**C**) Theta nesting for gamma and HFO frequency oscillations for an example tetrode illustrating coupling of theta, gamma, and HFO oscillations in PFC during REM sleep (see **Methods**). Briefly, averaged nesting plots were generated by aligning the unfiltered LFP to the peak power in the preferred theta frequency phase bin for either gamma or HFO oscillations separately. (**D**) Distribution of preferred phases for PFC cells locked to HFO or gamma events (U^2 = 4.74, ***p = 4.56×10^{-41}, Watson's U^2 test). (**E**) CA1-PFC theta (6-12 Hz) coherence centered on PFC REM HFOs is elevated relative to baseline theta coherence. The overlaid curve on the spectral plot represents the mean z-scored coherence across epochs, with shading indicating ± SEM. (**F**) Example REM HFO chain (doublet) plotted across 4 separate tetrodes with the average HFO power plotted below. (**G**) HFO chains showed higher PFC (Left) and CA1 (Right) theta PPC (pairwise phase consistency, a measure of phase-locking strength) compared to isolated HFOs (PFC: Chain = 0.22 ± 0.06, Isolated = 0.09 ± 0.04, *p = 0.013, WSR; CA1: Chain = 0.30 ± 0.08, Isolated = 0.14 ± 0.05, **p = 0.0016, WSR). (**H**) (Left) Chain and isolated HFO triggered spectrograms. (Right) Power in the gamma (top, 40-100 Hz) and theta (bottom, 6-12 Hz) frequency bands for isolated and chained HFOs. The average power in each band in the ±500 ms window surrounding HFO onset was used for comparison (Gamma: Chain = 0.72 ± 0.06, Isolated = 0.45 ± 0.03, ***p = 8.12×10^{-7}, WSR; Theta: Chain = 0.60 ± 0.20, Isolated = 0.15 ± 0.11, **p = 0.0021, WSR) (**I**) (Left) CA1-PFC theta (6-12 Hz) coherence during isolated vs chained events and (Right) quantification of the peak theta coherence in a ±1 second window from HFO onset (Chain = 0.93 ± 0.08, Isolated = 0.65 ± 0.05, **p = 0.0069, WRS). (**J**) (Left) Phase slope index (PSI), which is a measure of phase lag consistency across different frequencies, peaked at theta frequency, indicating a CA1 to PFC directed flow of information during HFO chains. (Right) Quantification of PSI in the theta band (6-12 Hz). Each data point corresponds to the averaged PSI across each electrode pair in an epoch. (PSI = -0.068 ± 0.021, **p = 0.0025, t-test against zero).

temporal clusters.[44-47] Importantly, chains of spindle events (termed, "spindle trains") in NREM sleep have been shown to underlie persistent reactivation of awake patterns and are associated with precise spatiotemporal coupling of sleep oscillations.[45] Similar to this previous study, we find spindle train events in PFC during NREM sleep (Figures S5A-D), supporting the claim that PFC can exhibit temporally clustered events during sleep.

We identified chains of HFOs as events that occur within 200 ms of each other (37.9% of all events). Chains were more prevalent in REM than NREM sleep (Figure S5E) and in putative phasic REM than tonic REM (Figures S3E,F). Similar to spindle trains, REM HFO chains predominantly occurred in doublets (Figures 3F and S5C,G). REM HFOs were more consistently locked to a preferred theta phase than NREM ripples, as quantified by pairwise phase consistency (PPC), which is a bias free measure of phase-locking strength (Figure S5F). Furthermore, REM HFO chains were strongly phase modulated by theta in both PFC and CA1 and had similar properties to isolated HFOs (Figures 3G and S5J). The strength of gamma was also elevated during HFO chains and exhibited phasic power fluctuations as well as suppression of population activity (as in Figure 2A) when coupled (within 500 ms) with HFOs, further demonstrating strong temporal coupling (Figures 3H and S4I,J).

Corroborating the strong phase locking of chain HFOs to theta oscillations in PFC and CA1 (Figure 3G), we find that hippocampal-prefrontal theta coherence is elevated during chain HFOs as compared to isolated events (Figure 3I), with CA1 theta leading PFC theta, as indicated by the phase slope index (PSI; negative values denote a CA1 to PFC direction of information flow at theta frequencies; Figure 3J). Together, these findings suggest that chains of HFOs can underlie coordinated hippocampal-prefrontal activity that supports REM sleep-mediated memory consolidation.

Differential modulation of PFC neuronal activity during NREM prefrontal ripples and REM prefrontal HFOs

Since we observed theta-modulated population activity aligned to REM HFOs that differed from activity aligned to NREM ripples (Figures 2A-C), we next examined PFC responses to determine how activity surrounding these events are organized at the level of single units and ensembles. Similar to population responses, many PFC neurons exhibited oscillatory spiking aligned to REM HFOs (Figure 4A). Unlike NREM ripples, REM events were associated with a broader distribution of activity peaks, suggesting a more sequential structure of neuronal firing surrounding these events (Figures 4A,B). Furthermore, we trained a binary linear classifier on the spike count vector across PFC neurons during each event and tested its ability to label held-out events as NREM ripples versus REM HFOs (10-fold cross-validation, with event counts equalized across types). PFC neuronal activity reliably distinguished NREM and REM events, confirming differences in spiking content (Figure 4C). In line with elevated CA1-PFC theta coherence surrounding REM HFOs (Figure 3E), we found that a subset of CA1 neurons were modulated by these events (Figure 4D), indicating enhanced interregional coactivity, potentially delineating periods of CA1-PFC ensemble reactivation to support memory consolidation.

Overall cortical cofiring, which is a measure of coincident activity between neuron pairs during discreet events,[48] and assembly strength were reduced during REM HFOs relative to NREM ripples (Figure 4E), consistent with overall activity suppression during HFO chains (Figures 4F-H), which can create a permissive background for gating selective reactivation of PFC ensembles in REM sleep. Examining population spiking activity, we found that PFC activity was strongly theta-modulated during REM HFO chains on the background of transient local suppression, compared to both isolated and NREM events (Figures 4F-H and S5H-J). This phasic population activity pattern was seen during HFO chains in both putative phasic and tonic REM substates (Figure S3F).

To address the possibility that this theta-modulated spiking activity and suppression may simply reflect high-theta-power bouts (rather than HFO occurrence), we generated surrogate event times by randomly sampling time points that matched the preferred theta phase of HFOs, but were at

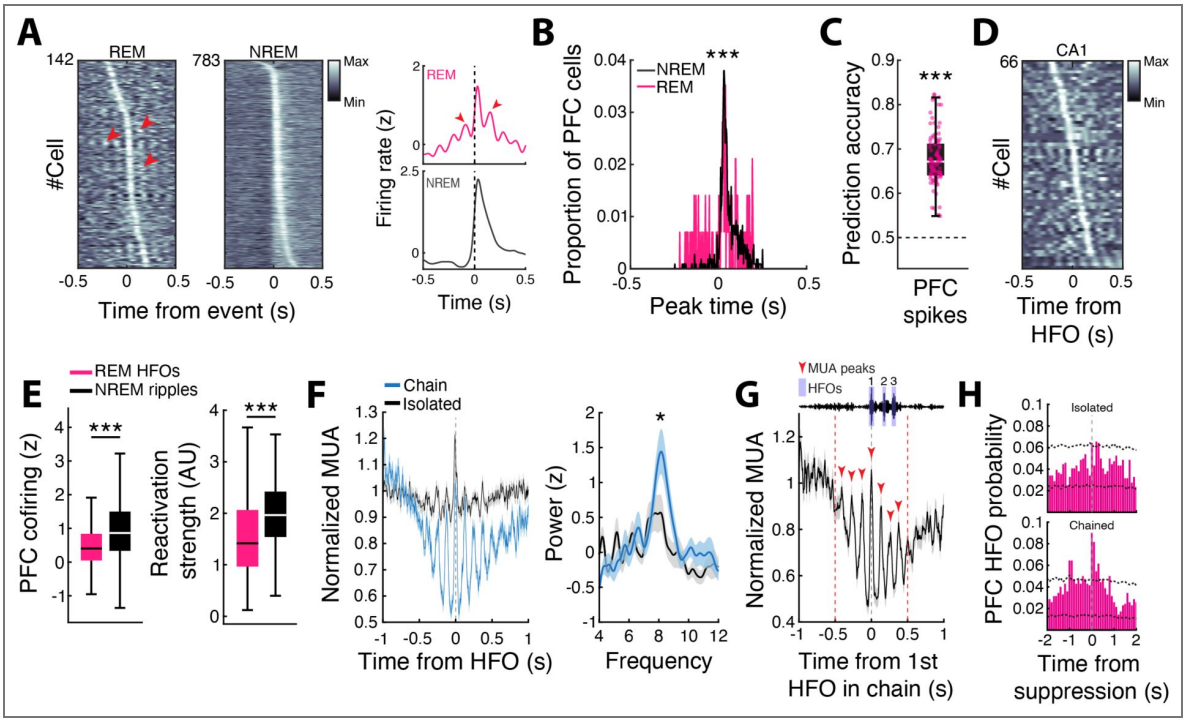

Figure 4. Differential modulation of PFC neuronal activity during NREM prefrontal ripples and REM prefrontal HFOs.

(**A**) (Left) PFC neurons that were positively modulated (EXC) during REM PFC HFO events and NREM PFC ripple events (REM EXC modulation = 142 out of 922 candidate neurons; NREM EXC modulation = 783 out of 1079 candidate neurons; See Methods section Ripple/HFO aligned modulation). (Right) Average z-scored peri-event time histograms (PETHs) aligned to events. Note the peaks in activity adjacent to REM HFO alignment at theta timescale denoted by the red arrowheads. (**B**) Timing of peak excitation for significantly modulated PFC cells during NREM and REM. Note the broader distribution of peaks during REM sleep (Comparison of peak timing distributions, ***p = 8.29×10^{-5}, WRS). (**C**) PFC event type (NREM vs REM) can be predicted by population spiking activity (PFC data = 0.68 ± 0.01, shuffle = 0.50 ± 8.00×10^{-5}, ***p = 2.56×10^{-34}, WRS). (**D**) Modulation of putative CA1 pyramidal neurons aligned to PFC REM HFO events (REM EXC modulation = 66 out of 680 candidate neurons). (**E**) PFC cofiring and assembly reactivation strength were overall stronger during NREM ripples (Cofiring: NREM = 0.96 ± 0.03, REM = 0.48 ± 0.03, ***p = 3.58×10^{-27}; Reactivation strength: NREM = 2.01 ± 0.05, REM = 1.56 ± 0.07, ***p = 6.91×10^{-16}, WRS). (**F**) (Left) PFC multiunit activity aligned to chained vs isolated REM HFO events. (Right) HFO aligned multiunit PSD illustrating stronger theta-modulated spiking activity in PFC during chained events (mean power in the 6-10 Hz band, *p = 0.029, WRS). (**G**) PFC multiunit activity aligned to the first HFO in each chained event. At top is a schematic of the multiunit alignment procedure. The initial HFO in a chain is at time 0. Note the peaks in the multiunit activity prior to the initial HFO within a chain, suggesting that fluctuations in PFC multiunit activity precede chained events. (**H**) The probability of (Top) isolated and (Bottom) chained REM PFC HFOs centered on population suppression events detected in REM sleep. Note the strong peak around 0 in the HFO chain distribution, indicating that REM PFC HFO chains are associated with overall decreases in population activity as compared to isolated HFOs. The black dotted lines indicate the 99% confidence intervals based on suppression events extracted from shuffled multiunit activity.

least 250 ms away from any detected HFO. PFC activity aligned to these surrogate events did not exhibit the same theta-modulated activity associated with real HFOs, even when the surrogate events were drawn from the highest-theta-power quartile (Figure S5K). Furthermore, we examined population activity as a function of distance from detected HFOs across all REM bouts, or subset by putative phasic REM, and did not observe the same magnitude of phasic response (Figure S5L-N), confirming that the transient theta-modulated population activity in PFC is specifically associated with the occurrence of HFOs. Interestingly, only HFO chains were uniquely associated with a transient suppression in overall local population activity (Figures 4F-H and S6), which is in contrast to the strong excitation seen in PFC and CA1 during NREM PFC ripples and SWRs, respectively.[28] Since REM HFOs predominantly occur in doublets (Figure S5G), the suppression of overall population activity is consistent with sublinear integration, in which subsequent events elicit less spiking activity than the first, thus likely creating privileged temporal windows for selective PFC ensemble reactivation and strengthening.

PFC ensemble activity is sequentially organized by REM HFO chains

Since we observed a broader temporal distribution of spiking activity (Figure 4B) as well as multiple peaks in population activity during REM HFO chains (Figures 4F,G), we next examined, in more detail, how ensemble activity is structured around these events. Previous studies have shown that the refractoriness of certain oscillatory events, such as spindles and SWRs, create distinct segregated periods for selective population activation.[44,45,47,49] Thus, we first examined population dynamics based on the temporal separation of REM HFOs. We observed selective activation of subsets of PFC ensembles during individual events in HFO chains (Figure 5A). To quantify this structure, we represented each HFO as a binary vector of PFC neurons active during the event, and computed the Pearson correlation between the vectors of every pair of consecutive HFOs. Spike content similarity as a function of Inter-Event-Interval (IEI) was examined using quartile ranges for the intervals between HFOs. Quartile 1 had the highest correlation, with the average IEI of this quartile as 114 ms (theta frequency, corresponding to HFO chains), indicating that adjacent HFO events within chains show a high degree of similarity as compared to adjacent isolated events (Figures 5A,B and S7A). Furthermore, we examined whether the order in which individual PFC neurons fired during HFOs within a chain was preserved across chains. For each chain, we extracted each cell's first-spike rank order and compared it to a leave-one-out template constructed from the average normalized rank across all other chains. This procedure revealed preserved sequences of PFC activity across multiple chain events (Figures 5C and S7B). These findings suggest that HFO chains stereotypically organize PFC activity, likely to support sequential reactivation of distinct assemblies.

Next, to test our hypothesis of sequential reactivation, we assessed PFC assemblies by examining time-locking of PFC reactivation strength to NREM and REM events. We detected behavioral PFC assemblies that are reactivated in sleep using established methods.[50,51] Similar to single unit modulation, the timing of PFC assembly reactivation aligned to NREM ripples was largely restricted to within 200-500 ms after ripple onset, depending on the ripple type examined (Figures 6A and S7F). For REM events, only the first HFO within a chain was selected for alignment, since we found that peaks in population activity occur prior to the onset of HFO chains (Figure 4G), possibly facilitated by strong phasic gamma surrounding HFO chains (Figures 3H and S4I). We found that unlike NREM ripples, where assembly reactivation is synchronous and consistently highest at the onset of events, PFC assemblies were sequentially organized on longer timescales surrounding REM HFOs, similar to single unit modulation (Figures 4A,B and 6A). This temporal tiling of assembly reactivation aligned to REM HFOs manifested in a relatively flat average response, highlighting the differential engagement of PFC assemblies during NREM and REM events (Figure 6B).

To confirm that the sequential tiling of assembly reactivation peaks in Figure 6A was a reliable phenomenon associated with HFO chains rather than an artifact, we used a split-half cross-validation. HFO events were first randomly partitioned into two halves, each assembly's peak reactivation bin was computed independently within each half, and the similarity of the temporal

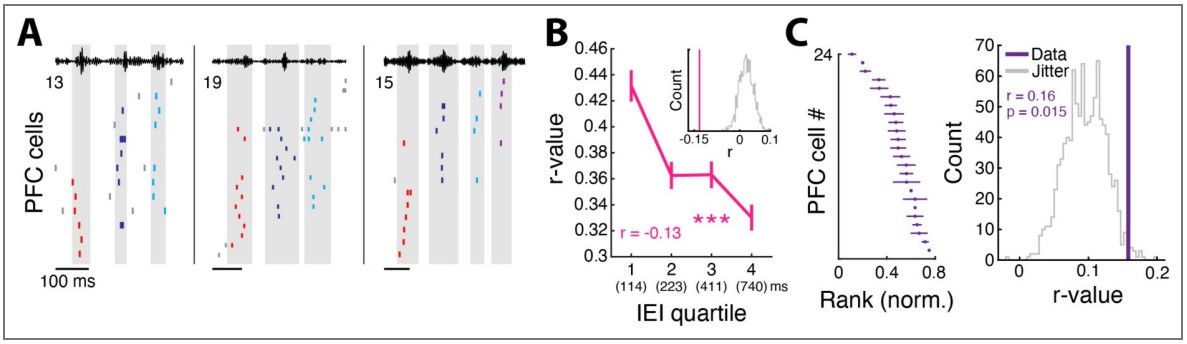

Figure 5. Temporally constrained sequential activity in PFC.

(**A**) Example rasters during HFO chains. Spikes are color-coded based on the HFO number within the chain during which the cell was active. Note the different cell assemblies active during each HFO within a chain. (**B**) Similarity of PFC population spiking between adjacent REM HFOs and its relationship with inter-event-intervals (IEI). Here, the PFC spiking activity during each HFO was binarized across all neurons and the Pearson correlation coefficient was calculated between adjacent events as a measure of pattern similarity. Then the relationship between pattern similarity and IEI was reported (r = -0.13, ***p = 6.00×10^{-8}, Pearson correlation). Below each quartile is the average IEI of that quartile in milliseconds. Note that the average for quartile 1 is 114 ms, which corresponds to 8-9 Hz during HFO chains. (Inset) The Pearson correlation coefficient compared to a distribution of r values generated from shuffling (n = 1000) HFO identity. (**C**) Rank-order correlation analysis. (Left) Example rank-order template from an example sleep epoch. Templates were generated by concatenating all HFOs in chained events (inter-event periods excluded) and averaging the normalized rank across chains. (Right) The mean rank-order correlation from the leave-one-out cross-validation procedure. Each event's rank was correlated with the averaged rank across all other events. The average across all events compared to a distribution of means generated by jittering (n = 1000) spike times is shown.

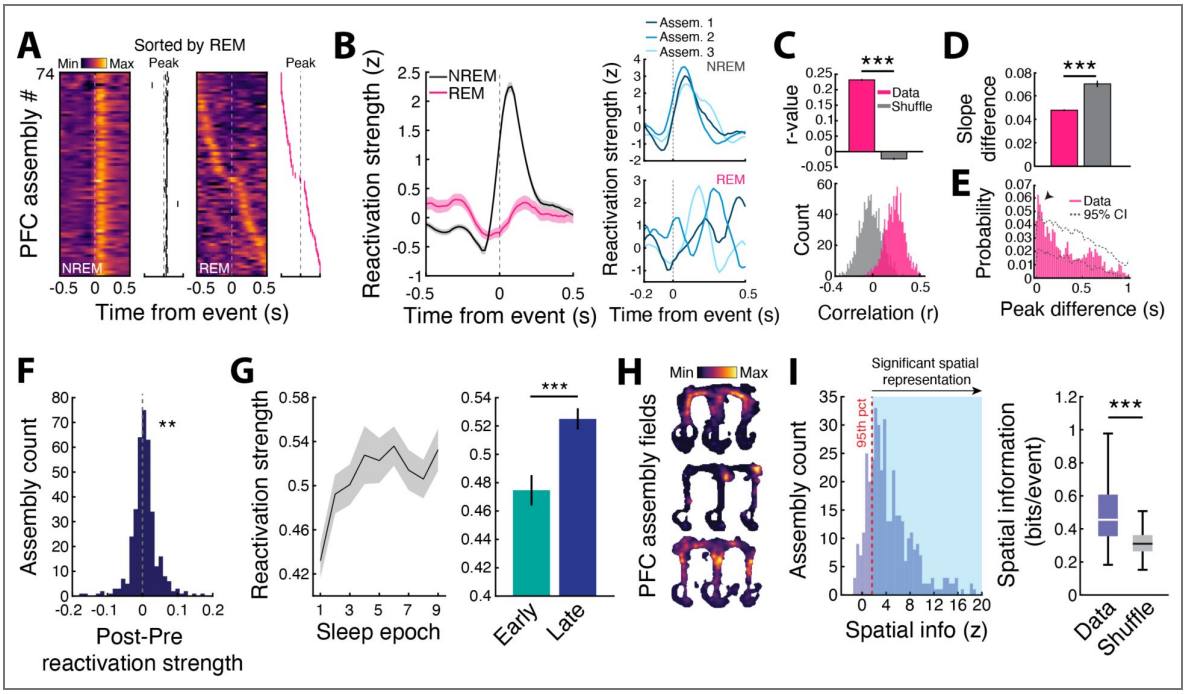

Figure 6. Structured reactivation in PFC during REM HFOs.

(**A**) (Left) PFC assembly reactivation aligned to NREM ripples or (Right) the first HFO of each REM HFO chain. Reactivation peak locations are shown alongside each plot. The assemblies are sorted based on the average peak reactivation bin within a ±500 ms window surrounding the first HFO in a chain. Note the tiling of assembly peaks aligned to HFO events in REM sleep, which manifests in the relatively flat average response in REM vs. a singular peak of synchronous assembly reactivation in NREM as shown in (**B**). (**B**) (Left) Averaged event triggered reactivation strength during NREM and REM. (Right) Mean reactivation strength of three example assemblies aligned to high-frequency events in NREM and REM, illustrating the tiling of assembly reactivation relative to events. The example assemblies shown come from the same animal and epoch. (**C**) Cross-validation of the REM reactivation sequences shown in (**A**), suggesting a consistent structure of reactivation surrounding REM HFO chains. (Bottom) Distributions of r values calculated from the Pearson correlation between peak reactivation bins across all assemblies for two randomly chosen halves (n = 1000 random splits) of the HFO aligned data (Data = 0.232 ± 0.003, Shuffle = -0.023 ± 0.004, ***p = 1.13×10^{-264}, WRS). (**D**) Differences in slope of the linear fit between the time of peak reactivation (in milliseconds) and assembly identity for two halves of the HFO aligned data (Data = 0.048 ± 2.21×10^{-4}, Shuffle = 0.070 ± 2.67×10^{-4}, ***p = 2.31×10^{-302}, WRS). (**E**) Probability of assembly peak displacement between randomly chosen halves of the HFO aligned data. For each assembly, the absolute difference in peak location was calculated between the two halves. To calculate 95% confidence intervals, assemblies were circularly shuffled, and the peak displacement probabilities were calculated over 1000 random splits of the data. Note the peak at small displacement values, indicating consistency of assembly peak activity across splits. (**F**) The distribution of PFC assembly reactivation strength differences between pre and post sleep. The same W-Track session was used as the template for each pair of sleep epochs. Thus, assemblies were matched across pre and post sleep epochs (**p = 0.006, t-test against zero). (**G**) (Left) PFC assembly reactivation strength during sleep over the course of learning. (Right) Comparison of reactivation strength during early (sleep sessions 1-3; epochs prior to grouped average of 75% correct performance on W-Track, see Figure S1B) and late (sleep sessions 4-9) sleep epochs (Early = 0.475 ± 0.010, Late = 0.525 ± 0.007, ***p = 1.78×10^{-4}, WRS). Except for sleep epoch 1, the preceding W-Track session was used as the template for reactivation. Only neurons that were tracked throughout the entire experiment were included for analysis. (**H**) Example PFC assembly rate maps. (**I**) (Left) Distribution of z-scored spatial information values for real assembly maps compared to maps generated from circularly shuffled (n = 1000) activation times. Each assembly's spatial information was expressed as a z-score relative to its shuffled distribution. The red dotted line at a z = 1.65 marks the one-tailed 95th percentile (p = 0.05). (Right) Observed spatial information vs. the median of each assembly's shuffle null distribution (Data = 0.535 ± 0.013, Shuffle = 0.325 ± 0.005, ***p = 2.82×10^{-65}, WSR).

ordering of assembly peaks between the two halves was calculated by taking the Pearson correlation (see **Methods**). Consistent with the structured PFC activity during chain events (Figures 5A-C), we found the greatest degree of sequence similarity during REM HFO chains compared to shuffled data (Figure 6C), confirming the tendency for PFC assemblies to be reactivated in a stereotyped, sequential manner as compared to isolated REM HFOs and NREM ripples (Figures S7C-F).

Finally, consistent with task-related reactivation, we found stronger PFC ensemble expression during sleep epochs following experience (Figure 6F). Importantly, assembly reactivation in sleep strengthened over the course of learning (Figures 6G and S1B), and a large proportion of detected assemblies had behaviorally relevant task representations with high spatial information (Figures 6H-I).

Differential engagement of distinct populations of CA1 neurons by PFC REM HFO chains

Theta coherence and phase amplitude coupling are two prominent modes of interregional coordination thought to underlie mnemonic processing.[42,52] Since we observed an overall increase in CA1-PFC theta coherence and gamma power during HFO chains (Figures 3H,I), as well as sparse modulation of CA1 activity during REM HFOs (Figure 4D), we reasoned that there may be specific populations of CA1 neurons that are engaged by these events. Examining CA1-CA1 cofiring during these cortical HFO events, we observed a higher degree of spatial rate map correlation for high cofiring pairs, suggesting HFO specific reactivation of behaviorally relevant hippocampal assemblies to support memory consolidation.[12] (Figures 7A,B). Additionally, the absolute CA1 cofiring, comprising both negative and positive magnitudes of cofiring, was higher during HFO chains, indicating a distinct activity profile compared to isolated HFOs (Figure S8A).

Next, we computed CA1-PFC cofiring across all cross-regional cell pairs and found that, during REM HFO chains, the distribution of cofiring values was bimodal, revealing a subpopulation of CA1 cells that are highly engaged with PFC neurons (Figure 7C). This distribution was unimodal during NREM PFC ripples, suggesting that the dual-population structure is specific to REM HFO chains. Analysis of low and high cofiring CA1 neurons during REM HFOs showed that high cofiring neurons exhibited elevated activity during HFO chain events as compared to low cofiring neurons (Figure 7D), independent of baseline firing rates (Figure S9A).

Interestingly, we also found a relationship between CA1 activation during REM PFC HFO chains and CA1 suppression by NREM PFC ripples. CA1 neurons that exhibited high cofiring with PFC (termed, “high HFO cofiring CA1 neurons”) specifically during REM HFO chains were more strongly suppressed during independent NREM PFC ripples, and the degree of suppression was correlated with the strength of REM CA1-PFC cofiring (Figures 7E and S8C,D). Given the sequential occurrence of NREM-REM sleep stages, this finding suggests that NREM ripples may tag specific CA1 populations for subsequent REM-dependent reorganization. However, although there was a strong relationship between CA1 suppression during independent PFC NREM ripples and excitation during coordinated SWRs in NREM sleep, as shown in a previous study.[28] (Figures S8C,E), we did not find correlations between CA1 REM HFO cofiring and CA1 SWR reactivation (Figure S8F), indicating that this CA1 sub-population that we identified as high co-firing with PFC neurons during REM HFOs is specifically engaged by high-frequency PFC events in sleep, with increased activity during REM and suppression during NREM.

Previous studies have shown that NREM and REM sleep are involved in modifying hippocampal excitability, with a net decrease in firing rates over the course of sleep.[33-35] To test whether REM HFO engagement predicted shifts in hippocampal excitability across sleep, we computed each CA1 cell’s firing rate change from the first to the last NREM bout within a sleep epoch and asked whether this change was related to how strongly the cell co-fired with PFC during HFOs. Interestingly, we observed that high REM HFO cofiring CA1 neurons differentially shifted their firing rates upward over the course of a sleep session, whereas most of the neuronal population, including low REM HFO cofiring cells, decreased their firing rates (Figures 7F, S8B, and S9B-

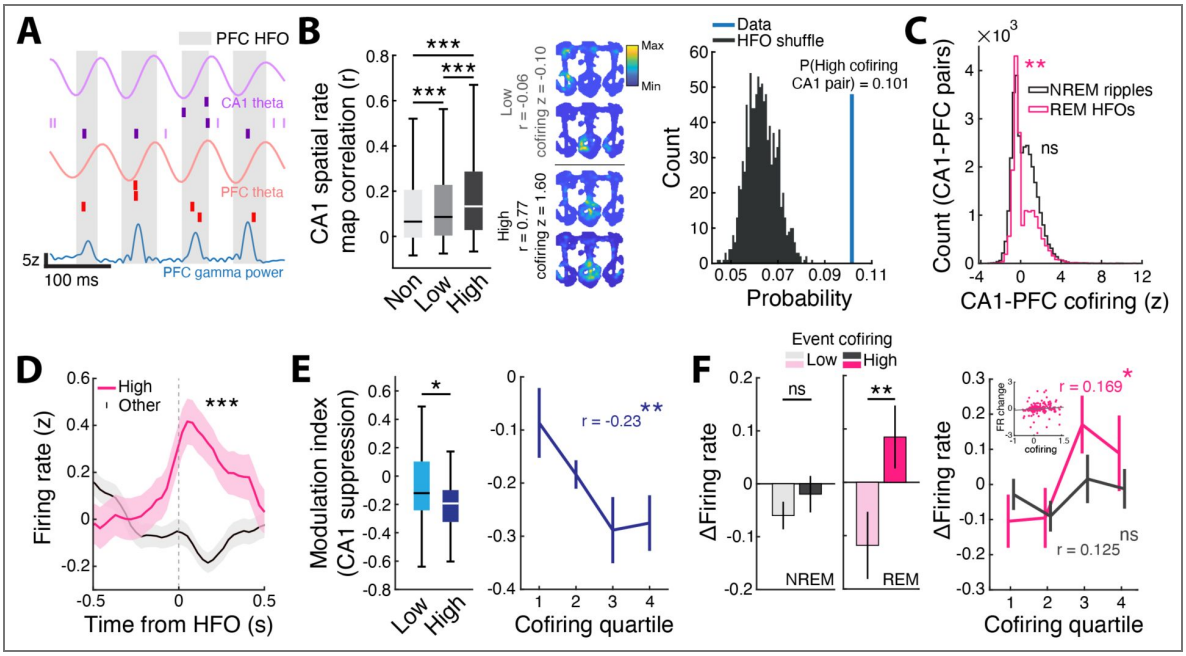

Figure 7. Differential engagement of distinct populations of CA1 neurons during PFC REM HFO chains.

(**A**) Example raster plot of CA1 and PFC cells during a HFO chain event. Only cells that were active during the plotted time window are shown. Note the coherence of theta band activity in CA1 and PFC with elevated PFC gamma power during each HFO event in the chain. (**B**) (Left) 2D spatial rate map correlation for non-active, low, and high HFO chain cofiring CA1 pairs (Non-active = 0.123 ± 0.001, Low cofiring = 0.127 ± 0.001, High cofiring = 0.176 ± 0.004, Non vs Low, ***p = 1.26×10^{-10}, Low vs High, ***p = 2.91×10^{-21}, Non vs High, ***p = 2.33×10^{-51}, Kruskal Wallis test with Bonferroni correction). Here, 'non-active' indicates cell pairs where cofiring was not assessed because at least one cell was inactive across all events. (Middle) Rate maps and spatial correlation of example low and high cofiring CA1 pairs. (Right) Real probability of high cofiring CA1-CA1 pairs during PFC HFOs (probability = 0.101) compared to a null distribution calculated by shuffling HFO times (n shuffles = 1000). (**C**) Histograms of CA1-PFC HFO cofiring during CA1-independent NREM PFC ripples and chained REM PFC HFOs. Cofiring during REM HFOs showed a bimodal distribution indicating separable populations of CA1 neurons based on PFC cofiring. (REM, **p = 0.001; NREM p = 0.23, Hartigan's dip test for bimodality). (**D**) Firing rate of high cofiring and "other" CA1 cells aligned to HFO chains. Here, 'other' includes low cofiring cells and cells that did not have a cofiring value because at least one of the cells in the pair emitted zero spikes across all events (similar to 'non-active' above). (Comparison of mean firing rates in the ±100 ms window from HFO onset, ***p = 7.77×10^{-5}, WRS). For comparisons between cofiring and other metrics (e.g. firing rate), a single cofiring value was calculated for each neuron by averaging the cofiring metric across all neuron pairings. Additionally, high and low cofiring CA1 neurons were split based on average cofiring values > 0 and < 0, respectively. (**E**) (Left) High REM PFC HFO cofiring CA1 neurons exhibited a greater degree of suppression during NREM PFC ripples. For a description of modulation index, see Methods section Ripple/HFO aligned modulation. Here, since CA1 neurons exhibit a robust decrease in activity in response to NREM PFC ripples,[28] we refer to the modulation as suppressive (Low cofiring = -0.08 ± 0.06, High cofiring = -0.25 ± 0.03, *p = 0.022, WRS). (Right) The CA1 cofiring magnitude during HFO chains was correlated with the degree of suppression during NREM PFC ripples (r = -0.23, **p = 0.0045, Pearson correlation). (**F**) (Left) Changes in CA1 firing rates from the first NREM bout to the last NREM bout within a sleep epoch plotted according to degree of cofiring with PFC (high, > 0; low, < 0), either during CA1-independent NREM ripples or chained REM HFOs (Low NREM = -0.06 ± 0.03, High NREM = -0.02 ± 0.03, p = 0.32; Low REM = -0.12 ± 0.063, High REM = 0.085 ± 0.059, **p = 0.0052, WRS). (Right) Firing rate change separated by cofiring quartile. The change in CA1 firing rates over the course of sleep was correlated with PFC cofiring during REM HFOs but not NREM ripples (NREM, r = 0.125, p = 0.46; REM, r = 0.169, *p = 0.012, Robust linear regression).

E), consistent with the role of REM sleep in hippocampal firing rate diversification.[53] This effect was hippocampal specific; there was no differential regulation of PFC firing rates over the course of sleep (Figure S9G). Furthermore, the degree of cofiring with PFC during REM HFOs predicted overall CA1 firing rate changes during sleep, and this relationship was absent for NREM PFC ripples (Figures 7F and S9E). Splitting the population in half based on mean firing rate changes further confirmed this relationship (Figure S9F), suggesting a REM specific role of PFC HFOs in modifying hippocampal excitability.

REM theta-phase shifting CA1 neurons are preferentially engaged during PFC REM HFOs

The dorsal CA1 pyramidal cell layer can be separated into subpopulations that are molecularly defined, have differential engagement with hippocampal SWRs and cortical areas,[54-57] and employ complementary spatial codes for effective coding of environments.[58] Notably, a subset of CA1 pyramidal cells preferentially shift their preferred theta phase from run to REM sleep[15] – a phenomenon that is experience dependent.[36] We therefore investigated whether there were differences in REM HFO recruitment for non-shifting and REM-shifting cells. We categorized REM-shifting neurons as cells that had a difference in phase preference greater than 90°.[15] As expected, there was a subset of CA1 neurons that shifted theta phase preference (n = 124/355 neurons significantly locked to both run and REM theta, Shift magnitude = 133.14 ± 2.35°) and were strongly engaged by SWRs (Figures S9H-J), as previously reported.[55] Similar to high cofiring CA1 neurons, these REM-shifting cells had higher cofiring with PFC than non-shifting cells (Figure 8A), and there was a significant relationship between HFO chain cofiring and suppression in the REM-shifting neurons, suggesting a specific modulatory effect on these neurons (Figures 8B and S9K). REM-shifting neurons also exhibited strong bursting activity during HFO chains as compared to isolated events and were more strongly phase locked to the PFC theta oscillation surrounding HFO chains (Figures 8C,D and S9L). Thus, PFC HFOs during REM sleep preferentially engage a specific population of REM-phase-shifting CA1 neurons, which are suppressed during NREM cortical ripples, and overall show an increase in firing rates during sleep, thus potentially increasing or stabilizing excitability to enhance signal-to-noise for efficient expression during future behavior.

Modeling high-frequency event-associated PFC activity during NREM and REM sleep

To gain a better understanding of how a cortical network can exhibit different activity patterns during NREM ripples and REM HFOs, we built a simplified network model (Figure 9A). 1,600 excitatory pyramidal and 400 inhibitory interneurons were pseudo-randomly connected based on cortical layer 2/3 connectivity probabilities (see **Methods**). Acetylcholine (ACh) concentration is an especially important factor for differentiating NREM and REM sleep states, with strong impacts on cell-spiking properties and network dynamics.[59-61] To incorporate one of the crucial impacts of ACh concentration on cortical neurons, each neuron in the model used a modified Hodgkin-Huxley (HH) formalism with an additional slow potassium (M-type) leak conductance term.[62] During NREM simulations, this slow potassium channel is opened to simulate low ACh concentration, and the channel is closed for REM simulations to simulate high ACh concentration.[63,64] By incorporating this additional conductance, a primary effect of the most abundant muscarinic ACh receptor in the brain (the M1 receptor) is included in the model. *In vivo* and in the model, activation of this potassium leak current alone reduces cell excitability and increases network synchronicity.[65-69] In the model, modulation of this M-type current also changes the excitatory-inhibitory balance of the network, supporting higher average interneuron rates (Figure S10A).

While the model does not possess the complexity to replicate the same HFO-range spiking frequencies, we found that by applying a stimulus input to a randomly chosen subset of cells of the network, we could recreate some essential characteristics of network activity patterns during NREM and REM cortical events. A brief moderately strong input during NREM, representing input during NREM ripples, was sufficient to induce a larger burst of synchronous spiking in the

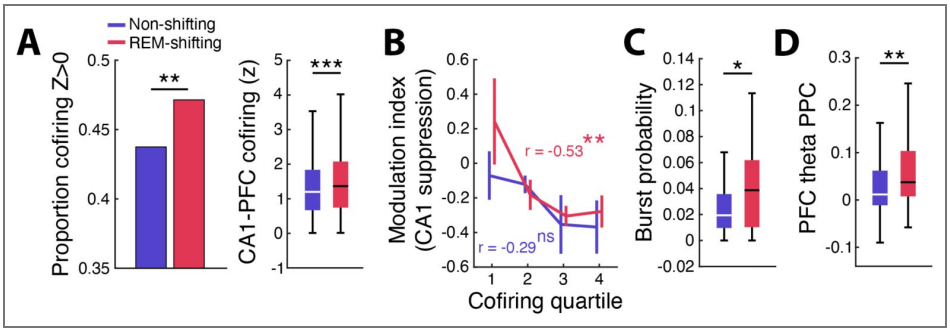

Figure 8. REM theta phase shifting CA1 neurons are preferentially active during PFC REM HFO chains.

(**A**) (Left) Proportion of CA1-PFC pairs with cofiring greater than 0 during REM HFO chains that contained either non-shifting or REM-shifting CA1 neurons (Non-shifting = 2216/5066 pairs, 43.7%, REM-shifting = 1057/2242 pairs, 47.2%, z = 2.70, **p = 0.0097, Z-test for proportions). (Right) Magnitude of CA1-PFC HFO cofiring (greater than 0) compared for non-shifting and REM-shifting CA1 neurons (Non-shifting = 1.35 ± 0.02, REM-shifting = 1.51 ± 0.03, ***p = 8.30×10^{-5}, WRS). Note that all cofiring pairs are assessed here. (**B**) Similar to Figure 7E, the REM PFC HFO cofiring magnitude of REM-shifting CA1 neurons was correlated with the degree of suppression during independent NREM PFC ripples (Non-shifting, r = -0.29, p = 0.066, REM-shifting, r = -0.53, **p = 0.0093, Pearson correlation). (**C**) Burst probability of non-shifting and REM-shifting CA1 neurons during REM HFO chains (Non-shifting = 0.028 ± 0.006, REM-shifting = 0.059 ± 0.017, *p = 0.022, WRS). (**D**) REM-shifting CA1 neurons showed higher PPC, indicating stronger phase locking to the PFC theta oscillation surrounding HFO chains (Non-shifting = 0.032 ± 0.006, REM-shifting = 0.064 ± 0.011, **p = 0.0026, WRS). Only periods surrounding REM HFO chains were used to evaluate phase locking strength of CA1 neurons.

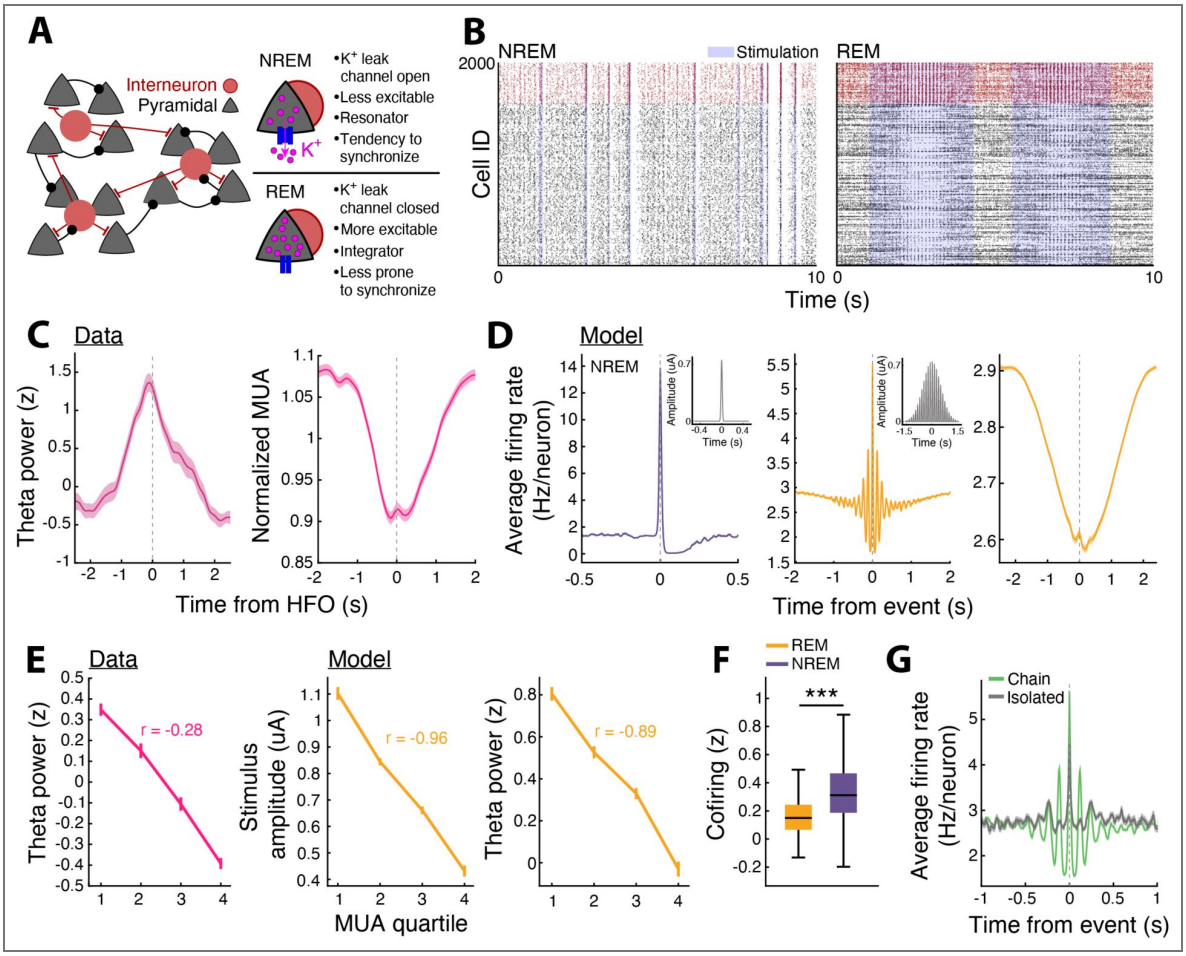

Figure 9. A simple network model incorporating acetylcholine recreates REM results.

(**A**) Model schematic. Network of Hodgkin-Huxley (HH) pyramidal and interneurons with an added slow potassium leak conductance. This channel is open in NREM, introducing an adaptation current that lowers cell excitability and bestows resonator properties to all neurons, altering their phase response curves such that connected cells are better able to synchronize spiking. In REM the channel is closed to simulate high ACh concentration, eliminating the adaptation current. (**B**) Example raster plots of network activity in NREM and REM. Spikes from 400 interneurons shown in red, spikes from 1600 pyramidal neurons shown in black. Shaded regions indicate periods of applied input current (see Methods). (**C**) Experimental data. (Left) Z-scored theta power surrounding REM PFC HFOs shows an average 3 second increase in theta power. (Right) Normalized MUA aligned to REM PFC HFOs using 100 ms bins shows suppression. (**D**) Modeling MUA results. (Left) NREM average network firing rate aligned to MUA peaks during stimulus periods, with inset depicting the average stimulus profile. (Center) same as (Left), but for REM. (Right) REM 100 ms binned firing rate aligned to MUA peaks within stimulus periods (i.e., a smoothened version of the Center panel) shows suppression, similar to experimental data. (**E**) (Left) Experimental data showing the negative correlation between peak theta power during REM HFOs and average MUA during HFOs. (Center) Peak amplitude of applied stimulus vs. average MUA quartiles during stimulus period in the model. (Right) Same as (Center), but for z-score of average theta power (measured from network MUA) during stimulus period. (**F**) Z-scored cofiring within MUA peaks in stimulus periods in the model. REM peak duration 37 ± 9 ms (mean ± std), NREM peak duration 35 ± 9 ms. (**G**) Average firing rate surrounding MUA peaks within stimulus periods in the model split between isolated and chained MUA peaks. Isolated peaks defined as having no other peak within a 200 ms.

network, causing a large peak in MUA (Figure 9B,D, left). In order to recreate the MUA surrounding REM PFC HFOs, we found that a theta-modulated gaussian input with a similar profile to the theta power observed around PFC REM HFOs (representing activity during phasic theta bursts in REM) was able to capture oscillatory and inhibitory features of the MUA (Figure 9C,D). We applied stimulus inputs of a variety of peak amplitudes to the network, and found that for temporally brief, discrete stimuli in NREM, stronger stimulation induced greater MUA (Figure S10D). Conversely, the strength of theta-oscillating input (and associated theta power as measured in the model's MUA) during REM correlated negatively with the MUA level during stimulation (Figure 9E). We found a similar negative relation in the experimental data between theta power surrounding REM HFO times and MUA level, suggesting that increased theta power in PFC is associated with stronger external input.

The cofiring analysis done on experimental spiking data during REM and NREM events (Figure 4E) was implemented for the spikes of a matched number of randomly chosen model neurons during REM and NREM stimulation periods, showing greater cofiring during NREM similar to the experimental data (Figure 9F). In addition, we divided peaks in MUA during REM stimulation periods in the same manner used to separate isolated and chained REM HFOs in the data (minimum 200 ms between MUA peaks, Figure 3). Similar to the data, we observed greater theta modulation in the MUA surrounding chained peaks compared to isolated peaks, as well as a larger dip in overall MUA (Figure 9G), with the difference especially clear in the pyramidal population of the model (Figure S10H). Overall, these results indicate an ability of the model to capture essential features of PFC activity in NREM and REM sleep, and suggest that REM HFOs reflect transient periods of elevated theta input to PFC neurons, leading to characteristic activity patterns in the network due to high cholinergic tone.

Stimulation in NREM induces widespread network activation compared to stimulation in REM

Analyzing stimulation periods in the model's NREM and REM states revealed intriguing differences in network activity (Figure 10A). While stimulus periods in REM tended to induce only a slight increase in the total fraction of cells spiking at any given time, stimulation in NREM induced a much wider spread of coactivity throughout the network (Figure 10B). We showed that the wider spread of coactivity depended on the decreased ACh concentration characterizing the NREM state in our model, and not the difference between REM- and NREM-inputs, because application of the brief NREM stimulus during REM did not produce the NREM level of peak coactivity (Figure S10G). Analysis of the percentage of PFC cells spiking in periods surrounding NREM and REM events in the model also showed this increased spread of coactivity in NREM, in agreement with the experimental results (Figures 4A,E, 6A,B, and 10B). However, it is unclear whether the widespread coactivity in NREM is a result of propagation of spiking due to recurrent excitation, or simply greater efficacy by the stimulus in directly inducing spikes in stimulated neurons during NREM. To investigate this, we analyzed model results by separating neurons within each stimulus event into stimulated and non-stimulated fractions. When stimulating in NREM, a widespread barrage of spiking from stimulated cells was followed by a smaller increase in the percentage of non-stimulated cell firing among both pyramidal and interneuron populations (Figure 10C). In contrast, during REM stimuli, the number of active stimulated neurons increased, but the effect on non-stimulated neurons was suppressive (Figure 10D). Again, swapping stimulus profiles showed that the cholinergic tone in the model plays a large role in creating this difference, especially as the brief NREM-like stimulus applied during REM produces no increase in percentage of coactive non-stimulated neurons (Figure S10I,J). These findings nicely align with experiments showing that ACh both suppresses the spread of cortical recurrent excitation and drives inhibition.[70-73] Our results suggest that the ACh level regulates the degree to which inputs can induce widespread synchronous network activity, leading to the distinct activity patterns in NREM and REM. Low ACh concentration and the associated reduced inhibitory tone in NREM leads to a rapid spread of activity to many non-stimulated cells upon transient excitatory input to a subset of the network. Such a result suggests

that the level of ACh regulates the fraction of cells in a circuit able to respond to a stimulus, accounting for the observation of synchronous bursts of activity among a large portion of cells during NREM (low ACh and low inhibition) whereas coactivity is restricted to smaller subsets of cells in the network during REM (high ACh and high inhibition).

Discussion

One of the key challenges in understanding the role of REM sleep in memory consolidation has been disentangling the interregional neurophysiological processes involved in memory-related processing. Previous studies have primarily focused on the role of theta oscillations in REM sleep as a brain-wide pattern that coordinates activity across various brain regions,[74] due to their similarity with patterns observed during wakeful behavior. While much attention has been focused on investigating theta oscillations due to their prominence in the hippocampus during REM sleep, the precise dynamics that drive the coordination of multiple brain areas to potentially support systems memory consolidation have been elusive. Furthermore, the prominence of oscillatory phenomena in NREM sleep—including slow oscillations, spindles, cortical ripples, and CA1 SWRs—has enabled systematic dissection of their spatiotemporal dynamics and their relationship to hippocampal-cortical reactivation that supports memory consolidation,[11-14] leaving REM sleep dynamics poorly understood in comparison.

Here, we show that phasic activity bursts in PFC during REM theta coincide with chains of local HFOs and elevated gamma power. These chains are associated with increased measures of oscillatory coupling between PFC and CA1, and show characteristic theta-modulated spiking activity patterns on background of local suppression. REM PFC HFO chains organize sparse, sequential reactivation in PFC over extended time periods, and recruit a sub-population of CA1 neurons that exhibit differential regulation of activity over the course of sleep. This contrasts with NREM sleep, where independent PFC ripples are associated with relatively brief, synchronous bursts of local reactivation along with suppression of CA1 activity. We also show that CA1 co-activation during REM PFC HFOs is related to the CA1 activity suppression seen during NREM PFC ripples, with CA1 neurons that are highly coactive with PFC during REM HFO chains being strongly suppressed during NREM ripples, suggesting a dual sleep-stage role of PFC ripples and HFOs in regulating excitability in hippocampal circuits. Thus, these results uncover a novel, high-frequency pattern of PFC activity in REM that can potentially bridge the gap between structured PFC and CA1 firing patterns in NREM-REM stages and changes in hippocampal plasticity during sleep.

In contrast to PFC ripples in NREM sleep, which are involved in suppressing CA1 activity as a possible mechanism for tagging specific memory traces for consolidation,[28] here we found that REM cortical HFOs engage specific populations of CA1 neurons to potentially regulate activity homeostasis. Of particular interest regarding this phenomenon of activity regulation is a recent study examining the differential roles of NREM and REM sleep in reorganization of drifting hippocampal assemblies over the course of sleep.[75] This study focused solely on hippocampal assemblies, and the results are in line with our finding of the potential roles of PFC ripples and HFOs in NREM and REM sleep, respectively. We have previously shown that independent NREM PFC ripples that are dissociated from hippocampal SWRs broadly suppress CA1 activity, and that this suppression is related to the strength of CA1 reactivation during SWRs and CA1 assembly reinstatement during subsequent behavior.[28] This bidirectional modulation of hippocampal representations during PFC ripples and CA1 SWRs may underlie assembly reorganization during NREM sleep. Relatedly, we report here that CA1 activity during REM PFC HFOs is associated with differential changes in excitability in a subset of hippocampal neurons during sleep, which may, in part, contribute to the stabilization of assemblies in REM sleep and thus drive the sleep-stage dependent reorganization of hippocampal assemblies. This finding is in line with REM sleep's role in recalibration of neural activity in hippocampal-cortical circuits.[5] We speculate that PFC REM HFO chains enable selective linkages between the sparsely reactivated PFC ensembles in coordination with a subset of CA1 neurons.

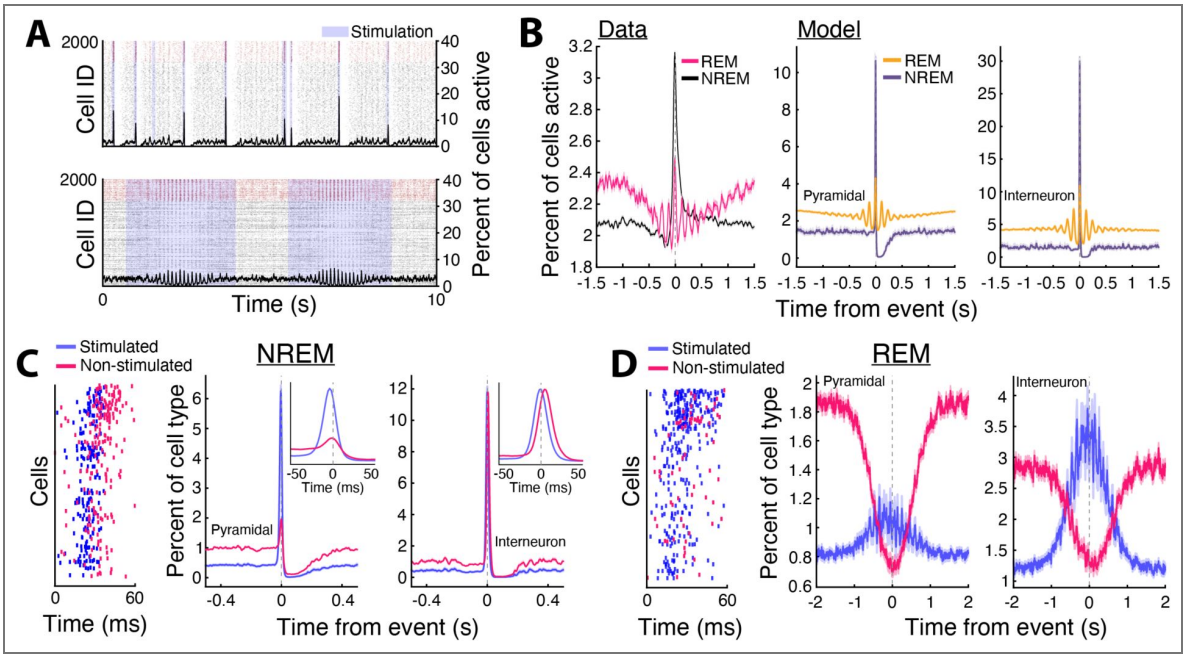

Figure 10. Stimulation in NREM induces widespread coactivity compared to stimulation in REM.

(**A**) Model raster plots during example NREM (Top) and REM (Bottom) periods with black trace indicating the percent of all pyramidal cells with at least one spike in 10 ms bins. (**B**) The same percent active measure (not distinguishing by cell type) calculated on experimental data aligned to NREM and REM events (Left), and in the model aligned to MUA peaks in NREM and REM as a fraction of all pyramidal neurons (Center). Similar plot for all interneurons in the model (Right). (**C**) Model NREM activity split by cells directly receiving stimulus input (blue) and receiving no external stimulus (pink). Raster of a single example population burst due to stimulation in NREM (Left). Percent of cells with at least one spike in 10 ms bins (as a percent of all pyramidal cells in the network) aligned to stimulus midpoints, the time of peak input amplitude (Center). Similar plot for interneurons (Right). (**D**) Same as (**C**), but for REM. Note that non-stimulated cell population (pink) comprise a greater percent of total active neurons outside stimulation times (average stimulation time of 3 sec centered at time of event), as there are more neurons in the non-stimulated group (only 30% of neurons are stimulated per stimulus event).

Cortical high-frequency oscillations (~120-160 Hz) in REM have been reported before, especially in parietal cortex, although they have been variously termed fast gamma or HFOs (high-frequency oscillations),[19,21,22,31] with previous reports of strong coupling with theta oscillations in REM.[31] HFOs have also been reported in parietal cortex and hippocampus during active waking behavior and REM, and it has been argued that HFOs in hippocampus are distinct from hippocampal SWRs.[22] We detected HFOs in REM sleep using a similar frequency band (150-250 Hz) as cortical NREM ripples. These high-frequency events in NREM are denoted as "ripples", a term used by previous studies for NREM high-frequency events in cortex,[23,25,27-29,76] although this is likely a separate phenomenon from hippocampal SWRs. PFC NREM ripples that occur independently of hippocampal SWRs are associated with temporally synchronized local PFC reactivation and suppression of hippocampal activity and reactivation,[28] while in REM, we show here that they present as PFC HFO chains during theta-modulated activity, associated with sparse, temporally extended local reactivation in the backdrop of suppression, along with co-activation of a hippocampal-subpopulation. These structured cortical sequences seen during HFO chains are gated by theta oscillation bursts in REM sleep, with higher rate of occurrence in phasic REM than tonic REM substages, and are reminiscent of hippocampal theta sequences,[77] but may have different underlying mechanisms. We examined PFC HFO events during behavior on the W-maze, but did not find similar spiking activity patterns as REM HFO events (Figure S11), confirming that this is a REM-exclusive phenomenon.

Based on previous studies, external drive can lead to the generation of PFC ripples and synchronized activity in NREM, whereas high acetylcholine (ACh) and high inhibitory tone in REM can lead to local suppression in response to external drive.[73,78,79] Notably, a recent computational study demonstrated that differential cholinergic modulation, together with the sequential architecture of sleep (NREM to REM transition), can support memory consolidation through the complementary shaping of ensemble activity during NREM and REM sleep.[64] We show here that a simple network model that incorporates the effect of differential ACh tone on excitatory and inhibitory neurons in REM vs. NREM states is able to reproduce the observed experimental activity patterns in response to stimulation, akin to phasic theta bursts during REM and isolated, brief inputs in NREM. It is likely that PFC NREM ripples and REM HFOs are generated locally and modulated by external inputs. We speculate that theta-modulated input to PFC during REM is driven by hippocampal inputs, but it is also possible that theta is driven by inputs arising from regions other than the hippocampal network, a possibility which will require further experimental investigation.

We observed that isolated REM HFOs in PFC were more prevalent than chains, especially in tonic REM, potentially reflecting the need for coordinated activation of distributed circuits to elicit HFO-associated phasic events. One possible mechanism driving this phenomenon could involve PGO waves, which are prominent during phasic REM and are known to play a role in modulating hippocampal plasticity during REM sleep.[80] These waves are also coordinated with both SWRs in NREM and theta states in REM,[80,81] suggesting that PGO-associated amplification of hippocampal theta oscillations could drive activity above a certain threshold for HFO generation in PFC. Additionally, ACh may also play a role in altering the threshold for HFO generation in PFC in conjunction with PGO coordination. It has been reported that there is coordinated release of ACh in PFC and dorsal hippocampus, potentially elevating theta coherence between the two areas.[82] Indeed, a number of studies have shown that ACh boosts theta oscillations.[83] Furthermore, ACh induces decorrelation in cortical circuits, which improves cortical representations of relevant stimuli,[84] and our finding that REM HFOs are associated with an overall decreases in PFC population activity, reactivation strength and cofiring, in stark contrast to NREM ripples, suggests a role for REM HFOs in amplifying local cortical signal to noise to enable linking of cortically encoded information with specific populations of hippocampal neurons. Lastly, cholinergic input to the hippocampus also suppresses SWR generation,[85,86] which could facilitate the sparse CA1 reactivation during REM sleep for selective changes in excitability and stabilization of salient representations in coordination with cortical networks for subsequent expression during

behavior. Future experimental and network modeling studies can investigate how neuromodulatory mechanisms and NREM and REM state-specific cortical activity patterns act in concert to support learning and memory consolidation.

Taken together, these results establish a new cortical LFP pattern in REM sleep (PFC REM HFO chains) associated with a distinctive neuronal population activity signature. The findings are aligned with REM sleep's role in memory consolidation and provide a neural basis for the cortical-hippocampal modifications that occur during sleep to support activity reorganization and mnemonic processing. The complex interplay between oscillations of varying frequencies revealed here further highlight the importance of segregating sleep into multiple states to uncover how systems memory consolidation can be supported through the multiplexing of distinct phases, both during NREM and REM sleep. The interareal dynamics associated with PFC REM HFOs involve both bottom-up and top-down processes operating in precise temporal coordination, with theta-mediated communication leading to PFC HFO-associated reactivation and modifications in hippocampal excitability. These findings, in conjunction with PFC-mediated suppression of CA1 during NREM sleep, suggests a dual sleep stage processing of mnemonic representations that have implications for understanding the circuit mechanisms underlying systems memory consolidation, and can reveal how neural processes in sleep go awry in disease states.

Limitations

While the present results establish a potential role for REM sleep PFC HFOs, several limitations of our study are acknowledged here. First, we were unable to directly link REM HFO specific reactivation to learning. Spatial memory tasks in rodents similar to our study have revealed causal links of NREM reactivation driven by CA1 SWRs to learning and memory consolidation,[87-90] but reports of REM reactivation are rare.[37] Investigation of the role of REM reactivation in learning and memory consolidation will need utilization of tasks known to require both REM and NREM states, such as schema-based inference or emotional memories.[38,91-93] Second, behavioral task learning and interleaved sleep sessions were conducted in a few hours within a single day, which did not allow us to densely sample the circadian cycle. Third, we did not record eye movements or ponto-geniculo-occipital (PGO) waves, both of which would have allowed for more accurate segregation of tonic and phasic REM sleep states.[94] Although we observed a bias for isolated and chain HFOs to occur in putative tonic and phasic REM substates, respectively, the scarcity of putative phasic REM bouts made the direct comparison based on substage difficult. Finally, although our model predicts that distinct cell-type activity profiles shape REM sleep HFO dynamics, we did not record a sufficient number of interneurons to test these predictions directly. Future studies using appropriate behavioral tasks, longitudinal sleep recordings, and cell-type specific opto-tagging will be able to resolve these limitations and further clarify the roles of high-frequency oscillations in REM sleep.

Method details

Surgical implant and electrophysiology

Surgical implantation procedures were as previously described.[95] Animals (n = 10) were implanted with a microdrive array containing 30, 32, or 64 independently moveable tetrodes targeting right dorsal hippocampal region CA1 (-3.6 mm AP and 2.2 mm ML) and right PFC (+3.0 mm AP and 0.7 mm ML). For 64 tetrode recordings (n = 1 animal), CA1 and PFC were targeted bilaterally. Tetrodes were split equally between PFC and CA1 (15, 16, or 32 tetrodes in each region). On the days following surgery, hippocampal tetrodes were gradually advanced to the desired depths using characteristic EEG patterns (sharp wave polarity, theta modulation) and neural firing patterns as previously described.[95] A CA1 tetrode in corpus callosum served as hippocampal reference, and another tetrode in overlying cortical regions with no spiking signal served as prefrontal reference. A ground (GND) screw installed in the skull overlying cerebellum also served as a reference. All spiking activity, gamma, and ripple/HFO-filtered LFPs (gamma: 40-100 Hz;

ripple/HFO: 150-250 Hz; see below) were recorded relative to a local reference tetrode. For detection of slower frequency components (i.e., theta and delta), LFP was recorded with respect to the GND screw. Electrodes were not moved at least 4 hours before and during the recording day.

Data were collected using a SpikeGadgets data acquisition system (SpikeGadgets LLC). Spike data were sampled at 30 kHz and bandpass filtered between 600 Hz and 6 kHz. LFPs were sampled at 1.5 kHz and bandpass filtered between 0.1 Hz and 400 Hz. The animal's position was recorded with an overhead color CCD camera (30 fps) and tracked by color LEDs affixed to the headstage. Additionally, the animals' speed was calculated based on predetermined cm/pixel values and the position displacement between frames captured at 30 fps.

Behavior

Ten animals were trained on a novel W-maze in a single day, as previously described.[28,40,95]. This single-day W-maze alternation learning task is SWR-dependent, and requires hippocampal-prefrontal interactions.[39,96,97] Briefly, following recovery from surgical implantation (~7–10 days), animals were food-deprived and again retrained on a linear track for 2-3 days before exposure to the W-Maze task. During the recording day, animals were introduced to the novel W-maze (~80 × 80 cm with ~7 cm wide tracks) for the first time and learned the task rules over eight behavioral sessions during the animals' light phase between the hours of 9 AM and 6PM. Each behavioral session lasted 15–20 min and was interleaved with 20–40 min rest sessions in the sleep box for a total of 17 separate sessions (8 W-maze and 9 sleep sessions). The total recording duration spanned ~6-7 hours within a single day. On the W-maze, animals were rewarded for performing a continuous spatial alternation. The task rules are as follows: returning to the center well after visits to either side well (left or right well; inbound trajectories) and choosing the opposite side well from the previously visited side well when at the center well (outbound trajectories). Rewards were automatically delivered to the animal through custom 3D printed reward wells upon nose poke.

Histological verification of recording sites

At the completion of each experiment, electrolytic lesions were made by sending current (30 uA) down 3 electrodes per tetrode for 3-4 seconds each. 24 hours later, animals were sacrificed by intraperitoneal injection of Euthasol and subsequent intracardial perfusion with 0.9% saline followed by 4% formaldehyde. The skull, with the attached drive, was submerged in 4% formaldehyde for 24 hours before tetrode retraction and brain extraction. Brains were stored in a 4% formaldehyde and 30% sucrose solution for at least 1 week before slicing with a freezing microtome (Leica) at 50 uM. Slices were Nissl stained and imaged at 4x on a brightfield microscope (Keyence) and stitched together to generate composite images for lesion localization.

Spike sorting

Single units were sorted using a custom manual clustering program (MatClust, M. P. Karlsson) and were distinguished based on spike width, peak and trough amplitude, and principal components. Cluster quality was measured using isolation distance,[98] and only well isolated neurons were included for analysis.

Sleep state identification

To detect bouts of NREM and REM sleep, animals' head speed and CA1 LFPs were used as previously described.[15,16] During sleep box sessions, times of awake activity and immobility were defined as periods where head speed was greater or less than 4 cm/s, respectively. Candidate NREM sleep bouts were identified as periods where head speed remained <4 cm/s after an immobility period of at least 60 s. NREM and REM sleep were further identified and separated by using a theta to delta ratio metric. Briefly, CA1 LFP (referenced to GND) for each tetrode was bandpass filtered (6-12 Hz for theta; 1-4 Hz for delta) and averaged, and the ratio of theta to delta (TD ratio) power was calculated.

Periods that exceeded a set threshold (mean + 1 SD) for >10 s were categorized as REM bouts within candidate NREM bouts.[99,100] Additionally, candidate REM bouts were visually inspected to further confirm the transition into REM sleep. For comparison of velocity and TD ratio, the average velocity and TD ratio in each epoch for NREM and REM sleep were computed and compared. Additionally, only epochs with at least 30 s of REM sleep were included for analysis. Unless otherwise stated, all analyses were restricted to the 36 (of 90) sleep epochs that satisfied the inclusion criteria.

Intracranial electromyogram (EMG)

To estimate EMG from the neck, jaw, and face muscles from intracranial LFP signals, a previously established method was used.[35,101] Briefly, we extracted the 300-600 Hz filtered signal (Butterworth filter at 300 – 600 Hz; filter shoulders from 275 – 625 Hz) and calculated the pairwise Pearson correlations in each 500 ms bin between pairs of electrodes during the entire sleep epoch. Since we used tetrode recordings and cannot determine the exact separation of electrode sites, we elected to calculate the correlations between the reference tetrode in corpus callosum and CA1 ripple detection tetrodes within the dorsal CA1 pyramidal cell layer (~500 μm separation between corpus callosum and the dorsal CA1 pyramidal cell layer), thus maximizing the separation between the electrode sites. Previous studies have used electrode channels on probes at least two shanks apart (~400 μm). The average of all reference/CA1 layer tetrode pairs was calculated and compared for wake and REM sleep. For the distributions of intracranial EMG values in Figure S1D, each 500 ms bin correlation value was reported, and for the comparison between wake and REM sleep, the averages during each wake and REM bout were calculated and compared. A strong relationship between intramuscular EMG and intracranial EMG has been reported.[101]

LFP event detection

PFC ripple/HFO detection: High-frequency events were detected during immobility periods (<4 cm/s) as previously described.[16] Tetrodes with recorded cells in CA1 and PFC were used as candidate electrodes for event detection as well as downstream LFP analysis. Each LFP from candidate electrodes were bandpass filtered in the ripple/HFO band (150-250 Hz), and the envelope power was calculated using a Hilbert transform and subsequently smoothed with a Gaussian kernel (σ = 6). Events were detected as contiguous periods where the ripple/HFO power exceeded 3 SD of the mean on at least one tetrode. A minimum event duration of 15 ms was implemented to exclude spurious noise in the LFP signal. Events were further refined as periods around the detected event that remained above the mean (start and end times). The amplitude of each event was reported as the number of SD above the mean.[40] To estimate the frequency of each event, the power in each frequency bin was calculated around each event (±500 ms) using multi-taper time-frequency analysis (Chronux toolbox; *http://chronux.org/*)[102] and was z-scored relative to a baseline spectrogram. The frequency of each event was defined as the frequency with the highest power in the ripple/HFO band (100-250 Hz) between the start and end time of each event.[103] Furthermore, HFO chains were defined as 2 or more events that occurred <200 ms apart. Average amplitude plots for each animal were generated by aligning the peaks of each event and averaging.

PFC gamma detection: Bouts of high gamma power were detected as above after bandpass filtering in the gamma band (40-100 Hz).

High theta power detection: Each LFP from candidate PFC tetrodes were used to delineate periods of high theta power during REM sleep. LFPs were bandpass filtered with a theta band filter (6-12 Hz), the envelope power was calculated using a Hilbert transform, averaged across tetrodes, and periods that exceeded 4 SD of the mean during REM sleep were designated as bouts of high theta power. Only high-power periods exceeding 900 ms were included as high theta power periods.

PFC spindle detection: Spindle events were detected as previously described.[45] The mean LFP across all candidate PFC electrodes was calculated and the resulting signal was bandpass filtered between 10-16 Hz with a zero-phase shifted, third-order Butterworth filter. The envelope power was calculated using a Hilbert transform and subsequently smoothed with a Gaussian kernel (α =

2.5). Events that exceeded 2.5 SD of the mean were extracted, and events separated by <300 ms were concatenated. Spindle events were restricted to NREM sleep before analysis. Spindle trains were defined as 2 or more spindle events that occurred ≤2.78 s apart as previously established.[45]

Spectral analysis

Wavelet spectral analyses were utilized to calculate the ripple/HFO aligned power spectra in PFC (2–350 Hz, Morlet wavelets). For each epoch, the PFC tetrode with the greatest number of detected PFC ripples/HFOs was used. The power at each level of the wavelet transform was calculated around each event (±500 ms) and was z-scored relative to a baseline spectrogram calculated for the entire epoch. For each animal, spectrograms from all candidate sleep epochs were averaged.

Event autocorrelation

To calculate the autocorrelation of ripples/HFOs to assess the structure of event occurrence, identical event time vectors were lagged (max time lag 1 second, 10 ms time bins), and the correlations were calculated. The results were smoothed with a Gaussian kernel ($\sigma = 3$) and averaged across all animals and epochs. Similarly, the cross-correlation between gamma and HFO time vectors was calculated by using the gamma times as the reference vector. Thus, positive and negative lag values indicate that the HFOs tended to occur before and after gamma events, respectively.

Event aligned multi-unit activity

To characterize population activity aligned to LFP events, spike trains of each neuron were binned into 5 ms time windows (Figures 2A and 4F). Multi-unit activity was aligned to PFC ripple/HFO and gamma events and was normalized by the mean population firing rate during either NREM or REM sleep, depending on the events assessed. Subsequently, the power spectral density of the ripple/HFO aligned multi-unit activity was assessed (frequency limits, 2-12 Hz; MATLAB, *pwelch*).

Control for periods of high theta power

To determine whether theta-modulated population activity in PFC can be largely explained by periods of high theta power, instead of association with HFO events, we extracted surrogate timestamps to align PFC activity to (Figures S5K-N). Briefly, for each epoch, the preferred theta phase bin of HFO events was calculated from the PFC tetrode with the highest average theta power and used to randomly select surrogate times to align PFC multiunit activity to. Each preferred phase bin at least 250 ms away from a detected HFO was considered a candidate event. Then, times were randomly chosen, and the number of events selected matched the number of HFO events in that epoch. Theta power at each surrogate time point as well as HFO event was extracted and z-scored to control for any inter-animal variability in theta power. Lastly, the event aligned multiunit activity was split into quartiles based on theta power and compared.

Theta inter-peak intervals during bouts of high and low theta power

Since previous studies have segregated putative tonic and phasic substages of REM sleep based on CA1 theta frequency,[15] we calculated the inter-peak intervals of the theta oscillation to determine whether bouts of low and high theta power may correspond to putative tonic and phasic substages, respectively (Figure S3B). We bandpass filtered and averaged the LFPs from candidate CA1 tetrodes between 5-12 Hz, and the peaks were extracted by detecting positive-to-negative zero crossings of the derivative of the filtered, averaged signal. Lastly, the inter-peak intervals were calculated within low and high theta power periods for each epoch and compared. Note that we defined low and high theta periods based on PFC electrodes, whereas we calculated inter-peak intervals based on CA1 electrodes.

Cross-frequency phase-amplitude coupling

Phase-amplitude coupling was assessed for a range of frequency combinations using a previously established approach.[104] Since the rate of REM HFOs was highest during bouts of high theta power, we focused on these periods for assessing phase-amplitude coupling. For each epoch, the tetrode with the highest HFO power was chosen, and an averaged comodulogram was generated across all animals and epochs for the phase and amplitude frequency ranges from 2-12 Hz and 40-250 Hz, respectively.

Comodulogram: Briefly, the phases were extracted from the Hilbert transform of the raw LFP of the candidate electrode and binned into 18 bins (intervals of 20°), and the envelope power of the amplitude modulated frequency band was calculated by taking the absolute value of the Hilbert transform. Then, the amplitude of each frequency from 40-250 Hz was calculated in each phase bin from 2-12 Hz and visualized (Figure 3B).

Modulation index: To quantify the depth of amplitude modulation by the phase frequencies, gamma (40-100 Hz) and HFO (150-250 Hz) signals were separately processed, and the mean gamma or HFO amplitude in each phase bin was calculated. The resulting values were used to calculate the modulation index,[104] which specifies the strength of phase modulation. Additionally, the phase bin with the maximum amplitude was reported as the preferred phase. For comparison, the phase and amplitude vectors were circularly shifted independently, and the modulation index was calculated.

Theta nesting

To further investigate the coupling of theta, gamma, and HFOs, in PFC during REM sleep, we examined theta nesting[105,106] in two different frequency bands (40-100 Hz for gamma and 150-250 Hz for HFO) relative to the theta oscillation (Figures 2C and S4E,F). Since we are evaluating the gamma and HFO coupling specifically during these transient HFO events, we restricted our analysis to high theta periods since the rate of REM HFOs was highest during these REM bouts (Figure S3D). For each PFC electrode, the theta phase bin for which gamma power was maximal was identified. Then, each instance of this phase bin during high theta periods in REM sleep was detected and the index of the highest gamma power within each preferred phase bin was identified. Only electrodes where there were at least 20 instances of the preferred phase were included. Lastly, the averaged waveform was calculated by averaging the unfiltered LFP centered on every instance of maximal gamma power in the preferred bin. The above procedure was performed separately for HFO band activity. For comparison between the frequency of averaged gamma and HFO waveforms and the preferred phase of theta coupling, electrodes that exhibited at least 5 local maxima within a 100 ms window surrounding the preferred phase were analyzed.

To further validate coupling of gamma and HFO to theta, surrogate waveforms were generated by randomly selecting a different phase bin for each theta cycle for alignment of gamma or HFO power. Then, peak-to-trough amplitudes were calculated from the average waveform within the 100 ms window centered on peak power, averaged, and compared between the preferred phase bin aligned data and the random phase bin surrogate.

Phase-locking

Phase-locking during active behavior on the W-Track and during REM sleep was quantified using previously developed methods.[107] The CA1 or PFC tetrode with the greatest ripple/HFO power was filtered in the theta (6-12 Hz), gamma (40-100 Hz), or ripple/HFO (150-250 Hz) range and was used to extract phase information. For HFO and gamma phase locking of PFC cells, each spike that occurred across all extracted events were assigned a phase, and the distributions of the peak phases of all cells were compared between gamma and HFO. During run sessions (for 'REM theta phase shifting' analysis below, Figures S9H,I), spikes were restricted to CA1 theta periods where the animals' speed was >5 cm/s and were assigned a phase between 0-360°. Only neurons with at least 10 spikes during theta periods were included in this analysis. The Rayleigh test was used to determine whether the phase distribution of each cell deviated from circular uniformity ($p < 0.05$

criterion). Additionally, for phase locking to gamma and HFOs, the preferred phases of each cell was calculated separately for gamma or HFOs. Thus, a cell could be significantly phase locked to both gamma and HFOs. To test for phase preference differences, the distributions were compared using a nonparametric Watson's U^2 test. Subsequently, for each theta-modulated cell, phase locking strength to the theta oscillation was measured using pairwise phase consistency (PPC).[108] PPC was calculated by taking the dot product of the angular difference between each pair of phase values then averaging. Similar procedures were performed to determine the HFO and gamma phase preference of PFC cells.

Additionally, PPC was used to assess the strength of theta phase locking of HFO/ripple events in REM or NREM sleep. Only epochs with at least 20 events of each type were included for analysis.

Theta coherence

Theta coherence between pairs of CA1 and PFC tetrodes was calculated during REM sleep periods centered on REM HFOs, and each frequency was normalized by the mean and SD of the baseline coherogram computed across the entire epoch (Figures 3E,I). Coherograms were averaged over CA1-PFC tetrode pairs. For quantification and comparison, theta coherence was measured as the peak coherence between 6-12 Hz in a ±1 s window around HFO events. For visualization of coherograms, the averaged coherograms across all animals and epochs were smoothed with a 2D Gaussian kernel ($\sigma = 4$). All coherence-based analyses were conducted using the Chronux toolbox.[102] Only epochs with at least 20 events were included for quantification of peak theta coherence.

Phase slope index

Since we observed elevated theta coherence between CA1 and PFC during chained events, we assessed the directionality of information flow at different frequency bands (0-50 Hz) centered on these events (±1 s) using the phase slope index (PSI, Figure 3J),[109] which was calculated with the FieldTrip analysis toolbox.[110] In practice, PSI is used to assess the consistency of phase lag relationships between two signals across different frequency bands and is a measure that is weighted by oscillatory coherence. We opted to use PSI to estimate the directional flow of information instead of other methods, such as Granger causality, since it has been demonstrated that PSI is less prone to false positives.[109] Briefly, for each epoch, the PSI was calculated and averaged across each candidate CA1-PFC tetrode pair. Here, positive PSI values indicate that PFC theta leads CA1, while negative values indicate that CA1 leads PFC. Then the distribution of mean PSI values within 6-12 Hz was tested against 0 with a t-test. Only epochs with at least 5 chained events were included for analysis.

Ripple/HFO aligned modulation

Single unit ripple/HFO modulation in CA1 or PFC was calculated as previously described (Figures 4A,D),[28,111] This analysis was restricted to neurons that fired >50 spikes cumulatively across all peri-event windows (±2 s). For each candidate neuron, an averaged event-triggered (NREM or REM event) time histogram (event-PSTH) was calculated. For comparison, 1000 shuffled event-PSTHs were generated by circularly shifting the spikes around each ripple/HFO event by a random amount. To determine whether a neuron was significantly modulated, the squared difference between the real event-PSTH and the shuffled data in the -200 to +200 ms window surrounding event onset was calculated. If this real value exceeded 95% of the shuffled values, the neuron was categorized as significantly modulated. The modulation index for each cell was given by calculating the average difference between the activity in the response window and a background window -600 to -200 ms from event onset. Furthermore, excited (EXC) and inhibited (INH) neurons were separated based on whether the modulation in the event response window was positive (EXC) or negative (INH). Modulation timing distributions for EXC PFC neurons during NREM and REM PFC events were compared by binning (2 ms bins) the peak responses within the modulation window.

Event type prediction

High-frequency event type (NREM or REM) in PFC was predicted by fitting a linear model (MATLAB, *fitclinear*, Figure 4C) to PFC spike count data. Since the NREM events largely outnumbered the REM events, the event counts were equalized prior to training by randomly excluding a subset of NREM events. The binary decoders were built using 10-fold cross validation, and prediction accuracy was assessed by comparing performance against models constructed with randomly permuted spike matrices (n = 1000). To account for the excluded events, this entire process was repeated 10 times for each animal and epoch.

Ripple and HFO cofiring

To quantify ripple/HFO cofiring during events, a pairwise cofiring z-score was calculated as previously described (Figures 4E and 7B,C).[48] Briefly, this cofiring measure estimates how likely two cells will fire together during events and is normalized by the incidence of spiking independent of the other cell:

$$Z_{\text{coactivity}_{a,b}} = \frac{n_{ab} - \frac{n_a n_b}{N}}{\sqrt{n_a n_b (N-n_a)(N-n_b)/(N^2(N-1))}}$$

where N is the number of events, n_a and n_b are the number of events where cell a and cell b were active, respectively, and n_{ab} is the number of events where both cells were active. Here, cofiring assesses coincident activity between neuron pairs within the start and end times of events, and thus, no explicit temporal threshold was implemented. The same procedure was used to calculate cofiring between pairs in the model simulations.

Detection of population suppression

To validate the suppression of PFC multiunit activity surrounding REM PFC HFOs, periods of decreased PFC activity were separately extracted, and the probability of REM HFOs surrounding these events was calculated (Figures 4H and S6B,C). First, multiunit activity was binned (5 ms bins), normalized by the average activity during REM sleep, and smoothed with a Gaussian kernel (σ = 3). The population activity was then z-scored, and periods that fell below 0 for 300-500 ms were extracted as population suppression events. Lastly, the probability of HFO occurrence surrounding these events was calculated in 100 ms bins. To obtain the 99 percent confidence intervals, suppression events were extracted from shuffled multi-unit data. Briefly, each cells' spike count was circularly shifted independently, and events were detected. A total of 1000 shuffles were performed, and the probability of HFO occurrence surrounding these events was calculated for each shuffle.

Relationship between inter-event-interval (IEI) and content of adjacent HFOs

To assess whether there was a relationship between IEI and population spike content between HFO events, the spiking activity of PFC neurons during HFOs was represented as ones and zeros for either active or inactive during all events (Figures 5B and S7A).

The Pearson correlation between population activity vectors of two adjacent HFOs was calculated, and the IEI was given by calculating the temporal difference between the centers of the HFO events. Then, the relationship between spike content and IEI was assessed using the Pearson correlation coefficient. To validate this relationship, we employed two other methods for quantifying similarity of activity across two events, the Jaccard index and cosine similarity. The Jaccard index, or the Jaccard similarity coefficient, was used to quantify the similarity between two sets. It is defined as the ratio of the size of the intersection of the two sets to the size of their union. The Jaccard index (J) is expressed as

$$J(A,B) = \frac{|A \cap B|}{|A \cup B|}$$

where A and B represent the two sets being compared (spike activity for HFO A vs HFO B), |A∩B| is the number of elements in the intersection of the sets, and |A∪B| is the number of elements in the union of the sets. The resulting value ranges from 0 to 1. Similarly, cosine similarity, which quantifies the cosine of the angle between two vectors, was used to measure the similarity between two spike vectors. Cosine similarity is given by

$$CS = \frac{A \cdot B}{\|A\|\|B\|}$$

where A and B are the two vectors being compared, $A \cdot B$ is the dot product, and $\| A \|$ and $\| B \|$ represent the magnitudes of the vectors. The values range from -1 to 1 where 1 indicates identical vectors and -1 indicates that the vectors have an angular difference of 180 degrees. Actual spike counts were used for cosine similarity calculation.

Rank-order correlation

To evaluate the consistency with which populations of neurons in PFC fired in sequence during chained events, we calculated the rank-order correlation between each chain and its template as previously described (Figures 5C and S7B).[112,113] The population activity during each HFO in a chained event was concatenated (inter-event activity excluded), and for each concatenated event with ≥5 cells active, the spiking activity was reduced to each unit's first spike time, chronologically ordered, and normalized from 0 to 1. Then, a cross-validated template-based method was used to calculate sequence similarity between each event and its template. For each event, a template was created by averaging the normalized rank of each cell across all events excluding the event in question. The rank correlation was reported as the mean Pearson correlation coefficient between the event and template across all events. For comparison, a null distribution was generated by jittering spike times (1000 jitters) and performing the rank-order analysis above. For the pseudo-chain control, each HFO chain was time-shifted ±5 seconds such that each HFO within the chain was shifted the same value (1000 time shifts), thus preserving the inter-event-intervals (i.e. The entire chain was shifted coherently). Additionally, the entire shifted chain must have stayed within a REM sleep bout. The above rank-order procedure was performed, and the real correlation was compared to the pseudo-chain null distribution.

Assembly detection

To detect cell assemblies in PFC populations, a previously described method was used (Figure 6).[50,51] Significant coactivity patterns in PFC were detected using a method based on principal and independent component analyses. For each W-Track epoch, the spike trains of each neuron were binned into 20 ms time windows and Z-scored to eliminate any biases due to differences in firing rates. Principal component analysis was then applied to the Z-scored spike matrix (Z). The resulting eigenvalue decomposition of the correlation matrix (C) was given by:

$$\sum_{i=1}^{n} \lambda_i p_i p_i^T = C$$

Where p_i is the i^{th} principal component of C and λ_i is the corresponding eigenvalue. Note that $C = \frac{1}{n} Z Z^T$ is the correlation matrix of Z. To determine the number of significant coactivity patterns in the data, the Marcenko-Pastur law was used to calculate a threshold eigenvalue λ_{max}, which was given by $\lambda_{\max} = (1 + \sqrt{n/B})^2$ where n is the number of recorded units and B is the total number of bins. Note that an eigenvalue exceeding λ_{max} indicates that the corresponding cell assembly explains more correlation than expected if the activity of neurons was independent of each other. The number of eigenvalues above λ_{max}, N_A, represents the number of significant patterns found in the data. These principal components were then projected back onto the original z-scored spike data:

$$Z_{\mathrm{PROJ}} = P_{\mathrm{SIGN}}^T Z$$

where P_{SIGN} is the nXN_A matrix with N_A columns. Independent component analysis (ICA, RobustICA)[114] was then used to identify patterns that were maximally independent from

each other. ICA was applied to the matrix Z_{PROJ} to find an $N_A X N_A$ unmixing matrix, W, which was used to obtain the weights of each cell in each assembly.

$$V = P_{\mathrm{SIGN}}\, W$$

Since the sign of the output of ICA is arbitrary, the signs of the weight vector were set such that the highest absolute weight was set to positive.

Assembly reactivation strength

To assess the reactivation of these detected assemblies during sleep sessions (Figure 6), the expression strength of each pattern over time was given by:

$$R_k(t) = z(t)^T P_k z(t)$$

$R_k(t)$ is the reactivation strength of assembly k at time t, $z(t)$ is the z-scored firing rate vector for all neurons at time t, and P_k is the projection matrix for assembly k, constructed by taking the outer product of its weight vector v_k. Additionally, the diagonal of the projection matrix was set to zero to reduce the influence of highly active neurons, and the reactivation strength was calculated such that only the positive weight cells were assessed. Thus, only patterns of coactivity are detected as periods of high reactivation strength.

Assembly sequence detection surrounding HFOs

The consistency of assembly reactivation surrounding REM HFOs was assessed by implementing a cross-validation process similar to procedures used for place cell sequences (Figures 6A-D).[115,116] We employed a split-event procedure where HFO events were randomly split into two halves. The average reactivation strength for each assembly was then calculated across all HFOs across both halves separately. This was performed across all animals and epochs. The assemblies aligned to the first half were subsequently sorted by peak reactivation strength within a ±500 ms window around HFO times, and the assemblies aligned to the second half were sorted using the same sort indices such that each row in the two matrices correspond to the same assembly. The consistency of temporal assembly reactivation was quantified as the Pearson correlation between the peak reactivation strengths of the first and second halves. This procedure was conducted 1000 times using different subsets of HFOs for the first and second halves to obtain a distribution or correlation coefficients. For comparison, a distribution of shuffled data was obtained by circularly shuffling assembly reactivation strength prior to HFO alignment, and the above procedure was performed. This procedure was also performed for gamma and NREM PFC ripples for comparison.

Furthermore, the slope and peak differences were calculated as additional metrics of sequence and temporal reactivation consistency between the two halves of data, respectively. For the slope difference metric, the slope of the best fit line between assembly ID and peak reactivation index was taken for the two halves of data and compared. A smaller slope difference compared to shuffled data indicates that assembly reactivation is structured in a more similar manner across the two halves of the real data. For peak reactivation difference, the temporal displacement of the peak reactivation index between the two halves of data was calculated and compared to shuffle. A high probability of small peak differences indicates that the timing of peak reactivation of assemblies relative to HFO chain onset is similar across the two halves of data. Shuffling of assembly strength was carried out as above.

Reactivation strength across epochs

For comparison of pre and post reactivation strengths, the same run-derived templates were projected onto the preceding and following sleep epochs (neurons were matched across pre, run, and post), and the pre and post strengths during periods of sleep were compared. Thus, each assembly was matched across pre and post. Furthermore, to assess reactivation strength changes over learning, the preceding run epoch's template (following run epoch for sleep epoch #1, since no preceding run) was projected onto the following sleep epoch, and the average reactivation

strength was calculated and compared for early (epochs 1-3) and late (epochs 4-9) sleep epochs during periods of sleep. Epochs prior to a grouped average of 75% correct performance on the W-Track task (Figure S1B) were defined as early.

2D#assembly maps

To generate assembly rate maps, a procedure similar to computing place fields was used.[51] For each assembly, all assembly activation timestamps during W-Track behavioral sessions that exceeded 5 at positional bins where occupancy was >20 ms were used for map generation. 2-D assembly maps were calculated by dividing the binned activation count by the occupancy in each 1 cm^2 positional bin and smoothed with a Gaussian kernel (σ = 2).

Spatial information of assembly fields

Spatial information (bits/event activation) was computed using the following formula:

$$I_{\text{spike}} = \sum_{i=1}^{N} p_i \frac{\lambda_i}{\lambda} \log_2 \frac{\lambda_i}{\lambda}$$

where p_i is the occupancy probability of bin *i*, λ_i is the mean assembly activation in bin *i*, and λ is the occupancy-weighted mean activation. Spatial information is reported in bits per activation event. The significance of each assembly's spatial information was assessed by a per-assembly circular-shift procedure. The full assembly activation time series was circularly shifted by a random offset >20 s, the activation shuffled 2D assembly field was computed, and the spatial information was calculated. This procedure was repeated 1000 times per assembly to generate a null distribution. The observed spatial information was expressed as a z-score relative to the assembly-specific shuffle distribution, and a one-tailed permutation p-value was computed as $p = (1 + \#[I_{\text{shuffled}} \geq I_{\text{Observed}}]) / (1 + 1000)$. Assemblies with $p < 0.05$ ($z > 1.65$) were classified as showing significant spatial structure (Figures 6H,I).

2-D rate maps

2-D spatial rate maps during active behavior on the W-Track were calculated during periods of high mobility (>5 cm/s; all SWR times excluded) at positional bins where occupancy was >20 ms. Then, the 2-D spatial maps were calculated by dividing the binned spike count by the occupancy in each 1 cm^2 positional bin and smoothed with a Gaussian kernel (σ = 2).

Calculation of a single cofiring metric and separation into populations of high and low cofiring neurons

Since we wanted to relate the above cofiring metric to other measures, we needed to obtain a single value cofiring metric for each neuron. To do this, we averaged the cofiring values across all pairings for a neuron (e.g. 1 CA1 neuron paired with all PFC neurons) and reported it as the cell's cofiring. Furthermore, since we observed a bimodal distribution of CA1-PFC cofiring values in REM sleep, we split the population based on whether the average (across all cell-cell combinations) cofiring value or correlation coefficient of a cell was above or below 0 (High cofiring > 0; low cofiring < 0). Also, since the NREM ripple cofiring distribution was unimodal, we additionally split the populations using the mean of the average cofiring or correlation coefficient distributions (High cofiring > mean; low cofiring < mean).

Change in firing rate across sleep

To assess differences in firing rate changes in CA1 and PFC over the course of sleep, populations were separated into low or high cross-regional cofiring units based on the z-scored cofiring metric above as well as the Pearson correlation between spike count vectors across all REM HFO chains or independent NREM ripples. Here, we are only including independent ripples for NREM analysis since we have shown that CA1-PFC cofiring is elevated when PFC ripples are coordinated with CA1 SWRs.[28] Exclusion of coordinated ripple events allows us to assess the influence of strictly PFC ripples in NREM on firing rate changes. For each cell, the change in the firing rate from the first

bout to the last bout of NREM sleep was calculated and compared for low and high coactive cells (Figures 7F and S9B-E). Only epochs that had first and last NREM bouts exceeding 30 s in length were included for analysis.

REM theta phase shifting

To assess shifts in the preferred CA1 theta phase of CA1 neurons between run sessions and REM sleep, the above procedure was performed, and only neurons that exhibited significant phase-locking during both run and REM sleep were included for analysis. Neurons that had a phase shift of >90° from the preceding run session to the subsequent REM sleep epoch were categorized as REM-shifting.

Single unit PFC HFO bursting

To determine HFO burst probability for each cell, the number of HFOs where burst spikes were detected (at least 2 spikes <6 ms apart[117]) was divided by the total number of events.

Network model

Computational simulations were done using a simplified model of a small cortical network. The model contains 1,600 excitatory pyramidal and 400 inhibitory interneuron modified Hodgkin-Huxley neurons laid out in a topographical grid. Connections are random, with probability of connection decaying with spatial distance on the grid. Connection probabilities were drawn from known layer 2/3 cortical connectivity rates of pyramidal cells and somatostatin (SST) interneurons. Synaptic weights were assigned randomly using log-normal distributions. Inhibitory cells in the model are regular-spiking with a voltage equation identical to pyramidal cells.

The voltage equation for the neuron model is:

$$C_M \frac{dV}{dt} = -m_\infty^3 h g_{Na} (V - E_{Na}) - n g_{Kdr} (V - E_K) - s g_{Ks} (V - E_K) - g_{\text{leak}} (V - E_{\text{leak}}) + I_{\text{base}} + I_{\text{noise}} - I_{\text{syn}} + I_{\text{stim}}$$

Where g_X are the maximal conductances, and each of the activation variables h, n, and s have a differential equation of the form:

$$\frac{dy}{dt} = \frac{1}{\tau(V)} (y_\infty - y)$$

Where y_∞ are the steady state values for each of the gating variables, each a function of voltage.[62]

For every presynaptic spike, the synaptic conductance between neurons is calculated as the difference between two decaying exponentials. Model pyramidal neurons and interneurons both elicit fast, large-amplitude synaptic inputs in connected postsynaptic cells modeled after glutamate and GABA-A receptors, respectively. Interneurons also elicit a slow, low-amplitude GABA-B-like conductance in connected neurons. In addition, a white noise current I_{noise} is applied to each neuron separately to introduce random variation.

Both pyramidal neurons and interneurons in the model feature a slow potassium conductance, g_{Ks}, that is active at neuronal resting potential and modeled after the slow potassium M-current.[64,118] The biological effect of acetylcholine (ACh) on the M-current through the M1 muscarinic ACh receptor is recreated in the model by raising or lowering g_{Ks} to simulate decreases or increases, respectively, in ACh concentration. As in biological neurons, lowering g_{Ks} shifts model neurons from Type 2 excitability (resonators) to Type 1 excitability (integrators), raising their excitability but lowering their tendency to synchronize spiking when connected.[66] The result for a connected network of neurons is, in general, lower sensitivity to inputs and an increased propensity for synchronous spiking in simulations modeling a low ACh condition, but increased sensitivity and less correlated spiking in simulations modeling a high ACh condition, as is

observed experimentally.[119,120] Model simulations of NREM sleep use g_{Ks} = 1.5 for all neurons, while simulations of REM sleep use g_{Ks} = 0. I_{base} is used to slightly hyperpolarize interneurons during REM to maintain balanced excitation and inhibition.

Each external stimulus input to the network I_{stim} is modeled as a depolarizing current injection to a random 30% of neurons. For the NREM brief stimuli, a gaussian profile that peaks at the midpoint of the stimulus was used, with duration drawn from a normal distribution with a mean of 70 ms and standard deviation 20 ms. Stimulus peak amplitude was calculated similarly, with a mean of 0.75 and standard deviation 0.3. For REM theta stimuli, the input was a sinusoid with frequency drawn from normal distribution with mean 8.5 Hz and 3 standard deviations within 7-10 Hz range. Stimulus amplitude was convolved with a gaussian profile peaking at the midpoint of the stimulus duration. Negative amplitude phases of the sinusoid were set to zero. For REM stimulus duration, mean 3000 ms and standard deviation 250 ms duration were used. Peak amplitude parameters were identical to NREM. No negative durations or amplitudes were allowed and set to zero if drawn from the distribution. Triggering of all stimulus events was determined by a Bernoulli process with a success rate of on average 1 Hz, with overlapping stimuli not permitted. For theta stimuli, a minimum delay of 1000 ms was enforced after the end of each stimulus to allow the network time to return to baseline activity.

Experimental model and subject details

All experimental procedures were approved by the Institutional Animal Care and Use Committee at Brandeis University and conformed to US National Institutes of Health guidelines. Ten adult male Long-Evans rats (450-600 g, 4-6 months; *RRID:RGD_2308852*) were used in this study. Animals were individually housed and kept on a 12-hr regular light/dark cycle.

Quantification and statistical analysis

All statistical analyses were performed with MATLAB (MathWorks, Natick, MA; R2022a) functions or custom scripts. No specific analysis was performed to predetermine sample size, but the number used in this study is similar to or larger than typically used. Nonparametric, two-tailed statistical tests (Wilcoxon rank-sum (WRS) and signed-rank (WSR), for unpaired and paired data, respectively) were used throughout the paper unless noted. $P < 0.05$ was considered the cutoff for statistical significance. Boxplots show the median (center line), interquartile range (box), and the furthest points not considered outliers (whiskers). Unless otherwise noted, values and errors in the text denote means ± SEM. p-values in the text are reported as follows: $p > 0.05$, *$p < 0.05$, **$p < 0.01$, ***$p < 0.001$.

Data availability

Data underlying these results are available in the NWB (Neurodata Without Borders) format on DANDI Archive (ID#000978). Code to replicate these results will be available on our lab GitHub (*http://github.com/JadhavLab*).

Supplementary figures and table

Animal	Epoch	NREM	REM	% REM	Animal	Epoch	NREM	REM	% REM
	1	590	0	0.00%		1	715	121	14.47%
	2	574	0	0.00%		2	548	0	0.00%
	3	389	11	2.75%		3	1064	13	1.21%
	4	362	0	0.00%		4	1063	137	11.42%
JS17	5	629	0	0.00%	**BG1**	5	623	72	10.36%
	6	404	0	0.00%		6	1778	275	13.40%
	7	1197	10	0.83%		7	1636	263	13.85%
	8	1139	0	0.00%		8	1284	270	17.37%
	9	916	74	7.47%		9	693	27	3.75%
	Total	**6200**	**95**	**1.51%**		Total	**9404**	**1178**	**11.13%**
	1	414	11	2.59%		1	595	31	4.95%
	2	499	15	2.92%		2	49	0	0.00%
	3	836	36	4.13%		3	186	38	16.96%
	4	1124	0	0.00%		4	678	0	0.00%
JS13	5	1040	139	11.79%	**JS14**	5	605	0	0.00%
	6	1926	120	5.87%		6	901	167	15.64%
	7	1322	118	8.19%		7	661	86	11.51%
	8	1440	122	7.81%		8	594	126	17.50%
	9	1180	141	10.67%		9	814	95	10.45%
	Total	**9781**	**702**	**6.70%**		Total	**5083**	**543**	**9.65%**
	1	8	0	0.00%		1	138	177	56.19%
	2	840	98	10.45%		2	750	158	17.40%
	3	497	275	35.62%		3	1066	124	10.42%
	4	1266	202	13.76%		4	863	128	12.92%
KL8	5	1571	113	6.71%	**JS21**	5	435	14	3.12%
	6	629	182	22.44%		6	649	0	0.00%
	7	1346	256	15.98%		7	818	23	2.73%
	8	1193	243	16.92%		8	859	13	1.49%
	9	568	41	6.73%		9	743	0	0.00%
	Total	**7918**	**1410**	**15.12%**		Total	**6321**	**637**	**9.15%**
	1	3	0	0.00%		1	54	0	0.00%
	2	76	12	13.64%		2	5	0	0.00%
	3	291	45	13.39%		3	133	0	0.00%
	4	145	0	0.00%		4	637	26	3.92%
JS34	5	238	15	5.93%	**JS12**	5	562	11	1.92%
	6	1513	274	15.33%		6	1319	114	7.96%
	7	453	69	13.22%		7	1178	83	6.58%
	8	535	75	12.30%		8	1333	190	12.48%
	9	1070	112	9.48%		9	720	0	0.00%
	Total	**4324**	**602**	**12.22%**		Total	**5941**	**424**	**6.66%**
	1	731	30	3.94%		1	25	0	0.00%
	2	435	0	0.00%		2	504	16	3.08%
	3	742	0	0.00%		3	885	34	3.70%
	4	865	0	0.00%		4	919	14	1.50%
JS15	5	1115	191	14.62%	**ZT2**	5	1658	240	12.64%
	6	1476	0	0.00%		6	1484	151	9.24%
	7	938	116	11.01%		7	1573	47	2.90%
	8	1195	136	10.22%		8	1804	239	11.70%
	9	990	224	18.45%		9	716	12	1.65%
	Total	**8487**	**697**	**7.59%**		Total	**9568**	**753**	**7.30%**

Table S1. Amount of NREM and REM sleep (in seconds) across all animals and epochs.

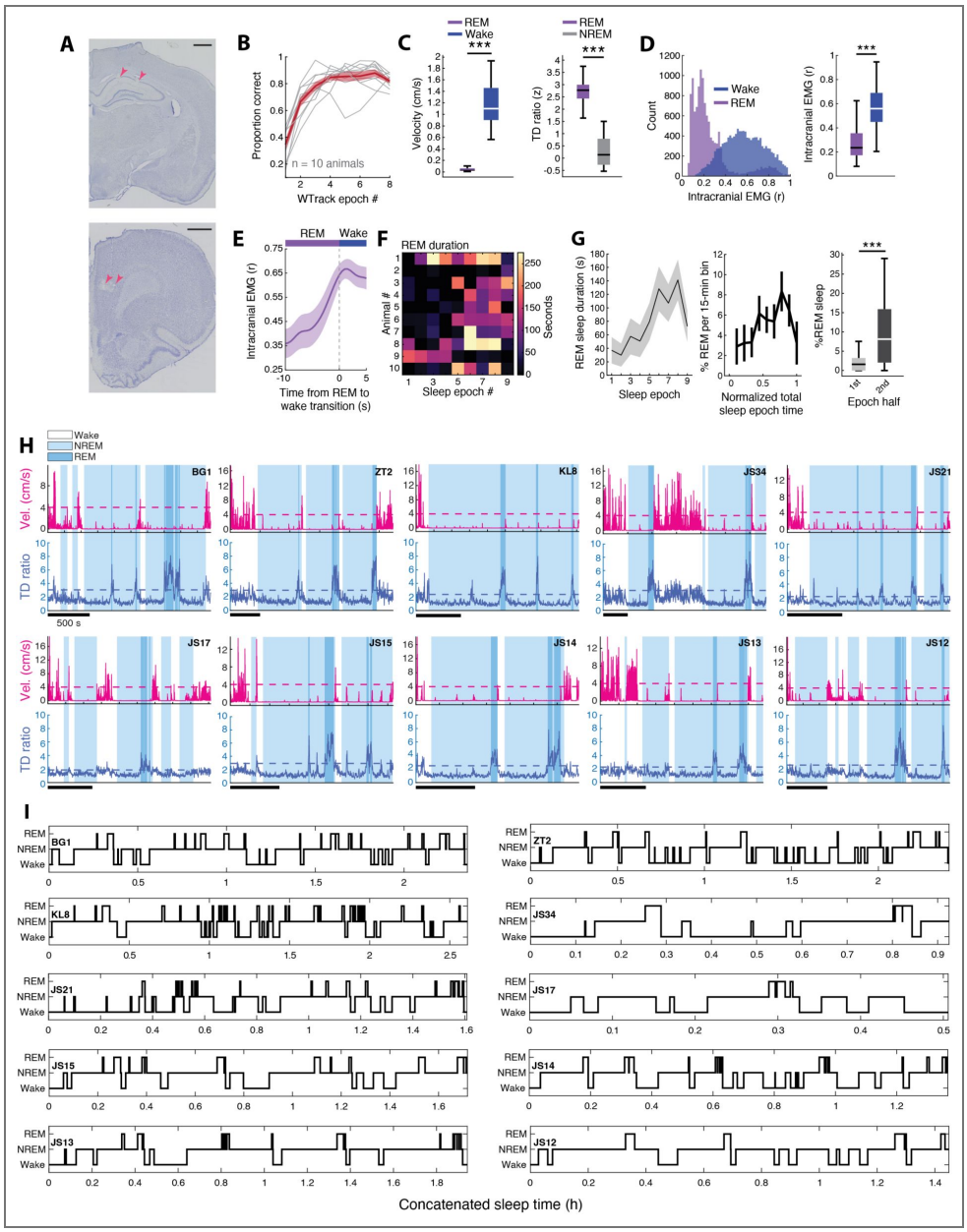

Figure S1. Characterization and validation of REM sleep (related to Figure 1).

(**A**) Histological verification of recording locations in dorsal CA1 (Top) and PFC (Bottom). Red arrows indicate electrolytic lesions, and scale bars represent 1 mm. (**B**) Performance of all 10 animals across 8 sessions on the W-Track task. Outbound and inbound trajectories were combined to calculated overall performance on the task. (**C**) (Left) Average velocity during wake and REM sleep (Wake = 1.16 ± 0.06 cm/s, REM = 0.05 ± 0.01 cm/s, *p = 5.39×10^{-7}, WSR). (Right) Theta-to-delta (TD) ratio in NREM and REM sleep (NREM = 0.30 ± 0.11, REM = 2.71 ± 0.10, ***p = 5.39×10^{-7}, WSR). (**D**) Distributions of intracranial EMG values for wake and REM sleep. All 500 ms binned Pearson correlation values are shown. (**E**) Comparison of the averaged intracranial EMG for bouts of wake and REM during all sleep epochs (Wake = 0.57 ± 0.01, REM = 0.32 ± 0.02, ***p = 5.26×10^{-37}, WRS) (**F**) Duration of REM sleep in each epoch (Total duration = 6089 s). Only epochs with at least 30 s of REM sleep were included for analysis. (**G**) (Left) Average REM sleep duration and (Middle) percentage of REM sleep out of total sleep epoch time (Wake, NREM, and REM) across all 9 sleep epochs. No animals had REM sleep in the first normalized bin, so that point isn't shown. (Right) Percentage of REM sleep during the first and second halves of the 36 sleep epochs included in analysis (First = 3.85 ± 0.93%, Second = 15.29 ± 0.94%, ***p = 1.93×10^{-6}, WRS). (**H**) Example sleep sessions for each animal showing each behavioral state detected using the sleep state algorithm that utilizes theta-to-delta ratio (TD ratio) and animal velocity (cm/s). Note that the plot for KL8 is the example shown in Figure 1B. (**I**) Hypnograms for animals showing sleep state across all concatenated sleep epochs that passed inclusion criteria (only sleep epochs are shown; behavior epochs are excluded).

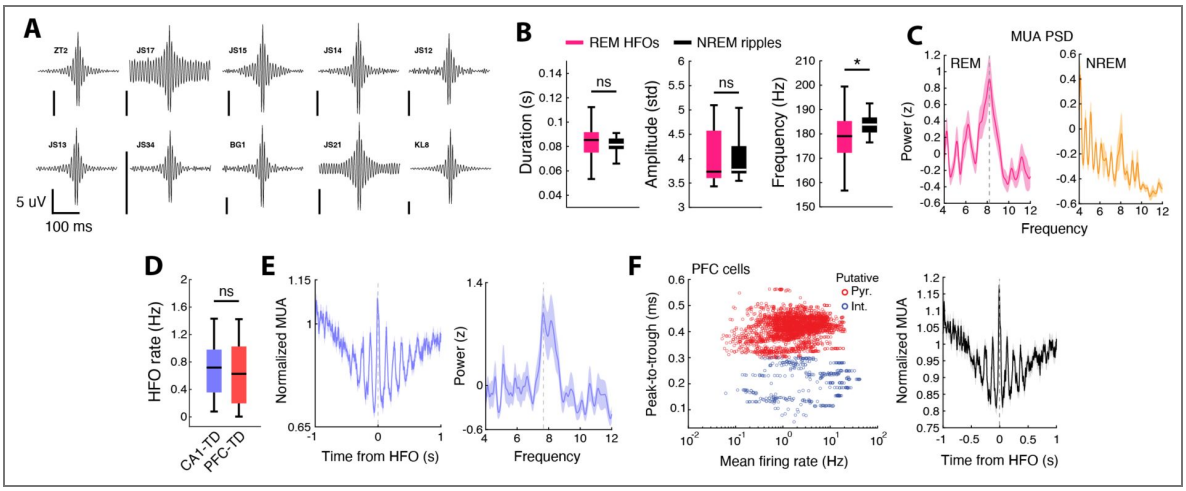

Figure S2. Characterization prefrontal REM sleep HFOs and event aligned multiunit activity (related to Figures 1 and 2).

(**A**) Average peak aligned amplitude plots across all detected REM HFO events for each animal. (**B**) Comparison of ripple/HFO duration, amplitude (standard deviations above the mean), and frequency for NREM and REM events (Duration: NREM = 0.111 ± 0.017 ms, REM = 0.126 ± 0.030 ms, p = 0.59; Amplitude: NREM = 4.13 ± 0.12, REM = 4.23 ± 0.20, p = 0.31; Frequency: NREM = 184.96 ± 1.68 Hz, REM = 179.02 ± 1.82 Hz, *p = 0.018, WRS). (**C**) Average power spectral density calculated from the REM and NREM event aligned multiunit activity in PFC. Note the peak around 8 Hz (theta frequency) for REM HFO aligned multiunit activity. (**D**) PFC HFO rates during REM sleep extracted from either CA1 or PFC TD ratio. HFO rates were similar during CA1 and PFC extracted REM sleep, validating the use of CA1-extracted REM sleep for further analysis. (**E**) PFC multiunit activity and average power spectral density aligned to REM HFO events extracted from the overlap of CA1 and PFC REM sleep. (**F**) (Left) Peak-to-trough of average spike waveforms and mean firing rate of PFC neurons. We separated populations based on peak-to-trough, since mean firing rate did not give us clear separation. Putative interneurons were identified as cells having a peak-to-trough <0.3 ms. (Right) REM HFO aligned PFC multiunit response when spikes from putative interneurons are excluded (compare to Figure 2A). Due to this similarity of the phasic PFC response when putative interneurons are omitted, we decided to pool PFC neurons for all further analyses.

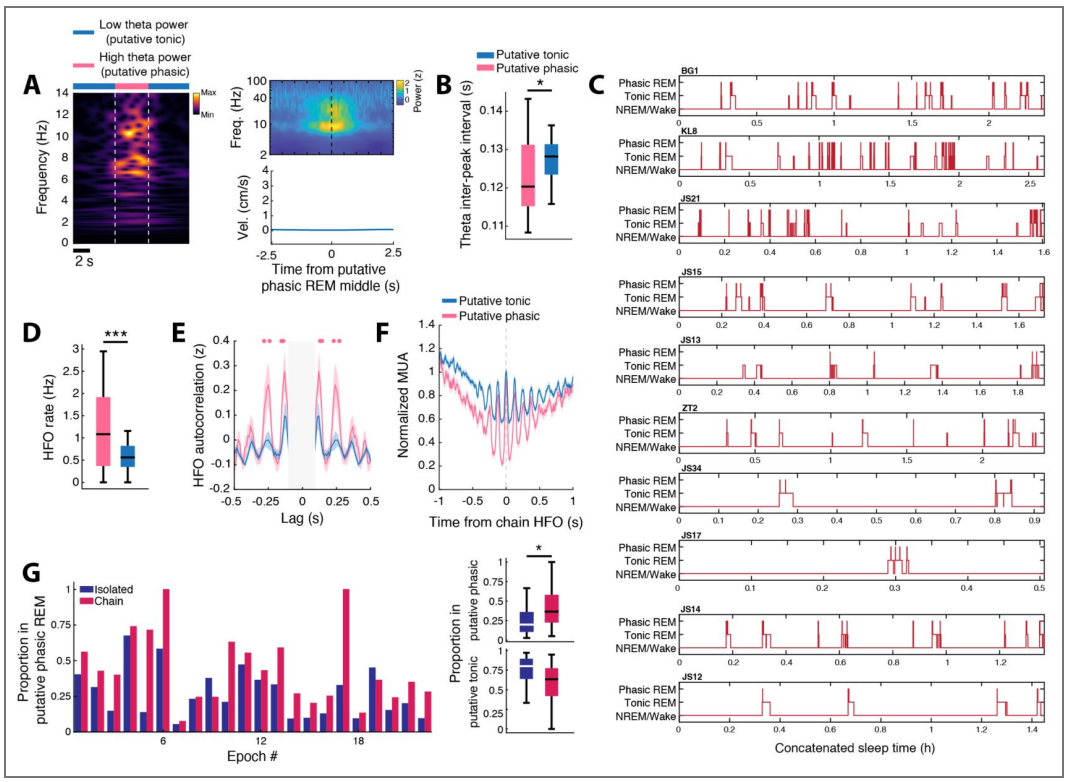

Figure S3. Putative tonic and phasic REM sleep (related to Figure 3).

(**A**) (Left) Example showing bouts of low and high theta power within a REM sleep bout. High theta periods were bouts within REM that exceeded 4 standard deviations above the electrode averaged theta power in REM sleep for at least 900 ms. (Right) Average spectrogram and speed surrounding putative phasic REM bouts. (**B**) The CA1 theta inter-peak intervals (IPI) during high PFC theta power periods during REM sleep were lower (corresponding to higher theta frequency) than during low power periods, indicating that these high and low theta power periods may correspond to putative phasic and tonic substages of REM sleep, respectively[15] (High theta IPI = 0.123 ± 0.002, Low theta IPI = 0.128 ± 8.3×10^{-4}, *p = 0.010, WRS). (**C**) REM sleep focused hypnograms for all animals illustrating sleep state concatenated across all epochs that were included for analysis (as in Figure S1I). Wake and NREM sleep are combined. (**D**) Rate of REM HFOs during bouts of high or low theta power (High = 1.19 ± 0.15 Hz, Low = 0.58 ± 0.05 Hz, ***p = 1.33×10^{-4}, WSR). (**E**) HFO autocorrelation during periods of high or low theta power. Dots indicate bins where high and low theta power HFO autocorrelations differ (p<0.05, WRS). (**F**) PFC multiunit activity aligned to chain HFOs in either putative tonic or phasic REM sleep. Similar patterns of PFC spiking modulation are elicited aligned to HFOs in both REM substates. (**G**) (Left) Proportion of isolated and chain HFOs that occurred in putative phasic REM sleep in all 22 sleep epochs that had at least 5 seconds of putative phasic REM sleep and (Right, top) a quantification of the difference between isolated and chain events (Isolated = 0.25 ± 0.04, Chain = 0.43 ± 0.06, *p = 0.018, WSR). (Right, bottom) Proportion of isolated and chain events in putative tonic REM shown as well.

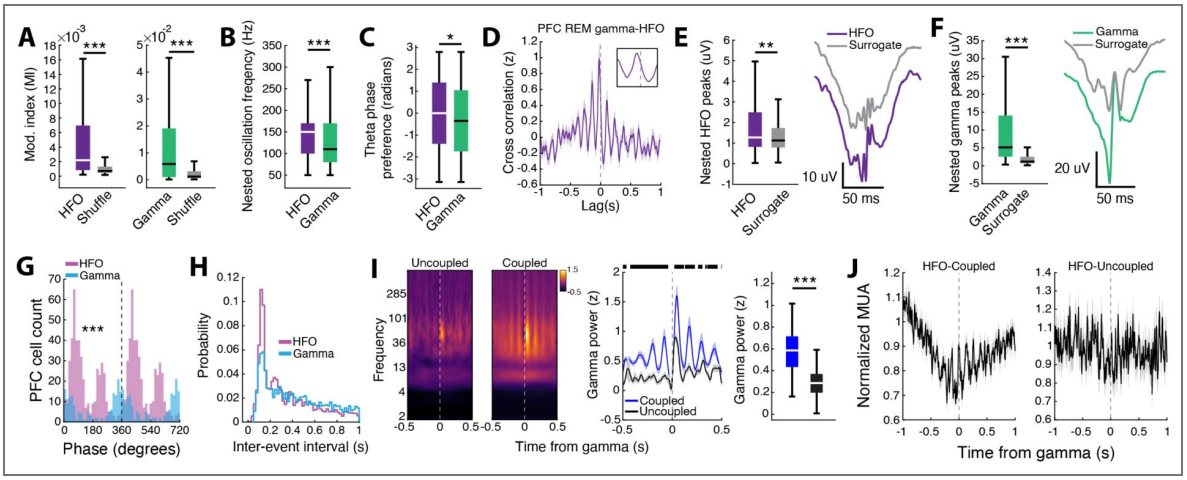

Figure S4. Coupling of gamma and HFOs with PFC theta oscillations (related to Figure 3).

(**A**) Modulation indices (MIs) for phase amplitude coupling (PAC) computed for HFO and gamma frequency oscillations compared to MIs calculated from circularly shifted theta phase and HFO/gamma amplitude vectors. Modulation was assessed for a phase frequency range from 2-12 Hz. The amplitude modulated frequencies were 150-250 Hz and 40-100 Hz for HFO and gamma, respectively (HFO = 0.005 ± 3.21×10^{-4}, shuffle = 0.001 ± 8.94×10^{-5}, ***p = 1.13×10^{-31}; Gamma = 0.011 ± 6.49×10^{-4}, shuffle = 0.002 ± 1.67×10^{-4}, ***p = 2.97×10^{-24}, WRS). (**B**) Frequency of the average theta nested oscillation either aligned to peak HFO or gamma power (See **Methods**). Note that aligning to peak HFO power at the preferred phase bin yields nested oscillations that are higher in frequency (HFO = 146.48 ± 2.82, Gamma = 128.96 ± 3.091, ***p = 2.85×10^{-7}, WRS). (**C**) Preferred theta phases of elevated HFO and gamma amplitude (HFO = -0.13 ± 0.08 radians, Gamma = -0.38 ± 0.08 radians, *p = 0.016, WRS). (**D**) Cross-correlation between PFC gamma and HFO events during REM sleep. The off-center peak at a negative lag (inset) indicates that gamma events tend to precede HFOs, corroborating the phase preference difference in (**F**). (**E**) Comparison of nested HFO peaks with a theta phase bin shuffled surrogate (See **Methods**; HFO = 4.09 ± 0.48 μV, Surrogate = 1.92 ± 0.19 μV, **p = 0.0058, WRS). (**F**) Same as in (**E**) but for gamma (Gamma = 11.33 ± 0.62 μV, Surrogate = 2.33 ± 0.20 μV, ***p = 9.46×10^{-94}, WRS). (**G**) Distribution of preferred phases for PFC cells that are significantly phase locked to either HFOs or gamma. Note the similarity in distribution to Figure 3D in the manuscript (HFO locked = 463 neurons, Gamma locked = 161 neurons, Dual locked = 110 neurons, U2 = 3.56, ***p = 6.37×10-31, Watson's U2 test) (**H**) Distributions of inter-event intervals for PFC gamma events and HFOs (***p = 5.09×10^{-30}, Kolmogorov-Smirnov test). (**I**) (Left) Gamma triggered spectrograms for events that were uncoupled or coupled to HFOs. (Middle) Comparison of gamma power (40-100 Hz power ±500 ms from event onset) for uncoupled and coupled events. Note the oscillating gamma power during coupled events. (Right) Quantification of average HFO power for coupled and uncoupled events (Coupled = 0.60 ± 0.04, Uncoupled = 0.34 ± 0.03, ***p = 1.03×10^{-7}, WRS). Coupled gamma events were defined as gamma periods that were within 500 ms of a HFO event. (**J**) (Left) Multiunit PFC activity aligned to gamma events that are coupled with or (Right) uncoupled from HFOs.

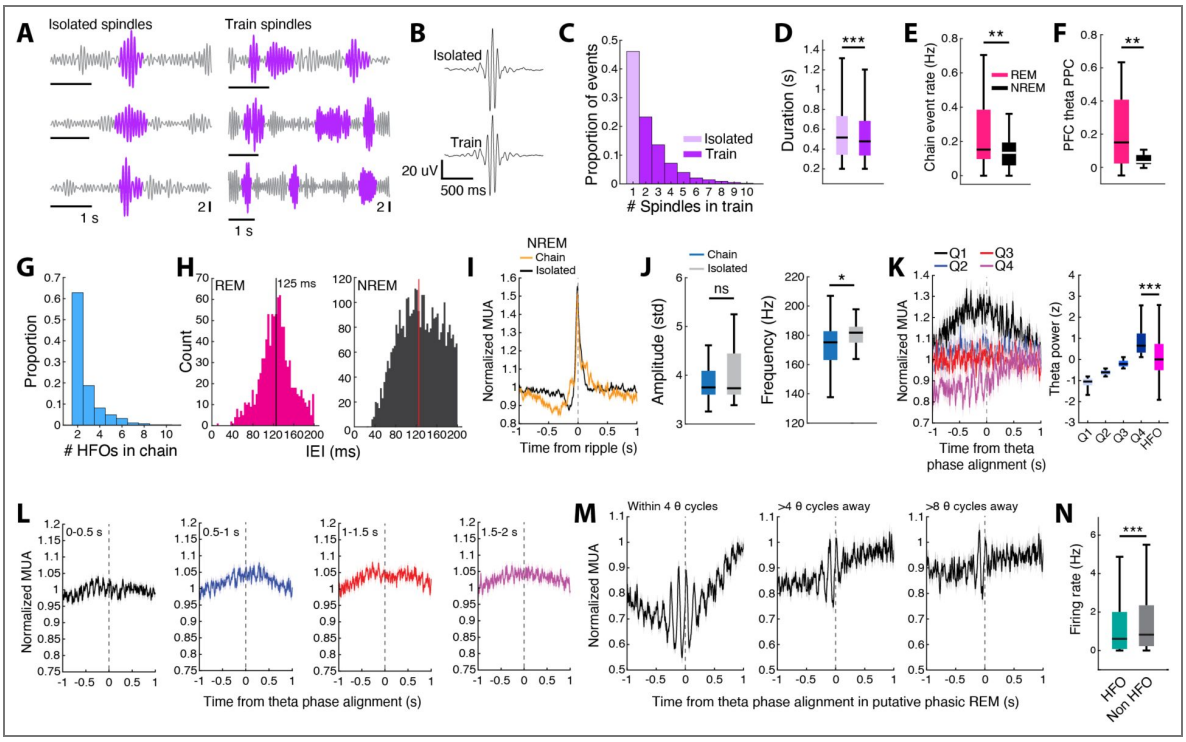

Figure S5. Chains of sleep oscillations in NREM (spindles) and REM (HFOs) sleep (related to Figures 3 and 4).

(**A**) Example isolated and train spindles, similar to previous reports.[45] (**B**) Averaged spindle peak aligned LFP for isolated and train spindles across all animals. (**C**) Histogram displaying the proportions of NREM spindle train events of specific lengths (Compare with Darevsky et al., 2024). (**D**) The durations of isolated and train spindles (Isolated = 0.579 ± 0.005 s, Train = 0.550 ± 0.003, ***p = 1.77×10^{-6}, WRS). (**E**) Rate of events designated as participating in a chain (<200 ms separation) during NREM and REM sleep (NREM = 0.15 ± 0.02 Hz, REM = 0.25 ± 0.04 Hz, **p = 0.0054, WSR). (**F**) PFC theta pairwise phase consistency (PPC) of HFO chains in REM vs NREM (REM = 0.22 ± 0.06, NREM = 0.06 ± 0.02, **p = 0.0097, WSR). (**G**) Histogram displaying the proportions of REM HFO chain events of specific lengths. (**H**) Histogram of all inter-event intervals (IEI) for HFO chains in (Left) REM or (Right) NREM sleep. Note the tight REM HFO IEI distribution centered around 125 ms, which corresponds to 8 Hz (theta frequency). Black and red vertical lines are displayed at 125 ms for both distributions. (**I**) PFC multiunit activity aligned to chained and isolated NREM ripple events. Note the absence of theta-modulated population activity during ripple chains in NREM sleep. (**J**) Comparison of HFO amplitude and frequency for chained and isolated PFC REM HFOs (Amplitude: Chain = 4.21 ± 0.26, Isolated = 4.17 ± 0.20, p = 0.995; Frequency: Chain = 172.54 ± 2.71 Hz, Isolated = 181.54 ± 1.51 Hz, *p = 0.018, WRS). (**K**) (Left) PFC multiunit activity aligned to the preferred theta phase of REM HFOs plotted according to theta power during surrogate events. (Right) Quantification of theta power in each quartile compared to the power during HFO events (Q1 = -1.10 ± 0.007, Q2 = -0.62 ± 0.004, Q3 = -0.20 ± 0.005, Q4 = 0.87 ± 0.024, HFO = 0.26 ± 0.018, ***p = 5.74×10^{-114}, WRS). (**L**) PFC multiunit activity aligned to preferred theta phase bins within the specified time window around HFOs. For example, for the figure on the left, theta phase bins must have been within 0-0.5 s from the beginning or end of HFO windows for inclusion. Note that this analysis sampled phase bins across both putative tonic and phasic REM sleep. (**M**) PFC multiunit activity aligned to preferred theta phase bins within the specified time window around HFOs. (**N**) PFC neuron firing rate comparison during chain HFOs and theta periods >4 theta cycles away from HFOs during putative bouts of phasic REM sleep. A ±250 ms window around events was used to calculate the average firing rate across events in each condition (HFO = 1.56 ± 0.10 Hz, non-HFO = 1.75 ± 0.11 Hz, ***p = 6.50×10^{-5}, WSR).

Figure S6. REM PFC HFOs are associated with decreases in PFC activity (related to Figure 4).

(**A**) PFC neurons that were negatively modulated (INH) during REM PFC HFO events (REM EXC modulation = 114). Although overall modulation in this subset of neurons surrounding PFC HFOs is suppressive, there are transient peaks in activity that occur approximately 125 ms apart (8 Hz theta frequency). (**B**) Extracted PFC population suppression events (see **Methods**) aligned by their troughs. (Left) All example suppression events in an example epoch. (Right) Averaged PFC multiunit activity aligned to these events. (**C**) The probability of NREM PFC ripples centered on population suppression events detected in NREM sleep. Unlike REM sleep, there is a decreased probability of NREM ripple occurrence surrounding suppression events, consistent with strong overall excitation during these events (Figure 2C). The slight peak to the right is likely reflective of the suppression in activity prior to the onset of NREM ripples (Figure 2C). The red dotted lines indicate the 99% confidence intervals based on suppression events extracted from shuffled multiunit activity.

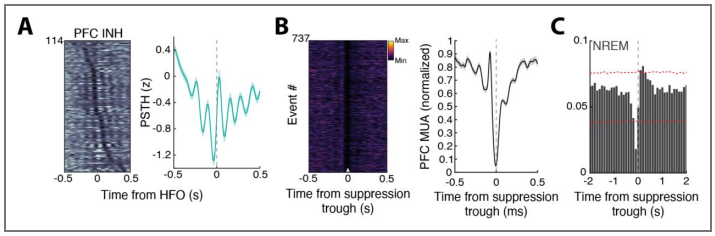

Figure S7. REM PFC HFOs are associated with sequential reactivation as compared to NREM PFC ripples (related to Figures 5 and 6).

(**A**) Relationship between IRI and (Top) Jaccard index and (Bottom) cosine similarity (Jaccard index, r = -0.094, ***p = 1.30×10^{-4}; Cosine similarity, r = -0.097, ***p = 7.16×10^{-5}, Pearson correlation). (**B**) Rank order correlation analysis on isolated REM PFC HFOs (Left) and pseudo-chain events (Right). (**C**) Cross-validation of the REM reactivation sequences surrounding gamma events (Data = 0.147 ± 0.003, Shuffle = -0.051 ± 0.004, ***p = 6.45×10^{-208}, WRS). (**D**) (Left) Same as in (**C**) but for isolated REM HFOs (Data = 0.050 ± 0.003, Shuffle = - 0.005 ± 0.004, ***p = 4.82×10^{-4}, WRS). (Right) Probability of assembly peak displacement between randomly chosen halves of the isolated REM HFO aligned data. Note the absence of peaks at small displacements as seen in Figure 6E. (**E**) Same as in (**C**) but for NREM ripple chains (Data = 0.084 ± 0.003, Shuffle = -0.019 ± 0.004, ***p = 1.37×10^{-75}, WRS). (**F**) Cross-validation of the NREM reactivation sequences in the post ripple window (+500 ms from first chained ripple onset) (Data = -0.007 ± 0.004, Shuffle = -0.018 ± 0.004, p = 0.062, WRS).

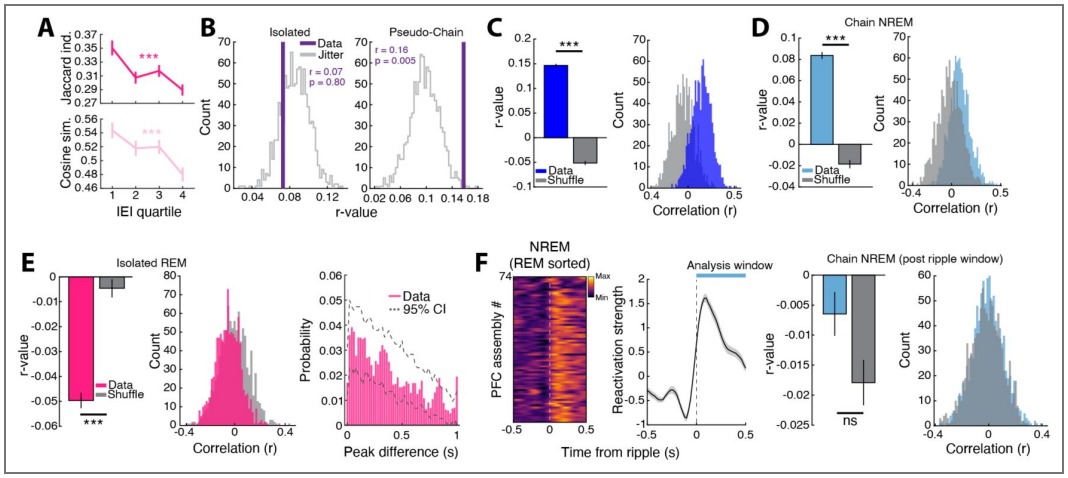

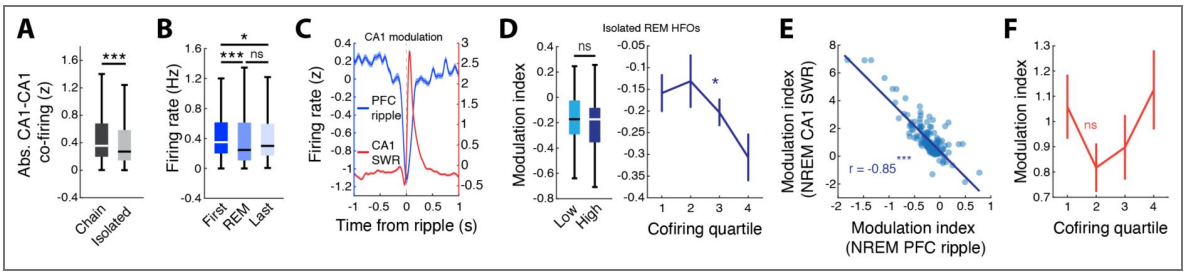

Figure S8. CA1 suppression during NREM PFC ripples and CA1 REM HFO cofiring (related to Figure 7).

(**A**) Absolute CA1-CA1 cell pair cofiring during chained and isolated HFOs (Chain = 0.53 ± 0.02, Isolated = 0.48 ± 0.02, ***p = 1.42×10^{-4}, WRS). The magnitude of cofiring (positive and negative) was greater for HFO chains as compared to isolated HFOs, suggesting differential engagement of CA1 neurons. (**B**) Firing rates of CA1 pyramidal neurons during the first 30 s of NREM, REM, and the last 30 s of NREM sleep within an epoch (First 30 s NREM = 0.54 ± 0.04 Hz, REM = 0.51 ± 0.04 Hz, Last 30 s NREM = 0.51 ± 0.03, First vs REM, ***p = 1.10×10^{-4}, REM vs Last, p = 0.61, First vs Last, *p = 0.013, Friedman test with Bonferroni correction). CA1 firing rates decreased during REM and later in NREM. (**C**) During NREM sleep, CA1 neurons were strongly suppressed during independent PFC ripples. (**D**) (Left) There was no difference in the degree of suppression during NREM PFC ripples for low and high cofiring (during isolated REM HFOs) CA1 neurons (Low cofiring = -0.16 ± 0.04, High cofiring = -0.21 ± 0.03, p = 0.40, WRS). (Right) The cofiring magnitude during isolated HFOs was correlated with the degree of suppression during NREM PFC ripples, similar to REM HFO chains (r = -0.19, *p = 0.011, Pearson correlation). (**E**) Correlation between CA1 modulation during independent NREM PFC ripples and coordinated SWRs. The more suppressed CA1 neurons are during PFC ripples, the stronger they are reactivated during coordinated SWRs (r = -0.85, ***p = 6.45×10^{-208}, Pearson correlation). (**F**) There was no relationship between CA1 cofiring (with PFC) during REM HFO chains and the degree of modulation during coordinated SWRs in NREM sleep (r = 0.04, p = 0.44, Pearson correlation).

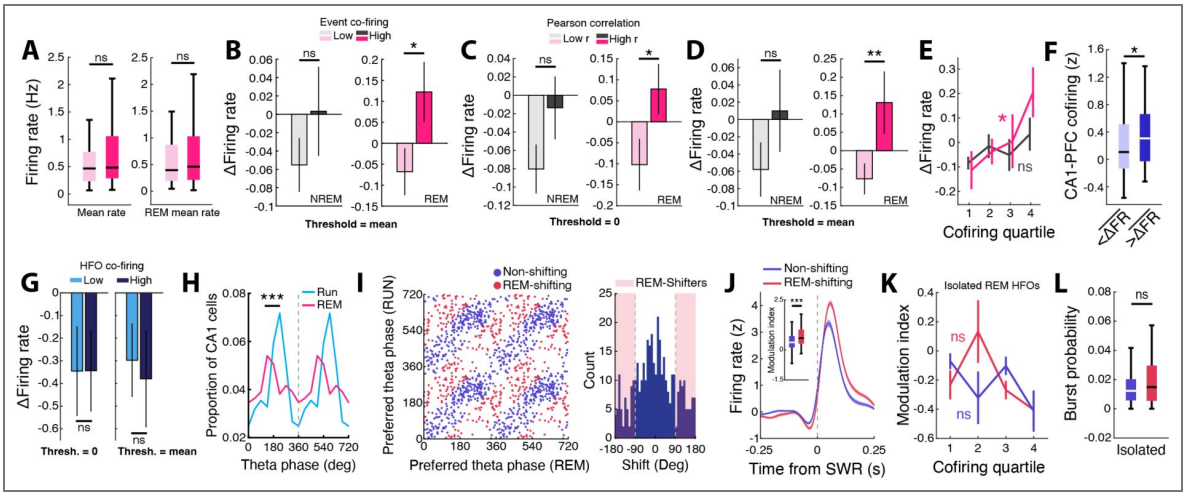

Figure S9. Relationship between REM PFC HFO cofiring, changes in CA1 firing rates over the course of sleep, and CA1 theta phase shifting neurons (related to Figures 7 and 8).

(**A**) (Left) Mean firing rates of high and low cofiring CA1 pyramidal neurons across the entire sleep epoch or (Right) restricted to REM sleep (Low cofiring mean rate = 0.69 ± 0.10, High cofiring mean rate = 0.79 ± 0.08, p = 0.41; Low cofiring REM mean rate = 0.73 ± 0.12, High cofiring REM mean rate = 0.78 ± 0.10, p = 0.49, WRS). (**B**) (Left) Changes in CA1 firing rates from the first NREM bout to the last NREM bout within a sleep epoch plotted according to degree of cofiring (cofiring as measured by the z-scored cofiring metric; high, z-cofiring > mean of distribution; low, z-cofiring < mean of distribution) with PFC either during CA1-independent NREM ripples or chained REM HFOs in PFC (Low NREM = -0.06 ± 0.03, High NREM = 0.003 ± 0.048, p = 0.40; Low REM = -0.068 ± 0.056, High REM = 0.122 ± 0.071, *p = 0.013, WRS). (**C**) Changes in CA1 firing rates from the first NREM bout to the last NREM bout within a sleep epoch plotted according to degree of cofiring (cofiring as measured by the Pearson correlation coefficient; high, r > 0; low, r < 0) with PFC either during CA1-independent NREM ripples or chained REM HFOs in PFC (Low NREM = -0.08 ± 0.03, High NREM = -0.01 ± 0.03, p = 0.080; Low REM = -0.10 ± 0.06, High REM = 0.08 ± 0.06, *p = 0.012, WRS). (**D**) Same as in (**E**) but using above or below the mean of the cofiring distribution to designate high or low cofiring CA1 units, respectively (Low NREM = -0.06 ± 0.03, High NREM = 0.01 ± 0.05, p = 0.30; Low REM = -0.08 ± 0.04, High REM = 0.13 ± 0.08, **p = 0.002, WRS). (**E**) Firing rate change separated by cofiring quartile. The change in CA1 firing rates over the course of sleep was correlated with PFC cofiring during REM HFOs but not NREM ripples (NREM, r = 0.13, p = 0.49; REM, r = 0.17, *p = 0.029, Robust linear regression). (**F**) CA1-PFC HFO cofiring compared for CA1 neurons with firing rate changes higher or lower than the mean (-0.04 Hz) of the distribution (Higher = 0.34 ± 0.04, Lower = 0.22 ± 0.06, *p = 0.038, WRS). Similar to (Figure 7F), CA1 neurons with positive shifts in firing rate over a sleep epoch had higher PFC cofiring than CA1 neurons with a decrease in rate. (**G**) Changes in PFC firing rates from the first NREM bout to the last NREM bout within a sleep epoch plotted according to degree of cofiring with CA1 during REM HFO chains in PFC. Results using 0 or the mean of the correlation coefficient distribution as the threshold shown on the left and right, respectively (0 threshold: Low = -0.35 ± 0.20, High = -0.34 ± 0.18, p = 0.90; Mean threshold: Low = -0.30 ± 0.21, High = -0.38 ± 0.21, p = 0.98, WRS). (**H**) Preferred CA1 theta phase of CA1 neurons during running behavior or REM sleep. A subset of CA1 cells shifted their preferred theta phase during REM sleep (U^2 = 0.48, ***p = 1.51×10^{-5}, Watson's U^2 test). Note that only cells that were significantly phase locked to the theta oscillation during both run and REM were used for analysis. (**I**) (Left) Distributions of preferred CA1 theta phases during run and REM sleep. Only CA1 neurons with significant phase locking during both run and REM sleep were included for analysis. (Right) Histogram of theta phase shifts between run and the subsequent REM sleep session. Red shaded areas indicate neurons that had a phase shift >90°. (**J**) (Left) SWR aligned firing rates of non-shifting and REM-shifting CA1 neurons. (Right) REM-shifting neurons had higher modulation indices, indicating stronger excitation during SWRs (Non-shifting = 0.60 ± 0.07, REM-shifting = 0.80 ± 0.07, ***p = 8.51×10^{-5}, WRS) (**K**) The cofiring magnitude during isolated REM HFOs of non-shifting or REM-shifting CA1 neurons was not correlated with the degree of suppression during independent NREM PFC ripples (Non-shifting, r = -0.25, p = 0.085, REM-shifting, r = -0.32, p = 0.13, Pearson correlation). (**L**) Burst probability of non-shifting and REM-shifting CA1 neurons during isolated REM H (Non-shifting = 0.015 ± 0.002, REM-shifting = 0.021 ± 0.003, p = 0.22, WRS).

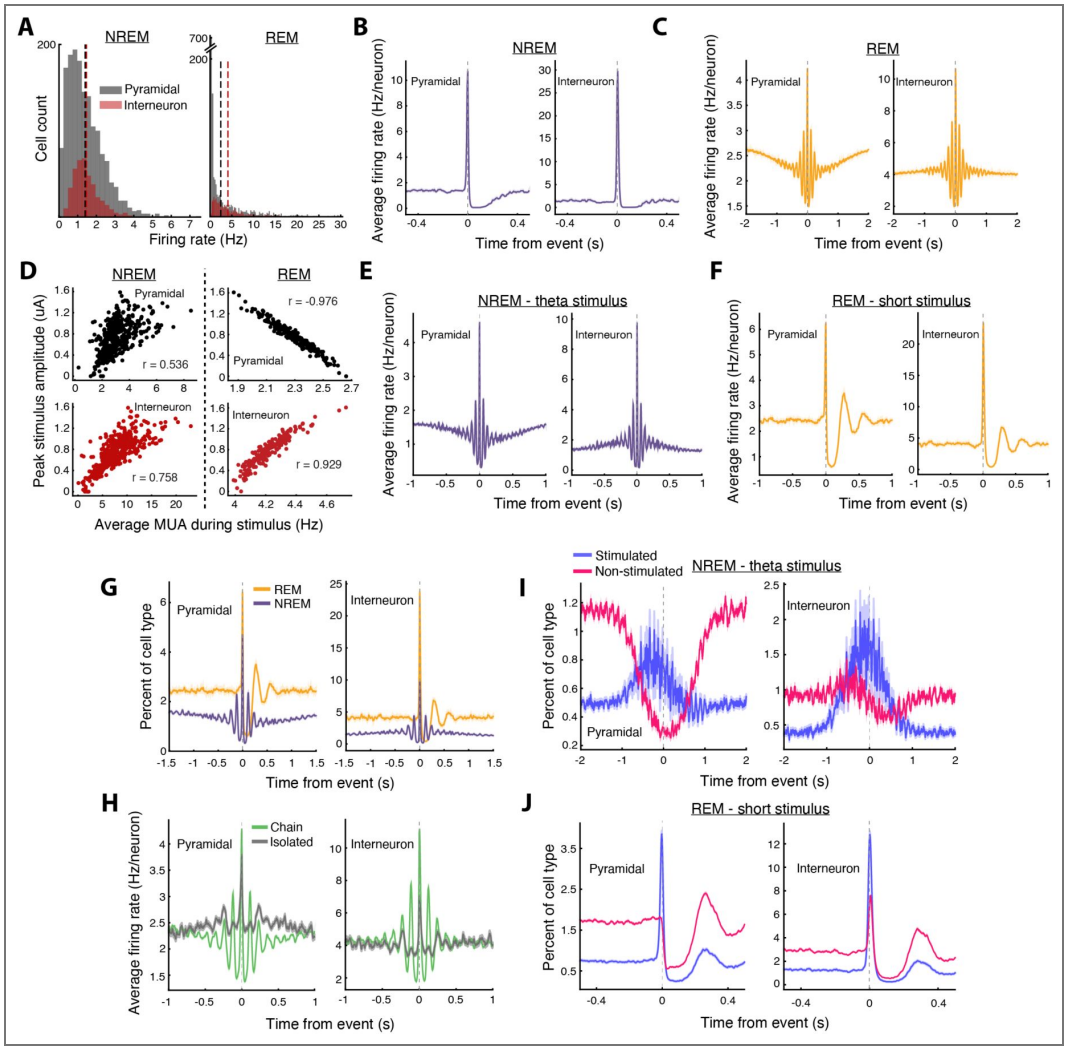

Figure S10. Model analyses split by cell type and reversed condition controls demonstrating the specific effects of ACh tone on network response (related to Figures 8 and 9).

(**A**) Firing rate histograms for NREM and REM simulations split by cell type. Bin size 0.25 Hz. NREM mean rate 1.41 Hz for pyramidal, 1.46 Hz for interneurons. REM mean rate 2.44 Hz for pyramidal, 4.14 Hz for interneurons. (**B**) Average network firing rate surrounding NREM MUA peaks in stimulus periods, split by cell type. (**C**) Same as (**B**), but for REM. (**D**) Peak stimulus amplitude vs average MUA within the stimulus period split by cell type for NREM (Left) and REM (Right). (**E**) Reversed stimulus condition for NREM. Same as (**B**), but swapping the stimulus profile by applying the REM theta-modulated stimulus profile during a low ACh (NREM) simulation. All other parameters are identical. (**F**) Reversed stimulus condition for REM. Same as (**C**), but for a simulation using the brief NREM stimulus combined with high ACh (REM). (**G**) Percent of each cell type with at least one spike in 10 ms bins for the swapped stimulus profile / ACh condition. Note the reduced breadth of pyramidal network activity when applying the brief stimulus in REM compared to NREM, compared to Figure 10B. (**H**) Same as Figure 9G, but split by cell type. (**I**) Swapped stimulus profile / ACh condition, applying the REM theta stimulus during a low ACh NREM simulation. Note the widespread recruitment of stimulated cells relative to non-stimulated cells, compared to REM response shown in Figure 10D. (**J**) Same as (**I**), but applying the NREM brief stimulus during a high ACh REM simulation. Note the lack of peak in non-stimulated cell recruitment by the stimulus compared to NREM response shown in Figure 10C.

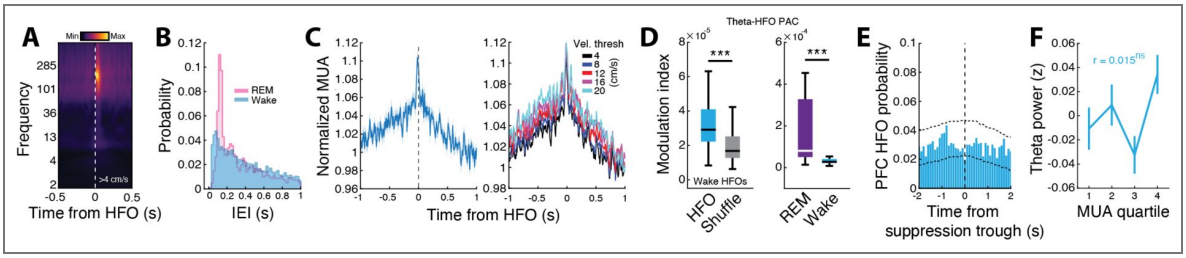

Figure S11. HFOs during awake behavior on the W-Track (related to Figures 1 through 4 and 9).

(**B**) Animal averaged wake HFO aligned PFC spectrogram. Note the absence of elevated gamma and theta power compared to REM events. Compare to Figure 1F. (**C**) Distributions of inter-event-intervals (IEIs) for Wake and REM HFOs (***p = 1.13×10^{-17}, Kolmogorov-Smirnov test) (**D**) (Left) Wake HFO aligned PFC multiunit activity. (Right) Wake HFO aligned multiunit activity stratified by velocity at HFO occurrence. Compare to Figure 2A. (**E**) (Left) Wake theta-HFO phase amplitude coupling compared to shuffle. Note the y-axis scale compared to Figure S4A (HFO = $3.81\times10^{-5} \pm 3.63\times10^{-6}$, Shuffle = $1.83\times10^{-5} \pm 1.24\times10^{-6}$, ***p = 3.16×10^{-12}, WRS). (Right) Comparison of theta-HFO phase amplitude coupling between wake and REM sleep (REM = $1.30\times10^{-3} \pm 4.54\times10^{-4}$, Wake = $3.65\times10^{-5} \pm 4.03\times10^{-6}$, ***p = 5.21×10^{-5}, WRS). Here, REM modulation index values are lower than in Figure S4A because, in this case, all of REM sleep was evaluated, whereas only putative phasic bouts were analyzed in Figure S4A. (**F**) The probability of wake HFOs centered on population suppression events detected during wake behavior. Compare to Figure 4H. The black dotted lines indicate the 99% confidence intervals based on suppression events extracted from shuffled multiunit data. (**G**) There was no correlation between theta power during HFOs and multiunit activity. Compare to Figure 9E (r = 0.015, p = 0.063, Pearson correlation).

Acknowledgements

This work was supported by the National Institutes of Mental Health (R01MH112661 to SPJ).

Additional information

Author contributions

J.D.S. and S.P.J. conceived the study. J.D.S. performed the experiments. J.D.S. processed and analyzed the data. M.S. conceptualized the model and P.M. advised on model implementation. J.D.S., M.S., and S.P.J. wrote the manuscript. S.P.J. provided supervision and funding for all aspects of the study.

Funding

Funder	Grant reference number	Author
HHS | NIH | National Institute of Mental Health (NIMH)	R01MH112661	Shantanu P Jadhav

Author ORCID iDs

Justin D Shin: https://orcid.org/0000-0002-7959-7772
Paul Miller: https://orcid.org/0000-0002-9280-000X
Shantanu P Jadhav: https://orcid.org/0000-0001-5821-0551

References

1. **Blumberg MS,** Lesku JA, Libourel PA, Schmidt MH, Rattenborg NC (2020) What Is REM Sleep?. *Curr Biol* **30**:R38-R49 https://doi.org/10.1016/j.cub.2019.11.045 | PubMed
2. **Peever J,** Fuller PM (2017) The Biology of REM Sleep. *Curr Biol* **27**:R1237-R1248 https://doi.org/10.1016/j.cub.2017.10.026 | PubMed
3. **Tempesta D,** Socci V, De Gennaro L, Ferrara M (2018) Sleep and emotional processing. *Sleep Med Rev* **40**:183-195 https://doi.org/10.1016/j.smrv.2017.12.005 | PubMed
4. **Mukai Y,** Yamanaka A (2023) Functional roles of REM sleep. *Neurosci Res* **189**:44-53 https://doi.org/10.1016/j.neures.2022.12.009 | PubMed
5. **Lendner JD,** Niethard N, Mander BA, van Schalkwijk FJ, Schuh-Hofer S, Schmidt H, Knight RT, Born J, Walker MP, Lin JJ, *et al.* (2023) Human REM sleep recalibrates neural activity in support of memory formation. *Sci Adv* **9**:eadj1895 https://doi.org/10.1126/sciadv.adj1895 | PubMed
6. **Dauvilliers Y,** Schenck CH, Postuma RB, Iranzo A, Luppi PH, Plazzi G, Montplaisir J, Boeve B (2018) REM sleep behaviour disorder. *Nat Rev Dis Primers* **4** https://doi.org/10.1038/s41572-018-0016-5 | PubMed
7. **Squire LR,** Alvarez P (1995) Retrograde amnesia and memory consolidation: a neurobiological perspective. *Curr Opin Neurobiol* **5**:169-177 https://doi.org/10.1016/0959-4388(95)80023-9 | PubMed
8. **Nadel L,** Moscovitch M (1997) Memory consolidation, retrograde amnesia and the hippocampal complex. *Curr Opin Neurobiol* **7**:217-227 https://doi.org/10.1016/s0959-4388(97)80010-4 | PubMed
9. **Buzsaki G** (1989) Two-stage model of memory trace formation: a role for "noisy" brain states. *Neuroscience* **31**:551-570 https://doi.org/10.1016/0306-4522(89)90423-5 | PubMed
10. **Sekeres MJ,** Winocur G, Moscovitch M (2018) The hippocampus and related neocortical structures in memory transformation. *Neurosci Lett* **680**:39-53 https://doi.org/10.1016/j.neulet.2018.05.006 | PubMed
11. **Staresina BP** (2024) Coupled sleep rhythms for memory consolidation. *Trends Cogn Sci* **28**:339-351 https://doi.org/10.1016/j.tics.2024.02.002 | PubMed

12. **Buzsaki G** (2015) Hippocampal sharp wave-ripple: A cognitive biomarker for episodic memory and planning. *Hippocampus* **25**:1073-1188 https://doi.org/10.1002/hipo.22488 | PubMed
13. **Girardeau G,** Zugaro M (2011) Hippocampal ripples and memory consolidation. *Curr Opin Neurobiol* **21**:452-459 https://doi.org/10.1016/j.conb.2011.02.005 | PubMed
14. **Klinzing JG,** Niethard N, Born J (2019) Mechanisms of systems memory consolidation during sleep. *Nat Neurosci* **22**:1598-1610 https://doi.org/10.1038/s41593-019-0467-3 | PubMed
15. **Mizuseki K,** Diba K, Pastalkova E, Buzsaki G (2011) Hippocampal CA1 pyramidal cells form functionally distinct sublayers. *Nat Neurosci* **14**:1174-1181 https://doi.org/10.1038/nn.2894 | PubMed
16. **Tang W,** Shin JD, Frank LM, Jadhav SP (2017) Hippocampal-Prefrontal Reactivation during Learning Is Stronger in Awake Compared with Sleep States. *J Neurosci* **37**:11789-11805 https://doi.org/10.1523/JNEUROSCI.2291-17.2017 | PubMed
17. **Boyce R,** Glasgow SD, Williams S, Adamantidis A (2016) Causal evidence for the role of REM sleep theta rhythm in contextual memory consolidation. *Science* **352**:812-816 https://doi.org/10.1126/science.aad5252 | PubMed
18. **Montgomery SM,** Sirota A, Buzsaki G (2008) Theta and gamma coordination of hippocampal networks during waking and rapid eye movement sleep. *J Neurosci* **28**:6731-6741 https://doi.org/10.1523/JNEUROSCI.1227-08.2008 | PubMed
19. **Brankack J,** Scheffzuk C, Kukushka VI, Vyssotski AL, Tort AB, Draguhn A (2012) Distinct features of fast oscillations in phasic and tonic rapid eye movement sleep. *J Sleep Res* **21**:630-633 https://doi.org/10.1111/j.1365-2869.2012.01037.x | PubMed
20. **Bandarabadi M,** Boyce R, Gutierrez Herrera C, Bassetti CL, Williams S, Schindler K, Adamantidis A (2019) Dynamic modulation of theta-gamma coupling during rapid eye movement sleep. *Sleep* **42** https://doi.org/10.1093/sleep/zsz182 | PubMed
21. **Bueno-Junior LS,** Ruckstuhl MS, Lim MM, Watson BO (2023) The temporal structure of REM sleep shows minute-scale fluctuations across brain and body in mice and humans. *Proc Natl Acad Sci U S A* **120**:e2213438120 https://doi.org/10.1073/pnas.2213438120 | PubMed
22. **Tort AB,** Scheffer-Teixeira R, Souza BC, Draguhn A, Brankack J (2013) Theta-associated high-frequency oscillations (110-160Hz) in the hippocampus and neocortex. *Prog Neurobiol* **100**:1-14 https://doi.org/10.1016/j.pneurobio.2012.09.002 | PubMed
23. **Ghosh M,** Yang FC, Rice SP, Hetrick V, Gonzalez AL, Siu D, Brennan EKW, John TT, Ahrens AM, Ahmed OJ (2022) Running speed and REM sleep control two distinct modes of rapid interhemispheric communication. *Cell Rep* **40**:111028 https://doi.org/10.1016/j.celrep.2022.111028 | PubMed
24. **Arndt KC,** Gilbert ET, Klaver LMF, Kim J, Buhler CM, Basso JC, McKenzie S, English DF (2024) Granular retrosplenial cortex layer 2/3 generates high-frequency oscillations dynamically coupled with hippocampal rhythms across brain states. *Cell Rep* **43**:113910 https://doi.org/10.1016/j.celrep.2024.113910 | PubMed
25. **Aleman-Zapata A,** Morris RGM, Genzel L (2022) Sleep deprivation and hippocampal ripple disruption after one-session learning eliminate memory expression the next day. *Proc Natl Acad Sci U S A* **119**:e2123424119 https://doi.org/10.1073/pnas.2123424119 | PubMed
26. **Yamada RG,** Ueda HR (2019) Molecular Mechanisms of REM Sleep. *Front Neurosci* **13**:1402 https://doi.org/10.3389/fnins.2019.01402 | PubMed
27. **Khodagholy D,** Gelinas JN, Buzsaki G (2017) Learning-enhanced coupling between ripple oscillations in association cortices and hippocampus. *Science* **358**:369-372 https://doi.org/10.1126/science.aan6203 | PubMed
28. **Shin JD,** Jadhav SP (2024) Prefrontal cortical ripples mediate top-down suppression of hippocampal reactivation during sleep memory consolidation. *Curr Biol* **34**:2801-2811.e2809. https://doi.org/10.1016/j.cub.2024.05.018 | PubMed

29. **Vaz AP,** Inati SK, Brunel N, Zaghloul KA (2019) Coupled ripple oscillations between the medial temporal lobe and neocortex retrieve human memory. *Science* **363**:975-978 https://doi.org/10.1126/science.aau8956 | PubMed

30. **van Schalkwijk FJ,** Weber J, Hahn MA, Lendner JD, Inostroza M, Lin JJ, Helfrich RF (2023) An evolutionary conserved division-of-labor between archicortical and neocortical ripples organizes information transfer during sleep. *Prog Neurobiol* **227**:102485 https://doi.org/10.1016/j.pneurobio.2023.102485 | PubMed

31. **Scheffzuk C,** Kukushka VI, Vyssotski AL, Draguhn A, Tort AB, Brankack J (2011) Selective coupling between theta phase and neocortical fast gamma oscillations during REM-sleep in mice. *PLoS One* **6**:e28489 https://doi.org/10.1371/journal.pone.0028489 | PubMed

32. **van Schalkwijk FJ,** Helfrich RF (2026) Aperiodic 1/f noise drives ripple activity in humans. *Nat Commun* **17**:746 https://doi.org/10.1038/s41467-026-68404-5 | PubMed

33. **Grosmark AD,** Mizuseki K, Pastalkova E, Diba K, Buzsaki G (2012) REM sleep reorganizes hippocampal excitability. *Neuron* **75**:1001-1007 https://doi.org/10.1016/j.neuron.2012.08.015 | PubMed

34. **Miyawaki H,** Diba K (2016) Regulation of Hippocampal Firing by Network Oscillations during Sleep. *Curr Biol* **26**:893-902 https://doi.org/10.1016/j.cub.2016.02.024 | PubMed

35. **Watson BO,** Levenstein D, Greene JP, Gelinas JN, Buzsaki G (2016) Network Homeostasis and State Dynamics of Neocortical Sleep. *Neuron* **90**:839-852 https://doi.org/10.1016/j.neuron.2016.03.036 | PubMed

36. **Poe GR,** Nitz DA, McNaughton BL, Barnes CA (2000) Experience-dependent phase-reversal of hippocampal neuron firing during REM sleep. *Brain Res* **855**:176-180 https://doi.org/10.1016/s0006-8993(99)02310-0 | PubMed

37. **Louie K,** Wilson MA (2001) Temporally structured replay of awake hippocampal ensemble activity during rapid eye movement sleep. *Neuron* **29**:145-156 https://doi.org/10.1016/s0896-6273(01)00186-6 | PubMed

38. **Abdou K,** Nomoto M, Aly MH, Ibrahim AZ, Choko K, Okubo-Suzuki R, Muramatsu SI, Inokuchi K (2024) Prefrontal coding of learned and inferred knowledge during REM and NREM sleep. *Nat Commun* **15**:4566 https://doi.org/10.1038/s41467-024-48816-x | PubMed

39. **Maharjan DM,** Dai YY, Glantz EH, Jadhav SP (2018) Disruption of dorsal hippocampal - prefrontal interactions using chemogenetic inactivation impairs spatial learning. *Neurobiol Learn Mem* **155**:351-360 https://doi.org/10.1016/j.nlm.2018.08.023 | PubMed

40. **Shin JD,** Tang W, Jadhav SP (2019) Dynamics of Awake Hippocampal-Prefrontal Replay for Spatial Learning and Memory-Guided Decision Making. *Neuron* **104**:1110-1125.e1117. https://doi.org/10.1016/j.neuron.2019.09.012 | PubMed

41. **Staresina BP,** Niediek J, Borger V, Surges R, Mormann F (2023) How coupled slow oscillations, spindles and ripples coordinate neuronal processing and communication during human sleep. *Nat Neurosci* **26**:1429-1437 https://doi.org/10.1038/s41593-023-01381-w | PubMed

42. **Canolty RT,** Knight RT (2010) The functional role of cross-frequency coupling. *Trends Cogn Sci* **14**:506-515 https://doi.org/10.1016/j.tics.2010.09.001 | PubMed

43. **de Almeida-Filho DG,** Koike BDV, Billwiller F, Farias KS, de Sales IRP, Luppi PH, Ribeiro S, Queiroz CM (2021) Hippocampus-retrosplenial cortex interaction is increased during phasic REM and contributes to memory consolidation. *Sci Rep* **11**:13078 https://doi.org/10.1038/s41598-021-91659-5 | PubMed

44. **Davidson TJ,** Kloosterman F, Wilson MA (2009) Hippocampal replay of extended experience. *Neuron* **63**:497-507 https://doi.org/10.1016/j.neuron.2009.07.027 | PubMed

45. **Darevsky D,** Kim J, Ganguly K (2024) Coupling of Slow Oscillations in the Prefrontal and Motor Cortex Predicts Onset of Spindle Trains and Persistent Memory Reactivations. *J Neurosci* **44** https://doi.org/10.1523/JNEUROSCI.0621-24.2024 | PubMed

46. **Antony JW,** Piloto L, Wang M, Pacheco P, Norman KA, Paller KA (2018) Sleep Spindle Refractoriness Segregates Periods of Memory Reactivation. *Curr Biol* **28**:1736-1743.e1734. https://doi.org/10.1016/j.cub.2018.04.020 | PubMed

47. **Mallory CS,** Widloski J, Foster DJ (2025) The time course and organization of hippocampal replay. *Science* **387**:541-548 https://doi.org/10.1126/science.ads4760 | PubMed

48. **Cheng S,** Frank LM (2008) New experiences enhance coordinated neural activity in the hippocampus. *Neuron* **57**:303-313 https://doi.org/10.1016/j.neuron.2007.11.035 | PubMed

49. **Judak L,** Chiovini B, Juhasz G, Palfi D, Mezriczky Z, Szadai Z, Katona G, Szmola B, Ocsai K, Martinecz B, *et al.* (2022) Sharp-wave ripple doublets induce complex dendritic spikes in parvalbumin interneurons in vivo. *Nat Commun* **13**:6715 https://doi.org/10.1038/s41467-022-34520-1 | PubMed

50. **Peyrache A,** Khamassi M, Benchenane K, Wiener SI, Battaglia FP (2009) Replay of rule-learning related neural patterns in the prefrontal cortex during sleep. *Nat Neurosci* **12**:919-926 https://doi.org/10.1038/nn.2337 | PubMed

51. **van de Ven GM,** Trouche S, McNamara CG, Allen K, Dupret D (2016) Hippocampal Offline Reactivation Consolidates Recently Formed Cell Assembly Patterns during Sharp Wave-Ripples. *Neuron* **92**:968-974 https://doi.org/10.1016/j.neuron.2016.10.020 | PubMed

52. **Fries P** (2005) A mechanism for cognitive dynamics: neuronal communication through neuronal coherence. *Trends Cogn Sci* **9**:474-480 https://doi.org/10.1016/j.tics.2005.08.011 | PubMed

53. **Miyawaki H,** Watson BO, Diba K (2019) Neuronal firing rates diverge during REM and homogenize during non-REM. *Sci Rep* **9**:689 https://doi.org/10.1038/s41598-018-36710-8 | PubMed

54. **Valero M,** Cid E, Averkin RG, Aguilar J, Sanchez-Aguilera A, Viney TJ, Gomez-Dominguez D, Bellistri E, de la Prida LM (2015) Determinants of different deep and superficial CA1 pyramidal cell dynamics during sharp-wave ripples. *Nat Neurosci* **18**:1281-1290 https://doi.org/10.1038/nn.4074 | PubMed

55. **Gu L,** Ren M, Lin L, Xu J (2023) Calbindin-Expressing CA1 Pyramidal Neurons Encode Spatial Information More Efficiently. *eNeuro* **10** https://doi.org/10.1523/ENEURO.0411-22.2023 | PubMed

56. **de la Prida LM** (2020) Potential factors influencing replay across CA1 during sharp-wave ripples. *Philos Trans R Soc Lond B Biol Sci* **375**:20190236 https://doi.org/10.1098/rstb.2019.0236 | PubMed

57. **Harvey RE,** Robinson HL, Liu C, Oliva A, Fernandez-Ruiz A (2023) Hippocampo-cortical circuits for selective memory encoding, routing, and replay. *Neuron* **111**:2076-2090.e2079. https://doi.org/10.1016/j.neuron.2023.04.015 | PubMed

58. **Sharif F,** Tayebi B, Buzsaki G, Royer S, Fernandez-Ruiz A (2021) Subcircuits of Deep and Superficial CA1 Place Cells Support Efficient Spatial Coding across Heterogeneous Environments. *Neuron* **109**:363-376.e366. https://doi.org/10.1016/j.neuron.2020.10.034 | PubMed

59. **Picciotto MR,** Higley MJ, Mineur YS (2012) Acetylcholine as a neuromodulator: cholinergic signaling shapes nervous system function and behavior. *Neuron* **76**:116-129 https://doi.org/10.1016/j.neuron.2012.08.036 | PubMed

60. **Eban-Rothschild A,** de Lecea L (2017) Neuronal substrates for initiation, maintenance, and structural organization of sleep/wake states. *F1000Res* **6**:212 https://doi.org/10.12688/f1000research.9677.1 | PubMed

61. **Colangelo C,** Shichkova P, Keller D, Markram H, Ramaswamy S (2019) Cellular, Synaptic and Network Effects of Acetylcholine in the Neocortex. *Front Neural Circuits* **13**:24 https://doi.org/10.3389/fncir.2019.00024 | PubMed

62. **Stiefel KM,** Gutkin BS, Sejnowski TJ (2009) The effects of cholinergic neuromodulation on neuronal phase-response curves of modeled cortical neurons. *J Comput Neurosci* **26**:289-301 https://doi.org/10.1007/s10827-008-0111-9 | PubMed

63. **Roach JP,** Ben-Jacob E, Sander LM, Zochowski MR (2015) Formation and Dynamics of Waves in a Cortical Model of Cholinergic Modulation. *PLoS Comput Biol* **11**:e1004449 https://doi.org/10.1371/journal.pcbi.1004449 | PubMed

64. **Satchell M,** Butel-Fry E, Noureddine Z, Simmons A, Ognjanovski N, Aton SJ, Zochowski MR (2025) Cholinergic modulation of neural networks supports sequential and complementary roles for NREM and REM states in memory consolidation. *PLoS Comput Biol* **21**:e1013097 https://doi.org/10.1371/journal.pcbi.1013097 | PubMed

65. **Czarnecki P,** Lin J, Aton SJ, Zochowski M (2021) Dynamical Mechanism Underlying Scale-Free Network Reorganization in Low Acetylcholine States Corresponding to Slow Wave Sleep. *Front Netw Physiol* **1** https://doi.org/10.3389/fnetp.2021.759131 | PubMed

66. **Stiefel KM,** Gutkin BS, Sejnowski TJ (2008) Cholinergic neuromodulation changes phase response curve shape and type in cortical pyramidal neurons. *PLoS One* **3**:e3947 https://doi.org/10.1371/journal.pone.0003947 | PubMed

67. **Gulledge AT,** Bucci DJ, Zhang SS, Matsui M, Yeh HH (2009) M1 receptors mediate cholinergic modulation of excitability in neocortical pyramidal neurons. *J Neurosci* **29**:9888-9902 https://doi.org/10.1523/JNEUROSCI.1366-09.2009 | PubMed

68. **Dasari S,** Gulledge AT (2011) M1 and M4 receptors modulate hippocampal pyramidal neurons. *J Neurophysiol* **105**:779-792 https://doi.org/10.1152/jn.00686.2010 | PubMed

69. **Mishra W,** Kheradpezhouh E, Arabzadeh E (2024) Activation of M1 cholinergic receptors in mouse somatosensory cortex enhances information processing and detection behaviour. *Commun Biol* **7**:3 https://doi.org/10.1038/s42003-023-05699-w | PubMed

70. **Kimura F,** Fukuda M, Tsumoto T (1999) Acetylcholine suppresses the spread of excitation in the visual cortex revealed by optical recording: possible differential effect depending on the source of input. *Eur J Neurosci* **11**:3597-3609 https://doi.org/10.1046/j.1460-9568.1999.00779.x | PubMed

71. **Dasgupta R,** Seibt F, Beierlein M (2018) Synaptic Release of Acetylcholine Rapidly Suppresses Cortical Activity by Recruiting Muscarinic Receptors in Layer 4. *J Neurosci* **38**:5338-5350 https://doi.org/10.1523/JNEUROSCI.0566-18.2018 | PubMed

72. **Zerimech S,** Chever O, Scalmani P, Pizzamiglio L, Duprat F, Mantegazza M (2020) Cholinergic modulation inhibits cortical spreading depression in mouse neocortex through activation of muscarinic receptors and decreased excitatory/inhibitory drive. *Neuropharmacology* **166**:107951 https://doi.org/10.1016/j.neuropharm.2020.107951 | PubMed

73. **Chen N,** Sugihara H, Sur M (2015) An acetylcholine-activated microcircuit drives temporal dynamics of cortical activity. *Nat Neurosci* **18**:892-902 https://doi.org/10.1038/nn.4002 | PubMed

74. **Boyce R,** Williams S, Adamantidis A (2017) REM sleep and memory. *Curr Opin Neurobiol* **44**:167-177 https://doi.org/10.1016/j.conb.2017.05.001 | PubMed

75. **Bollmann L,** Baracskay P, Stella F, Csicsvari J (2025) Sleep stages antagonistically modulate reactivation drift. *Neuron* https://doi.org/10.1016/j.neuron.2025.02.025 | PubMed

76. **Helfrich RF,** Lendner JD, Mander BA, Guillen H, Paff M, Mnatsakanyan L, Vadera S, Walker MP, Lin JJ, Knight RT (2019) Bidirectional prefrontal-hippocampal dynamics organize information transfer during sleep in humans. *Nat Commun* **10**:3572 https://doi.org/10.1038/s41467-019-11444-x | PubMed

77. **Drieu C,** Zugaro M (2019) Hippocampal Sequences During Exploration: Mechanisms and Functions. *Front Cell Neurosci* **13**:232 https://doi.org/10.3389/fncel.2019.00232 | PubMed

78. **Sanzeni A,** Akitake B, Goldbach HC, Leedy CE, Brunel N, Histed MH (2020) Inhibition stabilization is a widespread property of cortical networks. *eLife* **9** https://doi.org/10.7554/eLife.54875 | PubMed

79. **Niethard N,** Hasegawa M, Itokazu T, Oyanedel CN, Born J, Sato TR (2016) Sleep-Stage-Specific Regulation of Cortical Excitation and Inhibition. *Curr Biol* **26**:2739-2749 https://doi.org/10.1016/j.cub.2016.08.035 | PubMed

80. **Ramirez-Villegas JF,** Besserve M, Murayama Y, Evrard HC, Oeltermann A, Logothetis NK (2021) Coupling of hippocampal theta and ripples with pontogeniculooccipital waves. *Nature* **589**:96-102 https://doi.org/10.1038/s41586-020-2914-4 | PubMed

81. **Tsunematsu T,** Matsumoto S, Merkler M, Sakata S (2023) Pontine Waves Accompanied by Short Hippocampal Sharp Wave-Ripples During Non-rapid Eye Movement Sleep. *Sleep* **46** https://doi.org/10.1093/sleep/zsad193 | PubMed

82. **Teles-Grilo Ruivo LM,** Baker KL, Conway MW, Kinsley PJ, Gilmour G, Phillips KG, Isaac JTR, Lowry JP, Mellor JR (2017) Coordinated Acetylcholine Release in Prefrontal Cortex and Hippocampus Is Associated with Arousal and Reward on Distinct Timescales. *Cell Rep* **18**:905-917 https://doi.org/10.1016/j.celrep.2016.12.085 | PubMed

83. **Nunez A,** Buno W (2021) The Theta Rhythm of the Hippocampus: From Neuronal and Circuit Mechanisms to Behavior. *Front Cell Neurosci* **15**:649262 https://doi.org/10.3389/fncel.2021.649262 | PubMed

84. **Goard M,** Dan Y (2009) Basal forebrain activation enhances cortical coding of natural scenes. *Nat Neurosci* **12**:1444-1449 https://doi.org/10.1038/nn.2402 | PubMed

85. **Zhang Y,** Cao L, Varga V, Jing M, Karadas M, Li Y, Buzsaki G (2021) Cholinergic suppression of hippocampal sharp-wave ripples impairs working memory. *Proc Natl Acad Sci U S A* **118** https://doi.org/10.1073/pnas.2016432118 | PubMed

86. **Vandecasteele M,** Varga V, Berenyi A, Papp E, Bartho P, Venance L, Freund TF, Buzsaki G (2014) Optogenetic activation of septal cholinergic neurons suppresses sharp wave ripples and enhances theta oscillations in the hippocampus. *Proc Natl Acad Sci U S A* **111**:13535-13540 https://doi.org/10.1073/pnas.1411233111 | PubMed

87. **Girardeau G,** Benchenane K, Wiener SI, Buzsaki G, Zugaro MB (2009) Selective suppression of hippocampal ripples impairs spatial memory. *Nat Neurosci* **12**:1222-1223 https://doi.org/10.1038/nn.2384 | PubMed

88. **Maingret N,** Girardeau G, Todorova R, Goutierre M, Zugaro M (2016) Hippocampo-cortical coupling mediates memory consolidation during sleep. *Nat Neurosci* **19**:959-964 https://doi.org/10.1038/nn.4304 | PubMed

89. **Chang H,** Tang W, Wulf AM, Nyasulu T, Wolf ME, Fernandez-Ruiz A, Oliva A (2025) Sleep microstructure organizes memory replay. *Nature* **637**:1161-1169 https://doi.org/10.1038/s41586-024-08340-w | PubMed

90. **Gridchyn I,** Schoenenberger P, O'Neill J, Csicsvari J (2020) Assembly-Specific Disruption of Hippocampal Replay Leads to Selective Memory Deficit. *Neuron* **106**:291-300.e296. https://doi.org/10.1016/j.neuron.2020.01.021 | PubMed

91. **Porter BS,** Shi C, Kozlova E, Jadhav SP (2026) A novel rat spatial transitive inference paradigm reveals rapid deduction of transitive relationships using schemas and deliberation. *Behavioral Neuroscience* https://doi.org/10.1037/bne0000660 | PubMed

92. **Zeithamova D,** Schlichting ML, Preston AR (2012) The hippocampus and inferential reasoning: building memories to navigate future decisions. *Front Hum Neurosci* **6**:70 https://doi.org/10.3389/fnhum.2012.00070 | PubMed

93. **Cairney SA,** Durrant SJ, Power R, Lewis PA (2015) Complementary roles of slow-wave sleep and rapid eye movement sleep in emotional memory consolidation. *Cereb Cortex* **25**:1565-1575 https://doi.org/10.1093/cercor/bht349 | PubMed

94. **Simor P,** van der Wijk G, Nobili L, Peigneux P (2020) The microstructure of REM sleep: Why phasic and tonic?. *Sleep Med Rev* **52**:101305 https://doi.org/10.1016/j.smrv.2020.101305 | PubMed

95. **Shin JD,** Tang W, Jadhav SP (2023) Protocol for geometric transformation of cognitive maps for generalization across hippocampal-prefrontal circuits. *STAR Protoc* **4**:102513 https://doi.org/10.1016/j.xpro.2023.102513 | PubMed

96. **Jadhav SP,** Kemere C, German PW, Frank LM (2012) Awake hippocampal sharp-wave ripples support spatial memory. *Science* **336**:1454-1458 https://doi.org/10.1126/science.1217230 | PubMed

97. **Fernandez-Ruiz A,** Oliva A, Fermino de Oliveira E, Rocha-Almeida F, Tingley D, Buzsaki G (2019) Long-duration hippocampal sharp wave ripples improve memory. *Science* **364**:1082-1086 https://doi.org/10.1126/science.aax0758 | PubMed

98. **Schmitzer-Torbert N,** Jackson J, Henze D, Harris K, Redish AD (2005) Quantitative measures of cluster quality for use in extracellular recordings. *Neuroscience* **131**:1-11 https://doi.org/10.1016/j.neuroscience.2004.09.066 | PubMed

99. **Zhang LB,** Zhang J, Sun MJ, Chen H, Yan J, Luo FL, Yao ZX, Wu YM, Hu B (2020) Neuronal Activity in the Cerebellum During the Sleep-Wakefulness Transition in Mice. *Neurosci Bull* **36**:919-931 https://doi.org/10.1007/s12264-020-00511-9 | PubMed

100. **Rothschild G,** Eban E, Frank LM (2017) A cortical-hippocampal-cortical loop of information processing during memory consolidation. *Nat Neurosci* **20**:251-259 https://doi.org/10.1038/nn.4457 | PubMed

101. **Schomburg EW,** Fernandez-Ruiz A, Mizuseki K, Berenyi A, Anastassiou CA, Koch C, Buzsaki G (2014) Theta phase segregation of input-specific gamma patterns in entorhinal-hippocampal networks. *Neuron* **84**:470-485 https://doi.org/10.1016/j.neuron.2014.08.051 | PubMed

102. **Mitra P,** Bokil H (2008) *Observed brain dynamics* Oxford University Press.

103. **Sullivan D,** Csicsvari J, Mizuseki K, Montgomery S, Diba K, Buzsaki G (2011) Relationships between hippocampal sharp waves, ripples, and fast gamma oscillation: influence of dentate and entorhinal cortical activity. *J Neurosci* **31**:8605-8616 https://doi.org/10.1523/JNEUROSCI.0294-11.2011 | PubMed

104. **Tort AB,** Komorowski R, Eichenbaum H, Kopell N (2010) Measuring phase-amplitude coupling between neuronal oscillations of different frequencies. *J Neurophysiol* **104**:1195-1210 https://doi.org/10.1152/jn.00106.2010 | PubMed

105. **Vaz AP,** Yaffe RB, Wittig JH, Inati SK, Zaghloul KA (2017) Dual origins of measured phase-amplitude coupling reveal distinct neural mechanisms underlying episodic memory in the human cortex. *Neuroimage* **148**:148-159 https://doi.org/10.1016/j.neuroimage.2017.01.001 | PubMed

106. **Daume J,** Kaminski J, Schjetnan AGP, Salimpour Y, Khan U, Kyzar M, Reed CM, Anderson WS, Valiante TA, Mamelak AN, *et al.* (2024) Control of working memory by phase-amplitude coupling of human hippocampal neurons. *Nature* **629**:393-401 https://doi.org/10.1038/s41586-024-07309-z | PubMed

107. **Siapas AG,** Lubenov EV, Wilson MA (2005) Prefrontal phase locking to hippocampal theta oscillations. *Neuron* **46**:141-151 https://doi.org/10.1016/j.neuron.2005.02.028 | PubMed

108. **Vinck M,** van Wingerden M, Womelsdorf T, Fries P, Pennartz CM (2010) The pairwise phase consistency: a bias-free measure of rhythmic neuronal synchronization. *Neuroimage* **51**:112-122 https://doi.org/10.1016/j.neuroimage.2010.01.073 | PubMed

109. **Nolte G,** Ziehe A, Nikulin VV, Schlogl A, Kramer N, Brismar T, Muller KR (2008) Robustly estimating the flow direction of information in complex physical systems. *Phys Rev Lett* **100**:234101 https://doi.org/10.1103/PhysRevLett.100.234101 | PubMed

110. **Oostenveld R,** Fries P, Maris E, Schoffelen JM (2011) FieldTrip: Open source software for advanced analysis of MEG, EEG, and invasive electrophysiological data. *Comput Intell Neurosci* **2011**:156869 https://doi.org/10.1155/2011/156869 | PubMed

111. **Jadhav SP,** Rothschild G, Roumis DK, Frank LM (2016) Coordinated Excitation and Inhibition of Prefrontal Ensembles during Awake Hippocampal Sharp-Wave Ripple Events. *Neuron* **90**:113-127 https://doi.org/10.1016/j.neuron.2016.02.010 | PubMed

112. **Stark E,** Roux L, Eichler R, Buzsaki G (2015) Local generation of multineuronal spike sequences in the hippocampal CA1 region. *Proc Natl Acad Sci U S A* **112**:10521-10526 https://doi.org/10.1073/pnas.1508785112 | PubMed

113. **Valero M,** Viney TJ, Machold R, Mederos S, Zutshi I, Schuman B, Senzai Y, Rudy B, Buzsaki G (2021) Sleep down state-active ID2/Nkx2.1 interneurons in the neocortex. *Nat Neurosci* **24**:401-411 https://doi.org/10.1038/s41593-021-00797-6 | PubMed

114. **Zarzoso V,** Comon P (2010) Robust independent component analysis by iterative maximization of the kurtosis contrast with algebraic optimal step size. *IEEE Trans Neural Netw* **21**:248-261 https://doi.org/10.1109/TNN.2009.2035920 | PubMed

115. **Sosa M,** Plitt MH, Giocomo LM (2025) A flexible hippocampal population code for experience relative to reward. *Nat Neurosci* **28**:1497-1509 https://doi.org/10.1038/s41593-025-01985-4 | PubMed

116. **Plitt MH,** Giocomo LM (2021) Experience-dependent contextual codes in the hippocampus. *Nat Neurosci* **24**:705-714 https://doi.org/10.1038/s41593-021-00816-6 | PubMed

117. **Harris KD,** Hirase H, Leinekugel X, Henze DA, Buzsaki G (2001) Temporal interaction between single spikes and complex spike bursts in hippocampal pyramidal cells. *Neuron* **32**:141-149 https://doi.org/10.1016/s0896-6273(01)00447-0 | PubMed

118. **Delmas P,** Brown DA (2005) Pathways modulating neural KCNQ/M (Kv7) potassium channels. *Nat Rev Neurosci* **6**:850-862 https://doi.org/10.1038/nrn1785 | PubMed

119. **McCormick DA,** Wang Z, Huguenard J (1993) Neurotransmitter control of neocortical neuronal activity and excitability. *Cereb Cortex* **3**:387-398 https://doi.org/10.1093/cercor/3.5.387 | PubMed

120. **Meir I,** Katz Y, Lampl I (2018) Membrane Potential Correlates of Network Decorrelation and Improved SNR by Cholinergic Activation in the Somatosensory Cortex. *J Neurosci* **38**:10692-10708 https://doi.org/10.1523/JNEUROSCI.1159-18.2018 | PubMed

Shin Justin, Jadhav Shantanu (2024) Single Day W-Track Learning. The DANDI Archive. https://doi.org/10.48324/dandi.000978/0.240511.0307

Peer reviews

Reviewer #1 (Public review):

Summary and Strengths:

Shin et al deepen our understanding of high frequency oscillations in the frontal cortex during REM in a manner that sheds important light on the roles of these events. In particular, they reveal that cortical HFOs are modulated by theta oscillations, occur in chains and recruit cortical neuronal activation patterns in a manner that is distinct from other high frequency events during nonREM or in hippocampus. They also show that these events occur during increased oscillatory cross-talk between hippocampus and cortex and may protect cortical neurons from down regulation of firing during sleep. Overall, this is important work with several novel observations pointing towards an important role for these events that will open become increasingly understood over time.

I also wanted to comment that 2D is a beautiful illustration of separate and essentially exclusive communication channels used during HF events in NREM vs REM. They almost perfectly complement each other's frequencies.

Weaknesses:

I have only one major scientific critique, I believe we need to see quantification of how phasic REM theta waves with versus without HFOs differ. What do REM HFOs add to the "normal" theta oscillation? Without this, comparison it is more difficult to interpret the meaning of these events. Given that HFO chains have IEIs around the time of a theta cycle duration, are the repeating spiking activities stronger during HFO repeats than during adjacent theta waves without HFOs? What percentage of theta waves contain HFOs and what is the firing rate during those theta waves with vs without HFOs? Is there differential firing rate modulation? The authors may even consider that all REM-HFO-specific quantifications should be shown as differential from phasic theta cycles without HFOs.

As a non-scientific comment on the manuscript itself: unfortunately, the paper is difficult to read and understand at times, requiring great effort by the reader. This is to an extent that communication is hindered. The paper is dense with changing methods often from panel to panel. Unfortunately, the panel quantifications are not explained in the results section in a manner that readers can understand without going to read the methods for often each individual panel. These measures should be explained in a way that lets readers understand the conclusions of each panel and grossly what calculations were used to reach those. Instead, too much jargon is used rather than clear descriptions of overall calculations being done for each panel.

The authors mention in discussion that they see increased functional connectivity between mPFC and CA1, but most data suggesting that seems to be based on LFP rather than spiking. Functional connectivity is defined best by spiking-spiking relationships. And these authors have spiking data. So I believe either the descriptive language should be pulled back to something like "oscillatory coupling" or more analyses should be dedicated to showing spike-spike coordination across regions.

Comments on revised version.

Previously raised concerns are addressed.

https://doi.org/10.7554/eLife.110795.2.sa3

Reviewer #2 (Public review):

Summary:

In this study, the authors investigate high-frequency oscillations (HFOs) in the prefrontal cortex during REM sleep. They identify a specific pattern where these HFOs occur in "chains" that are phase-locked to theta oscillations, primarily during the "phasic" periods of REM. The study contrasts these events with isolated HFOs and NREM ripples, suggesting a unique role for these chains in coordinating activity between the prefrontal cortex and the hippocampus. Most notably, the authors report that a specific subset of hippocampal cells-those that co-fire with the prefrontal cortex during these HFOs-increase their firing rates over the course of sleep, suggesting a potential mechanism for selective memory consolidation.

Strengths:

The study addresses an under-explored area of sleep physiology: the fine-grained temporal coordination between the cortex and hippocampus during REM sleep. The identification of HFO "chains" and their association with higher theta power provides an interesting framework for understanding how the brain might organize information transfer outside of NREM sleep. The observation that specific hippocampal populations show differential firing rate changes based on their participation in these HFO events is a striking finding that warrants further investigation.

Comments on revised version.

I do have one remaining concern, which is about their continued use of the term "reactivation" during REM sleep, whereas it still seems "activation" is more appropriate. The only place they show more Post vs. Pre activation is in Figure 6F/6G which includes NREM sleep where indeed reactivation is robust (but not the main focus of this paper). There is no evidence offered that the REM ensembles are not already "pre-configured" and active at similar levels (with similar activation patterns) during Pre sleep. Notably Louie and Wilson 2001 found greater "replay" during Pre than Post during REM. Also, the first half vs. second half comparisons (e.g. Fig 6C) could be more effectively performed in Figure 6A, showing that

the same ordering persists across the periods. If this point were addressed, the significance of the findings could potentially increase.

https://doi.org/10.7554/eLife.110795.2.sa2

Reviewer #3 (Public review):

Summary:

Shin et al. examine hippocampal-prefrontal interactions during sleep using simultaneous CA1 and prefrontal cortex recordings in rats performing a spatial memory task. They identify high-frequency oscillation (HFO) events in PFC during REM sleep that occur in theta-modulated chains and are associated with increased CA1-PFC coherence and sequential, sparse reactivation of cortical ensembles. This pattern contrasts with the synchronous reactivation observed during NREM cortical ripples. Together with a simple cholinergic network model, the authors propose that REM HFO chains represent a distinct mechanism for hippocampal-cortical coordination that complements NREM ripple-mediated processing during sleep.

Strengths:

A major strength of the work is the extensive electrophysiological dataset, which includes simultaneous recordings of large neuronal populations in both hippocampus and prefrontal cortex across behaviour and subsequent sleep. The analyses linking high-frequency events to population dynamics, interregional coherence, and ensemble reactivation are technically sophisticated and provide an incredibly detailed description of REM-associated cortical activity patterns. In particular, the demonstration that REM HFOs occur in chains aligned to theta phase and organise sequential activation of cortical assemblies represents a potentially important advance in understanding the neural structure of REM sleep activity. The integration of experimental data with a computational model further provides a useful framework for interpreting the observed differences between REM and NREM network states in terms of neuromodulatory influences.

Weaknesses:

While overall this study provides a highly valuable body of work, there are two primary limitations, which if overcome, would provide substantially more significance to the overall characterisation of REM HFOs. Specifically:

Distinction from wake HFOs

The results largely support the authors' claim that REM HFO chains represent a distinct pattern of neural coordination compared to NREM cortical ripples. The analyses consistently show differences between REM and NREM events in terms of neuronal modulation, ensemble structure, and interregional coupling. However, similar high-frequency events during wake are not examined. Since REM sleep shares several network features with wakefulness, including strong theta oscillations, evaluating whether comparable PFC HFOs occur during wake would provide clarity on whether these events are specific to REM sleep (and its associated functions) or represent more general theta-associated phenomenon.

Link to memory consolidation

The manuscript proposes throughout that REM HFO chains may contribute to memory consolidation by coordinating hippocampal-cortical reactivation, but the evidence for this functional role remains indirect. The authors do highlight this as a limitation of the study - the inability to link their findings to learning - but it is not clear why. Further details of the behaviour results should be included. If no learning occurred across the eight behavioural

sessions, this should be reported. If learning did occur, but could not be linked to HFO events, this should also be reported.

Comments on revised version.

The authors have since addressed these weaknesses. In supplementary figure S11 the authors now show that while HFOs were detectable during wake, they were not associated with gamma/theta oscillations or theta modulation of unit activity. This suggests that HFOs during REM are a distinct feature of REM sleep and not comparable to HFOs during NREM or wake. It would be interesting for future work to identify the significance of wake PFC HFOs, whether there are differences between HFOs during running compared to stationary behaviour, and their relationship to hippocampal sharp-wave ripples and memory consolidation.

Regarding the link between REM HFOs and memory consolidation, the authors have further acknowledged this as a limitation of the study and requirement for a more specific experimental design to test related hypotheses. Nevertheless, they do show a clear trajectory of learning in the rats and corresponding increase in reactivation of task-related activity which could be associated with REM sleep HFOs. This study paves the way for future experiments to more directly test this link.

https://doi.org/10.7554/eLife.110795.2.sa1

Author response:

The following is the authors' response to the original reviews.

> ***Reviewer #1 (Public review):***
>
> *Summary and Strengths:*
>
> *Shin et al deepen our understanding of high-frequency oscillations in the frontal cortex during REM in a manner that sheds important light on the roles of these events. In particular, they reveal that cortical HFOs are modulated by theta oscillations, occur in chains and recruit cortical neuronal activation patterns in a manner that is distinct from other high-frequency events during non-REM or in the hippocampus. They also show that these events occur during increased oscillatory cross-talk between hippocampus and cortex and may protect cortical neurons from downregulation of firing during sleep. Overall, this is important work with several novel observations pointing towards an important role for these events that will become increasingly understood over time.*
>
> *I also wanted to comment that 2D is a beautiful illustration of separate and essentially exclusive communication channels used during HF events in NREM vs REM. They almost perfectly complement each other's frequencies.*
>
> *Weaknesses:*
>
> *I have only one major scientific critique: I believe we need to see quantification of how phasic REM theta waves with versus without HFOs differ. What do REM HFOs add to the "normal" theta oscillation? Without this comparison, it is more difficult to interpret the meaning of these events. Given that HFO chains have IEIs around the time of a theta cycle duration, are the repeating spiking activities stronger during HFO repeats than during adjacent theta waves without HFOs?*

Here, we provide additional analyses to demonstrate that the phasic, theta-modulated PFC activity that we observe during HFOs is specifically tied to the occurrence of HFOs and not a strong phenomenon during non-HFO-associated theta periods. In Figure S5 M (middle and

right), we find that aligning PFC multiunit activity to theta periods in phasic REM but temporally distant from HFOs does not elicit the same degree of theta-modulated activity as aligning to HFOs (as in Figure 2A and Figure S5 M, left).

Additionally, we provide analyses of the theta periods adjacent to HFOs (at different temporal thresholds) and demonstrate that this theta-modulated spiking activity is largely absent (Figure S5; compare to Figure 2A). Unlike Figure S5, this analysis was not restricted to putative phasic REM.

We have now added Supplementary Figures S5L-N to the revised manuscript.

> *What percentage of theta waves contain HFOs, and what is the firing rate during those theta waves with vs without HFOs? Is there differential firing rate modulation? The authors may even consider that all REM-HFO-specific quantifications should be shown as differential from phasic theta cycles without HFOs.*

Although theta oscillations are continuously expressed during REM sleep, HFOs occur only intermittently, such that only a small subset of theta cycles contain HFOs. Across all animals and epochs included for analysis, we found that ~7.4% of theta cycles contain HFOs. We present an epoch-level quantification of this in Author response image 1, where the proportions were calculated across all, tonic, and phasic theta cycles. As expected, a higher proportion of putative phasic theta cycles contain HFOs.

Regarding differential firing rate modulation, we refer reviewer to normalized MUA plots in the manuscript (Figures 2A and 4F). We would like the emphasize that what we show is PFC multiunit activity that is normalized by the mean population firing rate during REM sleep. Thus, these figures, specifically the chain HFO aligned figure, indicate that there are peaks in activity around baseline level in the background of an overall decrease in population activity relative to baseline (i.e. the troughs surrounding the peaks have lower activity compared to baseline, as in Figure 9C). While this suggests that there is an overall decrease in firing rates during HFOs as compared to baseline theta periods without HFOs, this simply provides a qualitative account of this difference. In Figure S5N, we present firing rate comparisons during HFO chains versus theta periods during putative phasic REM bouts at least 4 theta cycles away from HFOs. We find that HFO chain-associated PFC neuron firing rates are lower compared to non-HFO theta periods, supporting our finding of activity suppression during HFOs.

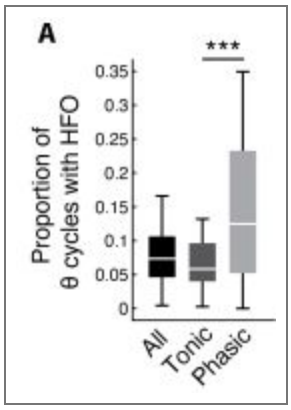

Author response image 1. Proportion of theta cycles with HFOs. (A) Proportion of theta cycles with HFOs across all, tonic, and phasic cycles (***p = 4.90e-05, rank sum test).

Lastly, we appreciate the reviewer's suggestion that REM HFO quantifications could be framed relative to phasic theta cycles without HFOs. We agree that such comparisons are

informative and ensure that the results we present are specific to periods with detected HFOs. In response, we have added additional analyses of theta periods outside of HFOs in Figure S5. Furthermore, while we found that a larger proportion of chain HFOs occurred during bouts of putative phasic REM compared to isolated events (Figure S5 and Figure S3C), most of the analyses that we performed were on events pooled across putative tonic and phasic, since putative phasic REM is relatively scarce (<10%).

We also refer the Reviewer to our response to Reviewer 2's major comment #1 below where we reiterate several of our findings that demonstrate the HFO-specificity of the reported dynamics, as well as our extended response to Reviewer 3's Public Review comment #1 where we show that the dynamics associated with REM HFOs are absent during HFOs detected during awake behavior (comparable theta state) on the W-Track (Figure S11). We hope that the additional control analyses we present as well as our expanded explanations adequately address the Reviewer's concerns.

> *As a non-scientific comment on the manuscript itself: unfortunately, the paper is difficult to read and understand at times, requiring great effort by the reader. This is to an extent that communication is hindered. The paper is dense with changing methods, often from panel to panel. Unfortunately, the panel quantifications are not explained in the results section in a manner that readers can understand without going to read the methods, often for each individual panel. These measures should be explained in a way that lets readers understand the conclusions of each panel and what gross calculations were used to reach those. Instead, too much jargon is used rather than clear descriptions of the overall calculations being done for each panel.*

We have now split and updated the figures in a more logical progression of ideas:

Figure 1: Prefrontal cortical HFOs in REM sleep using spectral analyses.

Figure 2: Characteristic spiking modulation in PFC during REM HFOs.

Figure 3: HFO and gamma distinction in theta cycles, and PFC-CA1 coherence (including chain/ isolated HFOs in phasic and tonic REM stages).

Figure 4: Differential modulation of PFC spiking activity during REM PFC HFOs vs. NREM PFC ripples.

Figure 5: Characteristic PFC population activity during REM HFO chains.

Figure 6: Comparison of PFC reactivation during REM PFC HFOs vs. NREM PFC ripples.

Figure 7: Differential engagement and excitability modulation of CA1 neurons by REM HFOs.

Figure 8: REM theta phase shifting CA1 neurons preferentially engaged by REM HFOs.

Figure 9: (Model) Network model with ACh reproduces spiking modulation during REM PFC HFOs vs NREM PFC ripples.

Figure 10: (Model) Model reproduces restricted REM coactivity vs. widespread NREM coactivity.

We have also rearranged the figures to parallel the main figures and results section.

> *The authors mention in the discussion section that they see increased functional connectivity between mPFC and CA1, but most data suggesting this seems to be based on LFP rather than spiking. Functional connectivity is best defined by spiking-spiking relationships. And these authors have spiking data. So I believe either the descriptive language should be pulled back to something like "oscillatory coupling" or more analyses should be dedicated to showing spike-spike coordination across regions.*

We have updated the manuscript accordingly. Specifically, we have modified the text on Page 13, Lines 23-24:

“These chains are associated with increased measures of oscillatory coupling between PFC and CA1…”

> ***Reviewer #1 (Recommendations for the authors):***
>
> *(1) Please ensure that analytical methods are presented in the same order in the methods section as they are in the results section - panel by panel. That said, the methods section is well-written and presented.*

We apologize for any confusion this may have caused. We have now reorganized the methods section to ensure they presented in the same order as the panels in the main figures.

> *(2) Please specify whether the recordings/behaviors occur during the animal's light circadian phase.*

We have added a statement in the methods under the “Behavior” section on Page 34, Lines 9-12 indicating that the experiments took place during the light phase:

“During the recording day, animals were introduced to the novel W-maze (~80 × 80 cm with ~7 cm wide tracks) for the first time and learned the task rules over eight behavioral sessions during the animals’ light phase between the hours of 9 AM and 6PM.”

> *(3) Please specify how many tetrodes are in mPFC and how many in CA1?*

We have added this clarification on Page 33, Lines 27-28:

“Tetrodes were split equally between PFC and CA1 (15, 16, or 32 tetrodes in each region).”

> *(4) All mentions of "coherence" should have frequency bands specified. "Theta coherence", for example.*

We have now added this information to all relevant mentions of “coherence”.

> *(5) The intuitive logic of the phase slope index (2K) should be briefly explained for maybe half a sentence in the results section. The intuition should be explained better in the methods section devoted to it.*

We have added more clarification on the phase slope index method, both in the legend of Figure 3 on Page 21, Lines 22-23:

“Phase slope index (PSI), which is a measure of phase lag consistency across different frequencies…” and in the methods section under “Phase slope index” on Page 39, Lines 21-26:

“In practice, PSI is used to assess the consistency of phase lag relationships between two signals across different frequency bands and is a measure that is weighted by oscillatory coherence. We opted to use PSI to estimate the directional flow of information instead of other methods, such as Granger causality, since it has been demonstrated that PSI is less prone to false positives.”

> *(6) "Cofiring" and "coactivity" should be defined clearly as measures - preferably in the results section if possible. They sound similar and are somewhat jargon-y without self-explanatory meaning (or difference from each other). How should readers understand and interpret them?*

We apologize for the confusion regarding these two terms, which are both used throughout the manuscript. Here, we specifically used to term “cofiring” to specify the explicit quantification of coincident activity between pairs of neurons (e.g. Figure 4E, left) as described in the Methods section under “Ripple and HFO co-firing”. There were instances where “coactivity” was used to refer to this quantification, and they have been changed to “cofiring”. We have now added a statement to the manuscript to clarify that “cofiring” is a quantification of coincident activity between neurons on Page 7, Lines 34-35:

“Overall cortical co-firing, which is a measure of coincident activity between neuron pairs during discrete events”

Additionally, the term “coactivity” in the manuscript is used when describing neuronal activity in the model or when there are mentions of coincident activity other than the explicit quantification described above.

> *(7) The temporal threshold for "cofiring" should be stated in the results to enable interpretation of the results.*

We apologize for the lack of clarity regarding the cofiring metric. Here, the temporal threshold that we are imposing is determined by the ripple/HFO event times (see Methods section “LFP event detection”). If both neurons in a pair emit spikes within the defined window of an event, they are considered to have “cofired” (Cheng and Frank 2008, Singer and Frank 2009, Sosa, Joo et al. 2020).

We have now clarified this in the results section on Page 7, Lines 34-35:

“Overall cortical cofiring, which is a measure of coincident activity between neuron pairs during discreet events…”

We have also added a clarifying statement in the Methods section under “Ripple and HFO cofiring” on Page 40, Lines 24-25:

“Here, cofiring assesses coincident activity between neuron pairs within the start and end times of events, and thus, no explicit temporal threshold was implemented.”

> *(8) Please clarify more systematically in which region the NREM ripples were detected. The natural assumption is the hippocampus, but at times it is mentioned that they are detected in the cortex. Are they cortical in all analyses? Readers could easily get confused about this and misinterpret "ripples". To clarify further, if these are always cortical events, I suggest renaming "ripples" in this text to "cortical NREM HFOs".*

We apologize for the confusion. For all mentions of “ripples” in the text, we are referring to PFC ripples specifically in NREM sleep. When hippocampal ripples are mentioned, we differentiate them by explicitly using “sharp-wave ripples” or “SWRs”. Our decision to use “ripples” for NREM sleep was based on previous studies that investigated NREM high-frequency events in cortex (Khodagholy, Gelinas et al. 2017, Helfrich, Lendner et al. 2019, Vaz, Inati et al. 2019, Aleman-Zapata, Morris et al. 2022, Ghosh, Yang et al. 2022, Shin and Jadhav 2024). Furthermore, we elected to use the “HFO” nomenclature for high-frequency events in REM sleep, since it has been used in previous studies to describe these events (Tort, Scheffer-Teixeira et al. 2013, Bueno-Junior, Ruckstuhl et al. 2023). Thus, to remain consistent with the literature, we decided to use these terms to describe these sleep-state-specific events throughout the manuscript:

Hippocampal sharp-wave ripples (SWRs) in NREM sleep

PFC ripples in NREM sleep

PFC HFOs in REM sleep

We have now added the following statement on Page 5, Lines 1-3:

“However, to avoid ambiguity, and to conform to previous nomenclature, we refer to cortical NREM events as ripples, cortical REM events as HFOs, and hippocampal sharp-wave ripples in NREM as SWRs throughout.”

> *(9) The analysis performed for 4B is not explained clearly. It is somewhat better explained in the methods. I believe the reader should understand that each HFO is treated as an event, and spiking participation per unit was measured, and then the similarity of that pattern was assessed between HFOs. I also find the x-axis being quartiles makes understanding this graph particularly difficult.*
>
> *Why not label by raw lag and show a correlation plot rather than break down by quartiles? Alternatively, labeling the millisecond values of these quartiles on the x-axis labels may make comprehension much easier.*

We apologize for the lack of clarity regarding this method. We have added points to clarify the analytical procedure used for Figure 4B (Now Figure 5B) on Page 8, Lines 25-28:

“We represented each HFO as a binary vector of PFC neurons active during the event, and computed the Pearson correlation between the vectors of every pair of consecutive HFOs” As well as in the Figure 5 legend on Page 24, Lines 7-10:

“Here, the PFC spiking activity during each HFO was binarized across all neurons and the Pearson correlation coefficient was calculated between adjacent events as a measure of pattern similarity. Then the relationship between pattern similarity and IEI was reported.”

In addition to the quartile labels, we have now added the average inter-event interval (IEI) of each quartile to the x-axis labels of Figure 5B to improve comprehension as well as a statement in the figure legend on Page 24, Line 11:

“Below each quartile is the average IEI of that quartile in milliseconds.”

> *(10) "Rank order analysis" should be again defined in the results in a manner that the reader can follow the point of the analysis and figure. For example, the goal is to assess the spike sequence across HFO events by looking at the regularity of spike timing rank for each neuron in each HFO event. Also, could this correlation be more simply calculated and presented as just a standard deviation around the mean of that cell's rank?*

We apologize for not including an explanation of this analysis in the results section. We have now added more detail about the rank order analysis to the Figure 5 legend on Page 24, Lines 18-21:

“The mean rank-order correlation from the leave-one-out cross-validation procedure. Each event’s rank was correlated with the averaged rank across all other events. The average across all events compared to a distribution of means generated by jittering (n = 1000) spike times is shown.”

We also provided a short description of the procedure in the results section on Page 8, Lines 32-36:

“Furthermore, we examined whether the order in which individual PFC neurons fired during HFOs within a chain was preserved across chains. For each chain, we extracted each cell's first-spike rank order and compared it to a leave-one-out template constructed from the average normalized rank across all other chains.”

Regarding the Reviewer’s second comment about the correlation, if we presented the result as the standard deviation around the mean of the cell’s rank, the result would be similar to the example rank order in Figure 5C, which we provided as a visualization of the rank-order template procedure we used. However, this would not necessarily demonstrate the consistency of population activity across HFO chains. To demonstrate consistency in activity across HFO chains, we used a leave-one-out cross-validated approach where each chain event was assessed separately. For each event, the neurons firing during that event was ranked and normalized 0-1. Then, the average rank of each neuron across all other events was calculated. Lastly, the correlation between the ranks of the left-out event and the average ranks of the template was taken to assess similarity in sequential activity. We opted to use this method since it has been demonstrated to be effective for evaluating similarities in sequential across events (Stark, Roux et al. 2015, Valero, Viney et al. 2021).

> *(11) In Figure 5B and the related results section, I gather that "spatial" relates to place field location rather than anatomical/tetrode location of the neuron? This was not my original understanding and should be stated clearly.*

We apologize for the lack of clarity regarding this result. Yes, the term “spatial” refers to spatial rate map correlation between CA1 neuron pairs, specifically during the behavioral W-Track session prior to the sleep session where cofiring was assessed. We have updated the y-axis label of Figure 5B (Now Figure 7B) to include “rate map” and have updated the results section on Page 9, Lines 32-33:

“…we observed a higher degree of spatial rate map correlation for high cofiring pairs…”

> *(12) Figure 5E and its caption are almost totally unable to be explained since axes aren't explained well in either. It is only by inference from the results text that meaning can be assumed.*

We apologize for the lack of clarity regarding Figure 5E (Now Figure 7E). We have now updated the y-axis labels on both updated figures (Figures 7E and 8B) and have reworded and added more detail to the figure legend on Page 28, Lines 1-5:

“High REM PFC HFO cofiring CA1 neurons exhibited a greater degree of suppression during NREM PFC ripples. For a description of modulation index, see Methods section Ripple/HFO aligned modulation. Here, since CA1 neurons exhibit a robust decrease in activity in response to NREM PFC ripples, we refer to the modulation as suppressive.”

> *(13) Figure 5F is interesting, supporting the concept that HFOs "protect" neurons from downscaling. However, how can a "neuron" be cofiring? Would cofiring not be defined in*

> *a pairwise manner, and so each unit of the cofiring measure would be a pair of neurons? This question applies to other panels in this figure. Please clarify this.*

We apologize for the lack of clarity regarding the exact cofiring metric that we use. For Figures 7D-F and 8A, since we wanted to relate cofiring to changes in firing rate and modulation state during NREM PFC ripples, we calculated single cofiring values for each CA1 neurons by averaging across all pairings with PFC neurons. Thus, this metric gives us an estimate of the overall cofiring strength of each CA1 neuron. We have now added a new section in the Methods under "Calculation of a single cofiring metric and separation into populations of high and low cofiring neurons" on Page 44, Lines 34-43:

"Since we wanted to relate the above cofiring metric to other measures, we needed to obtain a single-value cofiring metric for each neuron. To do this, we averaged the cofiring values across all pairings for a neuron (e.g. 1 CA1 neuron paired with all PFC neurons) and reported it as the cell's cofiring. Furthermore, since we observed a bimodal distribution of CA1-PFC cofiring values in REM sleep, we split the population based on whether the average (across all cell-cell combinations) cofiring value or correlation coefficient of a cell was above or below 0 (High cofiring > 0; low cofiring < 0). Also, since the NREM ripple cofiring distribution was unimodal, we additionally split the populations using the mean of the average cofiring or correlation coefficient distributions (High cofiring > mean; low cofiring < mean)."

We have also clarified this in the Figure 7 legend on Page 27, Lines 25-28:

"For comparisons between cofiring and other metrics (e.g. firing rate), a single cofiring value was calculated for each neuron by averaging the cofiring metric across all neuron pairings. Additionally, high and low cofiring CA1 neurons were split based on average cofiring values > 0 and < 0, respectively."

> ***Reviewer #2 (Public review):***
>
> *Summary:*
>
> *In this study, the authors investigate high-frequency oscillations (HFOs) in the prefrontal cortex during REM sleep. They identify a specific pattern where these HFOs occur in "chains" that are phase-locked to theta oscillations, primarily during the "phasic" periods of REM. The study contrasts these events with isolated HFOs and NREM ripples, suggesting a unique role for these chains in coordinating activity between the prefrontal cortex and the hippocampus. Most notably, the authors report that a specific subset of hippocampal cells-those that co-fire with the prefrontal cortex during these HFOs-increase their firing rates over the course of sleep, suggesting a potential mechanism for selective memory consolidation.*
>
> *Strengths:*
>
> *The study addresses an under-explored area of sleep physiology: the fine-grained temporal coordination between the cortex and hippocampus during REM sleep. The identification of HFO "chains" and their association with higher theta power provides an interesting framework for understanding how the brain might organize information transfer outside of NREM sleep. The observation that specific hippocampal populations show differential firing rate changes based on their participation in these HFO events is a striking finding that warrants further investigation.*
>
> *Weaknesses:*
>
> *The primary weakness of the study lies in the lack of a clear distinction between global brain states and the specific events being analyzed. Because the authors compare HFOs across different sleep stages (NREM, tonic REM, and phasic REM) without sufficient*

> *controls, it is difficult to determine if the observed differences are intrinsic to the HFOs themselves or simply a reflection of the different physiological states in which they occur.*

We would first like to note in case it was unclear – as clearly noted in our manuscript title, state-dependence is an integral part of our results, with the primary comparison in the manuscript being between REM cortical HFOs and NREM cortical ripples, and correspondingly spiking activity patterns observed in prefrontal cortical-hippocampal circuits during these event-types that occur in the two sleep stages. As noted in response to Reviewer 1's Comment #8 and Reviewer 3's Comment #1, to avoid ambiguity and to remain consistent with existing literature, we use the following terms to describe these sleep-state specific events throughout the manuscript: Hippocampal sharp-wave ripples (SWRs) in NREM sleep, PFC ripples in NREM sleep, and PFC HFOs in REM sleep.

We refer the Reviewer to our Response to Reviewer 1's first comment where we provide additional analyses of theta periods outside of HFO times (i.e. baseline REM periods), including Figure S5. We also further address these comments as a response to Reviewer 2's major comment #1 below.

> *Furthermore, the evidence for "structured reactivation" is not yet convincing. The temporal alignment of these reactivation events appears inconsistent, with peaks occurring well before the HFO itself, and the analysis does not sufficiently control for pre-existing cellular assembly strengths.*

We have now addressed this as a response to Reviewer 2's major comments #3 and #8 below, including Figure 6.

> *Additionally, some of the sleep architecture presented appears atypical, such as very short REM bouts and direct NREM-to-REM transitions that bypass standard progression, raising questions about the consistency of the sleep detection across animals.*

We have now addressed this as a response to Reviewer 2's major comment #2 below, including Figure S1 and Figure S3. We expect that addition of these figures will mitigate concerns about our sleep staging procedures and will clarify certain points raised by the Reviewer.

> *Finally, the study does not account for potential confounds like baseline firing rates when interpreting the behavior of "high-cofiring" neurons, which may simply be the most active cells in the population.*

We have now addressed this as a response to Reviewer 2's major comment #6 below.

> ***Reviewer #2 (Recommendations for the authors):***
>
> *In this study, the authors detect activity periods during REM sleep that feature high-frequency oscillations in the prefrontal cortex. They term these REM HFOs and report that they occur in "chains" phase-locked to theta oscillations. They contrast these with HFOs that appear in isolation and with ripples observed during NREM sleep, either in the PFC or in the hippocampus. The data presented is very interesting in places. The authors show that these HFOs are observed primarily during "phasic REM" periods that have higher theta power. It appears that overall firing is substantially lower surrounding these events. Intriguingly, it appears that CA1 cells that co-fire with the PFC during HFOs increase their firing rates over the course of sleep, whereas other neurons show a firing decrease. This seems to be the most striking finding of this study.*
>
> *Major:*
>
> *(1) The findings are generally intriguing, but the study makes some choices that are hard to understand. They begin comparing HFOs that occur in chains to HFOs that occur in*

> *isolation, even though it appears that chained and isolated HFOs likely occur at different times, some during tonic REM, some during phasic REM, and others during NREM. The lack of control for sleep state makes it difficult to determine if the reported differences are intrinsic to the HFO patterns or merely reflections of the underlying global brain state. Overall, I just didn't quite understand the motivation for comparing isolated and chain HFOs, as it seems natural that chains would occur during periods of greater synchrony.*

We appreciate the Reviewer for raising these points and agree that the properties of ripples and HFOs cannot be interpreted independently of the underlying brain state. As we mentioned in the initial response, we do expect that the generation of these ripples/HFOs in NREM and REM sleep are inextricably linked to global brain state (ex., cholinergic tone, as shown in the model in Figures 9-10), which results in differing patterns of activity across sleep states. We noted in the response to the public review comment #1 above that as clearly noted in our manuscript title, state-dependence is an integral part of our results, with the primary comparison in the manuscript being between REM cortical HFOs and NREM cortical ripples, and correspondingly, spiking activity patterns observed in cortical-hippocampal circuits during these event types that occur in the two sleep stages.

Sleep state: Our primary goal in comparing isolated and chain HFOs (chain vs. isolated HFOs are only compared in REM periods, not NREM periods) was not to suggest that the differences that we observe are state-independent, but rather to provide evidence that temporal clustering of HFOs underlies distinct PFC dynamics, as well as enhanced CA1 engagement. Rather than attempting to dissociate ripple/HFO occurrence and the differential physiology that underlie NREM and REM sleep states, we view them as complementary—both sleep states are permissive to generation of high-frequency oscillations. Similarly, putative tonic and phasic REM substates (low vs high theta power) are differentially permissive for isolated and chain HFOs (Figure S3C). We add additional detail on tonic vs. phasic REM substages in Supplementary Figure S3, showing that the rate of HFOs and HFO chains is significantly elevated in putative phasic REM. While we would have liked to analyze REM HFOs during tonic and phasic states separately to be able to make more concrete conclusions, the scarcity of phasic REM sleep made it difficult to make accurate comparisons between the two, especially for spiking modulation. We have therefore removed the qualifying term “phasic REM” from the abstract.

Also, we would like to clarify that while we investigated chains of events (ripples) in NREM sleep as a comparison to REM HFOs, we do not refer to them as HFOs in NREM anywhere in the manuscript. In NREM, while there are PFC ripples that are clustered into chains based on our definition (separation of <200 ms), we do not observe a prominent peak in the IEI distribution that would suggest entrainment by other oscillations (e.g. theta or spindles). This analysis was only to show that associated results are specific to REM HFO chains, and not seen during comparable chains of NREM cortical ripple events.

Chain vs isolated HFOs: Regarding the Reviewers comment about why we chose to compare isolated and chain HFOs, the motivation is clearly demonstrated by differences in these events in spectral properties (Figure 3H-I) and spiking modulation (Figure 4F-G). Our initial motivation to investigate these chains of events in REM sleep came from our observation that PFC population activity aligned to REM HFOs was theta-modulated (multipeaked, suggesting multiple high-frequency events over a short duration). This led us to hypothesize that there may be chaining of events in REM sleep, which in line with previous studies demonstrating the clustering of events, such as spindles in NREM sleep (Darevsky, Kim et al. 2024). In that study (Darevsky, Kim et al. 2024), the authors showed that reactivation of motor patterns was more persistent during trains of spindle events as compared to isolated spindles. Furthermore, trains/chains of multiple hippocampal SWRs have been shown to underlie the replay of extended experience (Davidson, Kloosterman et al. 2009). Thus, the separation of

high-frequency events into isolated and chained events has precedence and may have functional significance. Furthermore, since we see that isolated and chain events have a bias for occurring during putative bouts of tonic and phasic REM sleep, respectively (Figure S3C), characterization of both event types is an important step for understanding potential differences in interregional interactions during REM sleep. Furthermore, a recent appreciation for the role of sleep stage sub-states (Chang, Tang et al. 2025) further emphasizes the importance of investigating these events separately. We expect future studies to further dissect the roles of tonic and phasic REM states in memory and cognition, and our finding provides an account of the existence of different events for future reference.

HFO chains during periods of greater synchrony: While it may seem natural that chaining would occur during periods of high synchrony (theta synchrony here), we show that our result is HFO-specific, especially for spiking activity modulation (Figures 4F-H and Supplementary Figures S5K-N), which makes it novel and important. Previous studies have focused on theta-gamma cross-frequency phase amplitude coupling, which has been proposed as a mechanism where slower theta oscillations temporally organize faster local population activity, thereby synchronizing neural ensembles within and across brain regions (Belluscio, Mizuseki et al. 2012). Here, we present a comparison of HFOs and gamma events and show that while gamma events can also occur in chains (added to Supplementary Figure S4H), possibly due to increased synchrony as the Reviewer stated above, we do not observe theta-modulated population activity aligned to these events (Supplementary Figure S4J), which is a defining property of HFOs that we propose underlies our results. This indicates that our reported results are unique to periods of synchrony associated with HFOs.

Control analyses for theta periods: Regarding the comment about lack of control for sleep state, we refer the Reviewer to our response to Reviewer 1's comments. We have performed additional control analyses comparing PFC activity during REM theta periods adjacent to detected HFOs and demonstrate that phasic PFC population activity is largely absent (Figure S5).

We are aware that it is difficult to dissociate the generation of ripples and HFOs from the underlying brain state, since they are so tightly linked. However, we do expect that our clarifying points in addition to the REM theta state controls provide strong evidence that the results that we present are intrinsic to HFOs and not general reflections of activity during baseline theta activity in REM. Here, we further reiterate a few of the main results that demonstrate this:

(1) Phasic spiking modulation of PFC population activity associated with HFOs is not present during baseline theta periods (Supplementary Figure S5K).

(2) Phasic spiking modulation during HFOs is not linked to extracted gamma events (Supplementary Figure S4J).

(3) Phasic spiking modulation, as well as activity suppression, is strongest during chains of HFOs (Figure 4F, Supplementary Figure S4J).

(4) PFC-CA1 theta coherence surrounding HFOs increases relative to baseline (Figure 3E, z-scored relative to baseline coherence).

(5) Assembly peaks are sequentially organized surrounding HFO chains but not during isolated or shuffled (baseline) HFO times (Figure 6C, Supplementary Figure S7E, and Author response image 2).

(6) A higher proportion of CA1-CA1 pairs are high cofiring during HFOs as compared to baseline periods (Figure 7B), indicating specific CA1 engagement during HFOs (in addition to coherence).

Lastly, we show that HFOs detected during periods of active behavior (high theta) on the W-Track are not associated with many of the defining features of HFOs in REM sleep, thus demonstrating the specificity of REM HFOs despite similar background theta activity (Figure S11, in response to Reviewer 3 comment #1).

> *(2) It is crucial that the study provides REM-specific sleep examples for each of the data sessions, marking tonic and phasic REM and indicating when isolated and chain HFOs are observed. It remains unclear how interspersed these events are. Do some REM episodes just have isolated HFOs and others chains?*

We thank the Reviewer for raising this point and apologize for the lack of clarity. For additional transparency, we now provide example sleep state plots for each animal (Supplementary Figure S1H-I).

We also provide hypnograms that show bouts of putative phasic REM on top of REM periods (Supplementary Figure S3). Additionally, as a compact way of demonstrating the validity of our separation of putative tonic and phasic bouts, we provide a plot showing the average velocity and spectrogram surrounding putative phasic REM bouts across all putative phasic REM transitions (Supplementary Figure S3A). Regarding the incidence of HFOs in tonic and phasic REM, we refer the Reviewer to Supplementary Figure S3D, where we show that HFO rate is significantly higher during putative bouts of phasic REM, during which they tend to be organized in chains as compared to putative tonic bouts (Supplementary Figure S3E). In line with this, we additionally report that although both isolated and chain HFOs occur in putative tonic and phasic bouts of REM sleep, the proportion of chain HFOs during phasic REM is significantly higher than that of isolated HFOs (Figure S3), indicating a bias for chains to occur in phasic REM sleep, potentially due to stronger theta input. However, since putative phasic REM accounts for <10% of REM sleep in our dataset, consistent with previous reports using similar methods (Mizuseki, Diba et al. 2011), we were unable to restrict spiking analysis to HFOs in phasic REM. We found that chain HFOs during both putative tonic and phasic REM sleep elicited theta modulated population activity in PFC, thus we pooled HFOs across REM states for analysis.

While a larger proportion of chain events occur in putative bouts of phasic REM sleep as compared to isolated events (Figure S3), chain and isolated events occur in both putative tonic and phasic substates (Proportion of events in putative tonic REM is (1 - proportion in phasic) shown in Figure S3C, right). Thus, the majority of analyses comparing isolated and chain HFOs, especially for spiking data, were pooled across states. Instead of showing example plots for all 22 sleep epochs (22 out of 36 epochs with >5 s of putative phasic REM), we expect that this analysis will be sufficient to illustrate the distributions of isolated and chain HFOs across putative REM sleep substates. We have also removed the qualifying term “phasic REM” from the abstract.

To clarify this, we have added a statement to the new “Limitations” section of the manuscript on Page 16, Lines 10-20:

“Third, we did not record eye movements or ponto-geniculo-occipital (PGO) waves, both of which would have allowed for more accurate segregation of tonic and phasic REM sleep states. (Simor, van der Wijk et al. 2020) Although we observed a bias for isolated and chain HFOs to occur in putative tonic and phasic REM substates, respectively, the scarcity of putative phasic REM bouts made the direct comparison based on substage difficult. Finally, although our model predicts that distinct cell-type activity profiles shape REM sleep HFO dynamics, we did not record a suDicient number of interneurons to test these predictions directly. Future studies using appropriate behavioral tasks, longitudinal sleep recordings, and cell-type specific opto-tagging will be able to resolve these limitations and further clarify the roles of high-frequency oscillations in REM sleep.”

We have now added Supplementary Figure S3.

> *This is also important because some of the REM sleeps detected and shown in Figure S1H seem unusual. For example, in Animal 1, there are multiple bursts of REM that seem very irregular. In some other sessions, animals occasionally appear to enter REM sleep with very little preceding NREM, which goes against existing literature. It's not clear which ones of these meet the 30 s duration threshold. Are the chain events occurring in these periods?*

In reference to the hypnograms shown in Supplementary Figure S1H (Now Supplementary Figure S1I), these were generated by concatenating all 9 sleep epochs regardless of whether they passed the inclusion criterion of > 30 s of total REM sleep. Furthermore, only a subset of the epochs shown were included for analysis based on a secondary, manual inspection that is performed to confirm inclusion. Sleep state plots (e.g. Supplementary Figure S1H) were visually inspected to further confirm the transition into REM sleep, ensuring absence of noisy T/D ratio or spurious detection due to noisy signals – epochs where microarousals or persistent subthreshold fluctuations in animal movement induced noisy TD ratio increases, and thus inaccurate REM designation, were excluded. We thus used a total of 36 sleep sessions from a possible 90 sleep sessions.

We apologize for not specifying what portions of data represented by the hypnograms were included. We have now provided updated hypnograms only illustrating the sleep epochs included for analysis (Figure S1I).

We have now added Supplementary Figure S1.

Regarding the Reviewer's point "Are the chain events occurring in these periods?": Yes, all of the chain events (and isolated events) come from these updated epochs that are now shown. No events in the excluded epochs were included, since we wanted to only analyze the data that came from curated REM epochs that we were confident in.

> *(3) The analysis supporting structured reactivation was not generally convincing. Figure 4E does not provide convincing evidence of this. Indeed, reactivation strength is lowest around the time of the event, and appears highest 0.5s before. The example panel seems rather anecdotal. It's also not clear why REM reactivations should be compared to NREM ones here. I could not follow what was done in Figures 4F-H. Why should the first half and second half of an HFO event be correlated?*

We appreciate the Reviewer for raising these concerns. We agree that this section is somewhat dense and at time hard to follow, so we will clarify with further explanations and analyses (see also response to Comment #8 with new reactivation figures).

In Figure 6B (originally Figure 4E), our intention was to show that if you simply align assembly activation to REM HFOs, a relatively flat response is observed when averaged across all assemblies, in stark contrast to assembly reactivation during NREM cortical ripples. This could suggest a couple of things: 1) There is no real assembly activation in response to REM HFOs or 2) Assembly activation is organized differentially (compared to NREM) surrounding HFOs. What we hypothesized, and then quantified based on observations, is that assembly activity is sequentially organized around HFOs. If this were true, it would suggest a consistent temporal relationship between REM HFOs and assemblies (for example, assembly 1 tends to be active 115 ms after the onset of chains, assembly 2 is active 230 ms after, etc.). Of course, the sequential pattern that we show in Figure 6A may arise trivially, especially since these types of sequential visualization plots can simply arise from noise. Thus, a cross-validation method must be utilized to ensure the sequences are indeed reflective of an underlying computation.

In the methods section “Assembly sequence detection surrounding HFOs” we explain the splitripple/HFO procedure that we used to compare assembly sequences across two halves of the data, similar to methods used in hippocampal place cell sequence cross-validation (Plitt and Giocomo 2021, Sosa, Plitt et al. 2025). For every split and assembly alignment, a sequence similar to Figure 6A, right is generated based on the first half of aligned data. Then the second half of aligned data is sorted based on the peak indices of the first half of data and the correlation between the peak reactivation indices across all assemblies for the two datasets is calculated. A high correlation indicates high sequence similarity across the two halves of data (not two halves of an HFO as the Reviewer mentioned), suggesting temporal consistency of assembly reactivation. By utilizing this method, we show that assembly reactivation sequences across randomly chosen halves of data are most similar for chained HFOs (Figure 6C and Supplementary Figures S7C-F). We have now provided an additional control analysis that investigates this sequential assembly activity for time-shifted chain events (Author response image 2). As in Figure 6, assembly activity was aligned to the first event in each time-shifted chain. In addition to the analyses in Supplementary Figure S7, this control further indicates that sequential assembly activity is preferentially restricted to HFO chains.

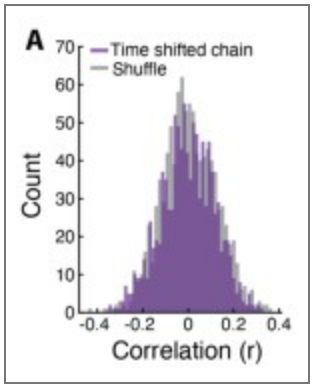

Author response image 2. Assembly sequences surrounding time-shifted HFO chains. (A) Distributions of r values calculated from the Pearson correlation between peak reactivation bins across all assemblies for two randomly chosen halves of the shifted HFO-aligned data. There was no difference between r values for time-shifted chains and shuffled data, indicating no structured assembly activity during periods outside of real HFOs chains.

To further quantify this, we calculated two additional metrics: 1) the slope difference between fitted lines for the two halves of data for each split and 2) the absolute peak difference between assemblies in the two halves of data. First, for the slope difference metric, the slope of the best-fit line between assembly ID and peak reactivation index was taken for the two halves of data and compared. A smaller slope difference compared to shuffled data in Figure 6D indicates that assembly reactivation is structured in a more similar manner across the two halves of the real data. Secondly, Figure 6E is a quantification of the peak reactivation displacement between the two halves of data. If there is a high probability of small peak differences, as in the real data, this indicates that the timing of peak reactivation of assemblies relative to HFO chain onset is similar across the two halves of data.

We apologize for the omission of the description of the slope and peak difference metrics that we used in Figures 6D,E. We have added information in the Methods section under “Assembly sequence detection surrounding HFOs” on Page 43, Lines 23-33:

“Furthermore, the slope and peak differences were calculated as additional metrics of sequence and temporal reactivation consistency between the two halves of data, respectively. For the slope difference metric, the slope of the best fit line between assembly ID and peak

reactivation index was taken for the two halves of data and compared. A smaller slope difference compared to shuffled data indicates that assembly reactivation is structured in a more similar manner across the two halves of the real data. For peak reactivation difference, the temporal displacement of the peak reactivation index between the two halves of data was calculated and compared to shuffle. A high probability of small peak differences indicates that the timing of peak reactivation of assemblies relative to HFO chain onset is similar across the two halves of data. Shuffling of assembly strength was carried out as above."

> *(4) The authors argue that the occurrence of HFOs, rather than theta power, is the reason for lower MUA activity, but the analysis for this (Figure S4I) is quite confusing. The left panel actually seems to indicate that MUA is indeed lower when theta power is high.*

We apologize for the confusion regarding this figure and appreciate the Reviewer's point that periods of high theta power can also appear to be associated with reduced MUA. We agree that the original presentation may not have clearly separated the contributions of theta and HFOs. What we convey with Supplementary Figure S5K (originally Supplementary Figure S4I) and new Supplementary Figures S5L-M is that the observed theta-modulated PFC spiking response (Figure 2A) cannot be solely explained by baseline theta periods (outside of HFOs) in REM sleep. Since theta oscillations are ubiquitous during REM sleep, an important control is to demonstrate that the theta-modulated population activity is not simply a consequence of ongoing theta activity. Thus, we aligned PFC activity to theta oscillations of varied power and show that the fluctuating, theta-modulated population activity is absent, indicating that HFOs associated with the theta oscillation are driving this phasic response.

We are not solely arguing that the presence of HFOs is the driver of decreased PFC multiunit activity. In both the data and model, we show that the magnitude of theta power detected in PFC (possibly input to PFC) is inversely related to multiunit activity (Figure 9E). Our interpretation is not that theta is unrelated to MUA, but rather that HFO occurrence provides additional explanatory power beyond theta alone. Accordingly, we show directly in Supplementary Figures S5L-M, in response to Reviewer 1's comment #1, that theta periods in phasic REM not associated with HFOs do not elicit the MUA activity suppression similar to HFOs.

> *The phase-alignment performed is hard to follow and is not being applied to HFO periods. If the study is trying to argue that high-theta periods without HFOs in the same recording sessions show lower MUA, then perhaps some sort of shuffle or jitter would be more suitable. For example, in Figure 1B, it seems there are some high-theta periods that don't have HFOs and appear to have higher MUA.*

We expect that the new analyses where we provide additional baseline theta controls for periods adjacent to HFOs in Supplementary Figures S5L-M now clarifies this point. Briefly, alignment to theta phases at different temporal distances from detected HFOs does not exhibit the same fluctuating PFC activity as HFO alignment.

Regarding the phase alignment procedure that we used for the control analysis, since REM sleep is characterized almost entirely by ongoing theta activity, the control condition was not a separate brain state but rather theta periods outside of HFOs. We therefore needed a systematic way to select comparable theta cycles and phase bins in order to make a valid comparison with HFO-aligned PFC population activity. Since we demonstrated that there is significant phase amplitude coupling between theta and HFOs, thus a theta phase preference of HFOs, we used that specific phase bin across multiple theta cycles to align PFC activity. This phase bin selection was performed separately for each epoch to account for inter epoch and animal variability in phase preference. We reasoned that this procedure would allow for a valid comparison as compared to random alignment, since activity was aligned to similar phases in the baseline theta vs HFO conditions.

> *(5) As far as I could tell, the study does not distinguish between putative excitatory and inhibitory neurons in the PFC, but only in the CA1, even though these play very different roles in the model. What is the rationale for not separating these? How are reactivations to be interpreted among interneurons?*

We apologize for the lack of emphasis on this point, which was originally highlighted in Supplementary Figure S2G (now in Supplementary Figure S2F), and for omitting the explanation as to why we did not separately analyze putative excitatory and inhibitory neurons. When we plot the average waveform peak-to-trough and mean firing rates of the PFC neurons, we observe a large cluster with moderate mean firing rates and peak-to-troughs consistent with recording primarily from pyramidal neurons (Supplementary Figure S2F, left). We therefore decided to pool and not separate the populations into putative pyramidal cells and interneurons for the spiking analyses presented. To further validate our decision to pool the cells, we separated the population into putative pyramidal cells and interneurons based on peak-to-trough. Putative interneurons were identified as cells with a peak-to-trough <0.3 ms (we obtained similar results when using a hyperplane to separate units based on both peak-to-trough and firing rate, with a smaller subset identified as putative interneurons). When these putative interneurons were excluded from the HFO-aligned multiunit PFC plot, we observed very similar activity to Figure 2A (Supplementary Figure S2F, right). We thus decided to pool the cells into a single population for the purpose of this manuscript, as we did not have enough interneurons to investigate them separately. We are, however, aware that different cell types may contribute to the phenomenon that we report here and attempt to more thoroughly differentiate the contribution of pyramidal cells and interneurons with our modeling result in Figures 9 and 10.

We have now added the following to the figure legend on Page 51, Lines 21-24:

“REM HFO aligned PFC multiunit response when spikes from putative interneurons are excluded (compare to Figure 2A). Due to this similarity of the phasic PFC response when putative interneurons are omitted, we decided to pool PFC neurons for all further analyses.”

Regarding the interpretation of reactivation in the context of interneurons, we expect reactivation reflects coordinated ensemble activity with excitatory neurons encoding task-relevant information, and inhibitory interneurons shaping timing and neural synchronization. We however did not record enough distinct interneurons to test the predictions of the model, which is now noted in the Limitations on Page 16.

Relatedly, we find that PFC assemblies detected from pooled data have task relevant representations (Figures 5F-G).

> *(6) Are the high-cofiring CA1 neurons generally higher-firing than the other cells? Could this perhaps explain why they behave differently?*

We apologize that this information was not more evident in the manuscript, as it is an important control. In Supplementary Figure S9A, we show that there was no difference in baseline firing rate between low and high cofiring CA1 neurons.

We have now explicitly referenced this figure in the main text on Page 9, Lines 42-45:

“Analysis of low and high cofiring CA1 neurons during REM HFOs showed that high cofiring neurons exhibited elevated activity during chained events as compared to low cofiring neurons (Figure 7D), independent of baseline firing rates (Figure S9A).”

> *(7) It appears that the decreased firing around HFO's could be a consequence of the stronger firing modulation around these periods, related to time averaging, rather than*

> *suppression per se. How does the firing rate compare to other periods with similar modulation that might not have HFOs?*

We thank the Reviewer for raising this important point. We expect that the new analyses, where we provide additional baseline non-HFO-associated theta periods, and theta periods adjacent to HFOs at different temporal distance as controls in also Supplementary Figure S5L-N now clarifies this point. These figures show that the decreased firing rate is specific to HFO chains (Supplementary Figure S5N). Indeed, if the suppression that we observe is related to time averaging, or another analytical artifact, our claims of suppression during HFOs would not be valid. We present a number of results and provide further explanations to support the accuracy of our characterization of PFC population suppression.

First, event-aligned multiunit activity was quantified as baseline-normalized population firing relative to detected events. For both NREM and REM, activity was normalized by the mean population firing rate during a baseline period within the same sleep state in which events were detected. Values are therefore expressed as deviations from baseline. This normalization allows comparison of relative changes in firing around events within each state. Importantly, values below baseline reflect reductions relative to the state-matched baseline period.

Second, we show that smoothing activity with a larger gaussian kernel preserves the dip in population activity, consistent with suppression of activity surrounding HFOs (Figure 9C, note that this is a data figure presented in the context of the model). However, as raised by the Reviewer, this normalized measure does not on its own distinguish sustained suppression from transient deviations introduced by event-locked temporal structure in firing.

Third, to address this, we employed an alternative method to demonstrate that HFO chains tend to occur during periods of PFC suppression (Figure 4G). Briefly, we detected events in PFC where activity fell below a threshold and calculated the probability of HFOs surrounding these “suppression” events. We refer the Reviewer to the Methods section under “Detection of population suppression” where we explain this procedure in more detail. We found that chain ripples, during which the strongest suppression is observed (Figure 4F), are associated with decreases in PFC activity (Figure 4G and Supplementary Figure S6).

Fourth, we refer the reviewer to Figure S5N, where we compare the firing rates of PFC neurons during HFO chains and theta periods outside of HFOs during putative phasic REM bouts. The observed reduction in firing during true HFO chains compared to non-HFO periods therefore reflects HFO event-specific activity suppression rather than a common occurrence during baseline REM periods.

Lastly, we performed a control analysis complimentary to Supplementary Figure S5K where we aligned PFC activity to the preferred theta phase of HFOs and investigated how distance from detected HFOs modulates PFC activity (Figure S5). We found that there was no consistent theta-modulated activity aligned to HFO-adjacent theta phases.

Regarding the final comment, if the Reviewer meant “modulation” as in the theta modulation or suppression observed when PFC population activity is aligned to HFOs (Figures 2A and 4F), we are not aware of any other REM periods where this strong theta modulation or suppression of PFC population activity is present. To our knowledge, we are the first to demonstrate such a modulation of PFC population activity in REM sleep. The closest comparison that we can make is PFC activity aligned to gamma events that are coordinated with HFOs (suppression of PFC), but this is explained only with association with HFOs, as shown in Supplementary Figure S4J.

> *(8) The assembly reactivation measure does not control for pre-existing assemblies. The term "activation strength" would therefore be more appropriate.*

We thank the reviewer for this important methodological point. The concern that ICA-based reactivation strength does not, by itself, distinguish behavior-induced reactivation from pre-existing assembly activity/structure is well-taken, and we have implemented several complementary analyses that directly address these concerns.

First, the interleaved structure of our recordings (8 run epochs interleaved with 9 sleep epochs) allows us to investigate the within-session pre/post assembly strength differences (i.e. each W-Track run session has a preceding (pre) and following (post) sleep session). An increase in assembly strength from pre to post is a hallmark of behaviorally relevant assembly reactivation (Kudrimoti, Barnes et al. 1999, Peyrache, Khamassi et al. 2009). For each run epoch, the same run-derived templates were projected onto the preceding and following sleep epochs, and the pre and post strengths were compared. The distribution of post-minus-pre reactivation differences across all epoch pairs is significantly skewed toward positive values (Figure 6F), indicating that templates from the run epochs are more strongly expressed in the post-sleep epochs. This asymmetry cannot be explained by pre-existing assembly structure, which would predict similar assembly strengths.

Second, reactivation strength in post-experience sleep increases across the experiment, with templates from later running epochs producing the strongest reactivation in the following post-sleep (Figure 6G). This increase in reactivation strength over time cannot be explained by preexisting assembly structure, which predicts similar assembly expression strength independent of experience.

Third, the detected assemblies carry behaviorally meaningful structure. Assembly activation maps computed during running exhibit spatially organized "assembly fields" similar to single-cell place fields (Figure 6H), demonstrating that the detected assemblies represent specific spatial locations or task variables rather than behavior-independent states. Pre-existing co-firing structure unrelated to ongoing experience would not be expected to produce spatially tuned, task-locked assembly activation. Furthermore, this spatial tuning of assemblies was verified by comparison with surrogates, where assembly maps were generated using circularly shuffled activation times (1000 shuffles). Assemblies with $p < 0.05$ ($z > 1.65$) were considered to have significant spatial structure (Figure 6I).

These results establish that what we measure is the selective re-expression of behaviorally relevant assemblies in subsequent sleep epochs, consistent with the use of "reactivation" in the established literature (Peyrache, Khamassi et al. 2009, Lopes-dos-Santos, Ribeiro et al. 2013). We have therefore retained the term "reactivation strength" and have added text to the manuscript noting these new results that justify the use of “reactivation” strength.

We have now added Figure 6.

We have also added the procedure for the calculation of spatial information to the Methods section under “Spatial information of assembly fields” on Page 44, Lines 8-23.

> *(9) Can the study rule out that the rank-ordering in Fig 4C is related to firing rates? Higher-firing rates tend to fire earlier, and lower-firing cells later.*

We thank the Reviewer for raising this interesting point. Here, we assume that the Reviewer meant the baseline firing rates of the neurons, not the intra-HFO firing rates of the neurons. Indeed, when we look at baseline REM firing rates of these PFC neurons, we do find that neurons with higher firing rates tend to fire earlier than low-firing-rate neurons (Author response image 3). This is also true when PFC rank and firing rate are assessed for isolated REM HFOs and NREM PFC ripples (Author response image 3). Similarly, we also observe this relationship in CA1 during SWRs, during which rank order correlation is typically assessed as a method for replay detection. In line with this, a previous study has shown that CA1 neurons with high excitability at animals’ current location tend to initiate replay events (Karlsson and

Frank 2009). Furthermore, high-firing-rate, rigid CA1 neurons are more active during SWRs than low-rate, plastic neurons (Grosmark and Buzsaki 2016), and there are distinct populations of neurons in both hippocampus and PFC that are preferentially active during immobility in sleep epochs (Jarosiewicz, McNaughton et al. 2002, Kay, Sosa et al. 2016, Tang, Shin et al. 2017), potentially biasing replay activity during high-frequency events. Similar dynamics may underlie activity during PFC ripples and HFOs in NREM and REM sleep, respectively. The critical point here is in the leave-one-out cross-validation that we implemented to determine sequence similarity—each left out event's cell rank was correlated with the averaged rank of the template that was generated from all other events. This analysis provides a basis for our claim that there is preserved sequential PFC activity across HFO chains. We did not observe neuron firing consistency during isolated HFOs or during pseudo-HFO chains (coherently shifted chain HFO times), which indicates that REM HFO chains are unique temporal windows during which PFC activity proceeds in a more structured manner.

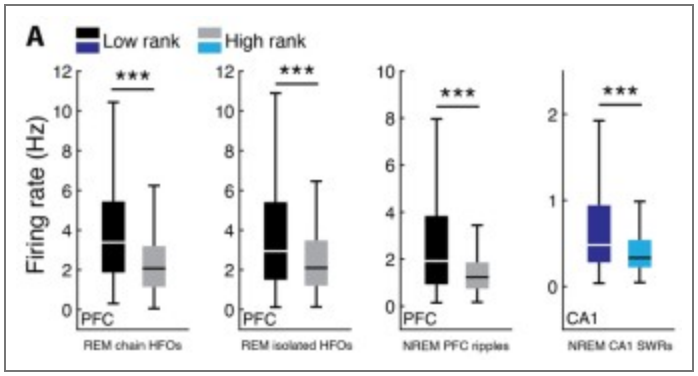

Author response image 3. Firing rate difference of low and high rank neurons (A) Comparison of baseline firing rates of PFC and CA1 neurons split by average rank across all PFC REM HFOs, PFC NREM ripples, or CA1 SWRs. Baseline rates were calculated separately for NREM and REM sleep.

> *Minor:*
>
> *(1) It gets confusing that the authors sometimes (but not always) refer to HFOs during NREM as "ripples" but not if they occur during REM. The terminology is inconsistent. When they refer to HFO chains, it seems they now pool between REM and NREM periods, as well as across phasic and tonic REM periods, which is confusing.*

We apologize for the confusion regarding the terminology. In the revised manuscript, we now use NREM ripples exclusively for NREM events and REM HFOs exclusively for REM events. We have removed mixed labels such as "ripple/HFO" except where a collective term is explicitly defined. We also clarified that HFO chains refer to REM events only and revised the relevant text/figure legends to avoid any implication that chain analyses pool NREM and REM events.

> *(2) P7 L8: It might be helpful to emphasize "broader temporal distribution".*

We thank the Reviewer for the suggestion. We have updated the text on Page 8, Line 18:

"Since we observed a broader temporal distribution of activity…"

> *(3) P8 L9: What do they mean by spatial? Do they mean the place-fields of these same neurons during a previous task period?*

We apologize for the confusion. The Reviewer is correct. Here, we calculated the spatial rate map correlation between CA1 neurons as a measure of place field similarity during the W-

Track session prior to the sleep epoch being assessed.

For clarification, we have added “rate map” to the text on Page 9, Line 33:

“…spatial rate map correlation…”

We have also updated the y-axis label for Figure 7B for clarity.

> *(4) P8 L27: What do they mean by "coordinated SWRs"? As opposed to what?*

Here, we are referring to our previous study where we investigated ripples in NREM sleep and showed that ripples and SWRs in PFC and CA1, respectively could either be independent from or coordinated with events in the other region (Shin and Jadhav 2024). A main result in the study showed that CA1 neurons are strongly suppressed during independent PFC ripples and that there was a relationship between activity suppression and reactivation during coordinated SWRs (CA1 SWR-PFC ripple coordination in NREM). We specifically mentioned “coordinated” since these are SWRs that are also coupled with SOs and spindles as compared to SWRs that are independent from PFC ripples (Shin and Jadhav 2024). Overall, we wanted to frame this result in the context of oscillatory coupling and mechanisms of memory consolidation.

> *(5) P37 L28 says "we observed a bimodal distribution" but L31 says "unimodal". Which is it?*

We apologize for the confusion. We observed a bimodal distribution for CA1-PFC cofiring in REM sleep, but a unimodal distribution in NREM sleep. Because of these two observations, we decided to split the CA1 population into high and low cofiring neurons based on two different thresholds:

(1) Splitting the population by cofiring values greater than (high cofiring) or less than (low cofiring) 0.

(2) Splitting the population by cofiring values greater than (high cofiring) or less than (low cofiring) the mean of the distribution of averaged cofiring values.

Using two separate thresholds to split high and low cofiring CA1 neurons demonstrates the robustness of the firing rate change result in Figures 7F and Supplementary Figures S9B-D.

We added a statement that clarifies that the bimodal distribution was seen in REM sleep only on Page 44, Lines 37-43:

“Furthermore, since we observed a bimodal distribution of CA1-PFC cofiring values in REM sleep, we split the population based on whether the average (across all cell-cell combinations) cofiring value or correlation coefficient of a cell was above or below 0. Also, since the NREM ripple cofiring distribution was unimodal, we additionally split the populations using the mean of the average cofiring or correlation coefficient distributions.”

> ***Reviewer #3 (Public review):***
>
> *Summary:*
>
> *Shin et al. examine hippocampal-prefrontal interactions during sleep using simultaneous CA1 and prefrontal cortex recordings in rats performing a spatial memory task. They identify high-frequency oscillation (HFO) events in PFC during REM sleep that occur in theta-modulated chains and are associated with increased CA1-PFC coherence and sequential, sparse reactivation of cortical ensembles. This pattern contrasts with the synchronous reactivation observed during NREM cortical ripples. Together with a simple cholinergic network model, the authors propose that REM HFO chains represent a*

> *distinct mechanism for hippocampal-cortical coordination that complements NREM ripple-mediated processing during sleep.*
>
> *Strengths:*
>
> *A major strength of the work is the extensive electrophysiological dataset, which includes simultaneous recordings of large neuronal populations in both hippocampus and prefrontal cortex across behaviour and subsequent sleep. The analyses linking high-frequency events to population dynamics, interregional coherence, and ensemble reactivation are technically sophisticated and provide an incredibly detailed description of REM-associated cortical activity patterns. In particular, the demonstration that REM HFOs occur in chains aligned to theta phase and organise sequential activation of cortical assemblies represents a potentially important advance in understanding the neural structure of REM sleep activity. The integration of experimental data with a computational model further provides a useful framework for interpreting the observed differences between REM and NREM network states in terms of neuromodulatory influences.*
>
> *Weaknesses:*
>
> *While overall this study provides a highly valuable body of work, there are two primary limitations, which, if overcome, would provide substantially more significance to the overall characterisation of REM HFOs. Specifically:*
>
> *(1) Distinction from wake HFOs*
>
> *The results largely support the authors' claim that REM HFO chains represent a distinct pattern of neural coordination compared to NREM cortical ripples. The analyses consistently show differences between REM and NREM events in terms of neuronal modulation, ensemble structure, and interregional coupling. However, similar high-frequency events during wake are not examined. Since REM sleep shares several network features with wakefulness, including strong theta oscillations, evaluating whether comparable PFC HFOs occur during wake would provide clarity on whether these events are specific to REM sleep (and its associated functions) or represent a more general theta-associated phenomenon.*

To investigate PFC high-frequency oscillations during running behavior on the W-Track, events were extracted in the same manner as NREM and REM events (Methods). Events during wake were subset by periods where the animals' velocity was >4 cm/s to provide a comparison of events during periods of high theta. While we were able to detect HFOs during wake that exhibited a similar spectral profile in the high frequency band, we did not observe 1) strong association with gamma or theta oscillations, 2) prominent HFO chaining, 3) HFO aligned theta modulated PFC activity, 4) comparable levels of theta phase amplitude coupling, 5) association with population suppression, or 6) a relationship between peri-event theta power and multiunit activity (Supplementary Figure S11). Many of the defining features of PFC REM HFOs are absent during wake, indicating REM specificity of the results we present.

> *(2) Link to memory consolidation*
>
> *The manuscript proposes throughout that REM HFO chains may contribute to memory consolidation by coordinating hippocampal-cortical reactivation, but the evidence for this functional role remains indirect. The authors do highlight this as a limitation of the study - the inability to link their findings to learning - but it is not clear why. Further details of the behaviour results should be included. If no learning occurred across the eight behavioural sessions, this should be reported. If learning did occur, but could not be linked to HFO events, this should also be reported.*

To address these concerns, we have now added an explicit “Limitations” section in the main text of the manuscript that includes a statement about learning. We have also added Supplementary Figure S1 in the manuscript, which illustrates the performance of all 10 animals on the W-Track task. Finally, we have also included Figures 6F G in the manuscript, showing that PFC assembly reactivation strength during sleep epochs increases during learning.

> ***Reviewer #3 (Recommendations for the authors):***
>
> *Most of my specific comments were related to further clarification that will help the reader's understanding.*
>
> *(1) I'd recommend simplifying terminology. Open to debate, but would it not be simpler and clearer to just say NREM HFO vs REM HFO? Obviously, there is a need to mention how NREM HFOs have previously been referred to as cortical ripples, but I'm not sure it is such a helpful terminology to continue for the field, given, as you state, how different cortical ripples are from hippocampal SWRs. If not, I'd at least provide a clearer explanation early in the manuscript, distinguishing NREM ripples from REM HFOs but collectively still calling them 'cortical events'.*

We appreciate the Reviewer’s suggestion regarding terminology and agree that it would be simpler and clearer to use a single term, ripple or HFO, to describe these events. Initially, we had used a unified term (ripples across both states) but ultimately decided to switch to state-specific terminology due to previous comments we received on the manuscript and to emphasize the distinctions between NREM and REM events. Ultimately, we decided on calling them ripples in NREM and HFOs in REM since there is precedence for both terms in each respective sleep state (Khodagholy, Gelinas et al. 2017, Vaz, Inati et al. 2019, Bueno-Junior, Ruckstuhl et al. 2023, Shin and Jadhav 2024), but we do agree that this distinction can be confusing if not clearly stated. Thus, we have added an additional statement in the manuscript on Page 4, Line 44 to Page 5, Lines 1-3 for clarity:

“Similar criteria were used to detect cortical high-frequency events in NREM and REM states; however, to avoid ambiguity and to conform to previous nomenclature, we refer to cortical NREM events as ripples, cortical REM events as HFOs, and hippocampal sharp-wave ripples in NREM as SWRs throughout”

> *(2) I assume experiments occurred during the light phase, but it would be good if this could be stated explicitly.*

We have now added text specifying that these experiments took place in the light phase on Page 34, Lines 9-12 of the Methods section under “Behavior”:

“During the recording day, animals were introduced to the novel W-maze (~80 × 80 cm with ~7 cm wide tracks) for the first time and learned the task rules over eight behavioral sessions during the animals’ light phase between the hours of 9 AM and 6PM.”

> *(3) Page 2 Line 14: Rephrase to make clearer, e.g. 'that have a shift in...'.*

We have rephrased the sentence for clarification on Page 2, Lines 13-15:

“REM HFO chains also preferentially engage CA1 neuronal populations that demonstrate a shift in their preferred theta-phase from behavior to REM sleep.”

> *(4) Page 4 Line 36 - 'and find coherent shifts in TD', this is self-fulfilling. I would rephrase to something like 'resulting in...'.*

We have rephrased the sentence on Page 4, Lines 36-38:

"We separated NREM and REM sleep stages based on theta-to-delta (TD) ratio in CA1, which revealed coherent shifts in TD ratio across CA1 and PFC at the onset and offset of REM sleep…"

> *(5) Figure 1H left - clarify how many animals or multiunits this is based on.*

We have now updated Figure 1 legend to specify the number of animals and epochs included on Page 19, Line 4:

"REM HFO aligned multiunit activity (MUA) in PFC (n = 10 animals, 36 epochs)…"

> *(6) Figure 1I (right), it would be useful to see the x-axis frequency start from 0, since you are cutting the peak in power.*

We thank the Reviewer for this suggestion. We had initially set the frequency limits to 4 and 12 to specifically illustrate the absence of theta-modulated activity during NREM ripples. However, as suggested by the Reviewer, it is informative to expand the frequency range to ascertain the location of the peak frequency for NREM. Indeed, the peak frequency of NREM ripple-aligned PFC activity tends to be lower than 4 Hz, which is consistent with a single peak of activity that lasts <1 s.

We have now updated Figure 2C with these new panels.

> *(7) Figure 5 E/I - use of ** is confusing, it looks like a significance comparing e.g. quartile 2 to 1, but I think this is the correlation significance. I'd move ** to the top right corner and ideally include rho values.*

We thank the Reviewer for this suggestion. We have now added the r values for the correlation to Figures 7E and 8B to resolve any ambiguity. In addition, we updated Figure 7F, right and Figure 5B to maintain consistency across main figures.

> *(8) Figure 7D - Why are stimulated and non-stimulated cells so different at baseline? This is not the case for the NREM results.*

The y-axes in Figures 10C,D (Formerly Figure 7) show the fraction of cells with at least one spike per 10ms bin, either for all pyramidal cells or all interneurons. We report in the figure legend that the stimulated cells represent only 30% of the network for any given stimulus (Page 32, Line 18), so at baseline in both the NREM and REM simulations, there are roughly 3x as many non-stimulated cells with a spike per 10ms bin compared to stimulated cells, as these populations are active at roughly equal firing rates per neuron outside of stimulation periods.

> *(9) Methods - there is limited info on spike sorting procedure - can you provide a reference with further details (I couldn't find)? Is this method equally valid for identifying PFC units?*

Matclust is a MATLAB-based spike sorting graphical user interface that allows for manual curation of neuron clusters through the visualization of spike waveform amplitude, peak-to-trough, and principal components. Polygons or boxes are drawn around spike data points, and single unit clusters are resolved through refinement in multiple dimensions. It was developed by Mattias Karlsson and was first used in a publication reporting replay of remote experiences in the hippocampus (Karlsson and Frank 2009). Although there is no formal reference, it can be found at *https://bitbucket.org/mkarlsso/matclust/src/master/*. Other labs have used the software for clustering neurons from cortical areas (Yu, Liu et al. 2018, Proskurin, Manakov et al. 2023), which demonstrates its robustness across multiple brain areas.

Additionally, examples of clustered neurons in PFC over the course of the experimental paradigm used here can be found in our previous publication (Shin, Tang et al. 2019). In addition to the aforementioned references, we show that PFC neurons can be accurately clustered and that neurons are stable over time, according to a number of cluster metrics.

> *(10) Why were there no further analyses of pyramidal cells and interneurons beyond Figure S2?*

We thank the Reviewer for bringing up this important point, which is similar to Reviewer 2, comment #5 above. We repeat our response here. When we plot the average waveform peak-to-trough and mean firing rates of the PFC neurons, we observe a large cluster with moderate mean firing rates and peak-to-troughs consistent with primarily recording from pyramidal neurons (Supplementary Figure S2F, left). All results are similar if we exclude putative interneurons. To validate our decision to pool the cells, we separated the population into putative pyramidal cells and interneurons based on peak-to-trough. Putative interneurons were identified as cells with a peak-to-trough <0.3 ms (we obtained similar results when using a hyperplane to separate units based on both peak-to-trough and firing rate, with a smaller subset identified as putative interneurons). When these putative interneurons were excluded from the HFO aligned multiunit PFC plot, we observed very similar activity to Figure 2A (Supplementary Figure S2F, right). We thus decided to pool the cells into a single population for the purpose of this manuscript. We are, however, aware that different cell types may contribute to the phenomenon that we report here and attempt to more thoroughly differentiate the contribution of pyramidal cells and interneurons with our modeling result in Figures 9 and 10.

We have now added the following to the figure legend on Page 51, Lines 21-24:

“REM HFO aligned PFC multiunit response when spikes from putative interneurons are excluded (compare to Figure 2A). Due to this similarity of the phasic PFC response when putative interneurons are omitted, we decided to pool PFC neurons for all further analyses.”

> *(11) Looking at Figure S1B, the second to last main block of NREM sleep shown has a clear peak passing TD threshold, but oddly not classed as REM - I can only assume this is due to the duration limits on your classification?*

Yes, this is due to the REM duration threshold that we implement in our sleep scoring algorithm. We used a minimum REM bout threshold criterion of 10 s for inclusion, as in previous reports (Rothschild, Eban et al. 2017, Zhang, Zhang et al. 2020). Additionally, we have included example sleep plots for all 10 animals in Supplementary Figure S1.

> *(12) Include details of how head speed was calculated - just based on the 30fps video?*

Yes, the head speed of the animal was determined by tracking the animals’ position and calculating the speed based on cm/pixel values. We have now added more detail on this in the Methods section under “Surgical implant and electrophysiology” on Page 33, Line 44 to Page 34, Lines 1-2:

“Additionally, the animals’ speed was calculated based on predetermined cm/pixel values and the position displacement between frames captured at 30 fps.”

> *(13) Page 31 line 7 - With the reference you cite, they didn't really show tonic and phasic REM can be segregated based on theta frequency - they just defined it as such. You've done it for some, but I'd ensure all references to phasic REM are defined as putative - mostly missed within the discussion - I'd also add this as a brief limitation (without recording of eye movements or PGO waves).*

We thank the Reviewer for these suggestions. We have now ensured that all mentions of "phasic REM" are qualified with "putative" and have added the requested limitation in the Limitations section on Page 16, Lines 10-15:

"Third, we did not record eye movements or ponto-geniculo-occipital (PGO) waves, both of which would have allowed for more accurate segregation of tonic and phasic REM sleep states.(Simor, van der Wijk et al. 2020) Although we observed a bias for isolated and chain HFOs to occur in putative tonic and phasic REM substates, respectively, the scarcity of putative phasic REM bouts made the direct comparison based on substage difficult."

We have also modified the wording in the Methods section under "Theta inter-peak intervals during bouts of high and low theta power" on Page 37, Lines 14-15 to indicate that the referenced article simply used the theta frequency-based method to define tonic and phasic REM – not to explicitly separate the two states:

"Since previous studies have segregated putative tonic and phasic substages of REM sleep based on CA1 theta frequency…"

References:

Abdou, K., M. Nomoto, M. H. Aly, A. Z. Ibrahim, K. Choko, R. Okubo-Suzuki, S. I. Muramatsu and K. Inokuchi (2024). "Prefrontal coding of learned and inferred knowledge during REM and NREM sleep." Nat Commun 15(1): 4566.

Aleman-Zapata, A., R. G. M. Morris and L. Genzel (2022). "Sleep deprivation and hippocampal ripple disruption after one-session learning eliminate memory expression the next day." Proc Natl Acad Sci U S A 119(44): e2123424119.

Belluscio, M. A., K. Mizuseki, R. Schmidt, R. Kempter and G. Buzsaki (2012). "Cross-frequency phase coupling between theta and gamma oscillations in the hippocampus." J Neurosci 32(2): 423–435.

Bueno-Junior, L. S., M. S. Ruckstuhl, M. M. Lim and B. O. Watson (2023). "The temporal structure of REM sleep shows minute-scale fluctuations across brain and body in mice and humans." Proc Natl Acad Sci U S A 120(18): e2213438120.

Cairney, S. A., S. J. Durrant, R. Power and P. A. Lewis (2015). "Complementary roles of slow-wave sleep and rapid eye movement sleep in emotional memory consolidation." Cereb Cortex 25(6): 1565–1575. Chang, H., W. Tang, A. M. Wulf, T. Nyasulu, M. E. Wolf, A. Fernandez-Ruiz and A. Oliva (2025). "Sleep microstructure organizes memory replay." Nature 637(8048): 1161–1169.

Cheng, S. and L. M. Frank (2008). "New experiences enhance coordinated neural activity in the hippocampus." Neuron 57(2): 303–313.

Darevsky, D., J. Kim and K. Ganguly (2024). "Coupling of Slow Oscillations in the Prefrontal and Motor Cortex Predicts Onset of Spindle Trains and Persistent Memory Reactivations." J Neurosci 44(43). Davidson, T. J., F. Kloosterman and M. A. Wilson (2009). "Hippocampal replay of extended experience." Neuron 63(4): 497–507.

Ellenbogen, J. M., P. T. Hu, J. D. Payne, D. Titone and M. P. Walker (2007). "Human relational memory requires time and sleep." Proc Natl Acad Sci U S A 104(18): 7723–7728.

Foster, D. J. and M. A. Wilson (2006). "Reverse replay of behavioural sequences in hippocampal place cells during the awake state." Nature 440(7084): 680–683.

Ghosh, M., F. C. Yang, S. P. Rice, V. Hetrick, A. L. Gonzalez, D. Siu, E. K. W. Brennan, T. T. John, A. M. Ahrens and O. J. Ahmed (2022). "Running speed and REM sleep control two distinct modes

of rapid interhemispheric communication." Cell Rep 40(1): 111028.

Grosmark, A. D. and G. Buzsaki (2016). "Diversity in neural firing dynamics supports both rigid and learned hippocampal sequences." Science 351(6280): 1440–1443.

Helfrich, R. F., J. D. Lendner, B. A. Mander, H. Guillen, M. PaD, L. Mnatsakanyan, S. Vadera, M. P. Walker, J. J. Lin and R. T. Knight (2019). "Bidirectional prefrontal-hippocampal dynamics organize information transfer during sleep in humans." Nat Commun 10(1): 3572.

Jarosiewicz, B., B. L. McNaughton and W. E. Skaggs (2002). "Hippocampal population activity during the small-amplitude irregular activity state in the rat." J Neurosci 22(4): 1373–1384.

Ji, D. and M. A. Wilson (2007). "Coordinated memory replay in the visual cortex and hippocampus during sleep." Nat Neurosci 10(1): 100–107.

Karlsson, M. P. and L. M. Frank (2009). "Awake replay of remote experiences in the hippocampus." Nat Neurosci 12(7): 913–918.

Kay, K., M. Sosa, J. E. Chung, M. P. Karlsson, M. C. Larkin and L. M. Frank (2016). "A hippocampal network for spatial coding during immobility and sleep." Nature 531(7593): 185–190.

Khodagholy, D., J. N. Gelinas and G. Buzsaki (2017). "Learning-enhanced coupling between ripple oscillations in association cortices and hippocampus." Science 358(6361): 369–372.

Kudrimoti, H. S., C. A. Barnes and B. L. McNaughton (1999). "Reactivation of hippocampal cell assemblies: effects of behavioral state, experience, and EEG dynamics." J Neurosci 19(10): 4090–4101. Lee, A. K. and M. A. Wilson (2002). "Memory of sequential experience in the hippocampus during slow wave sleep." Neuron 36(6): 1183–1194.

Leemburg, S., V. V. Vyazovskiy, U. Olcese, C. L. Bassetti, G. Tononi and C. Cirelli (2010). "Sleep homeostasis in the rat is preserved during chronic sleep restriction." Proc Natl Acad Sci U S A 107(36): 15939–15944.

Lopes-dos-Santos, V., S. Ribeiro and A. B. Tort (2013). "Detecting cell assemblies in large neuronal populations." J Neurosci Methods 220(2): 149–166.

Mizuseki, K., K. Diba, E. Pastalkova and G. Buzsaki (2011). "Hippocampal CA1 pyramidal cells form functionally distinct sublayers." Nat Neurosci 14(9): 1174–1181.

Nitsche, M. A., M. Jakoubkova, N. Thirugnanasambandam, L. Schmalfuss, S. Hullemann, K. Sonka, W. Paulus, C. Trenkwalder and S. Happe (2010). "Contribution of the premotor cortex to consolidation of motor sequence learning in humans during sleep." J Neurophysiol 104(5): 2603–2614.

Peyrache, A., M. Khamassi, K. Benchenane, S. I. Wiener and F. P. Battaglia (2009). "Replay of rule-learning related neural patterns in the prefrontal cortex during sleep." Nat Neurosci 12(7): 919–926.

Plitt, M. H. and L. M. Giocomo (2021). "Experience-dependent contextual codes in the hippocampus." Nat Neurosci 24(5): 705–714.

Proskurin, M., M. Manakov and A. Karpova (2023). "ACC neural ensemble dynamics are structured by strategy prevalence." Elife 12.

Rothschild, G., E. Eban and L. M. Frank (2017). "A cortical-hippocampal-cortical loop of information processing during memory consolidation." Nat Neurosci 20(2): 251–259.

Shin, J. D. and S. P. Jadhav (2024). "Prefrontal cortical ripples mediate top-down suppression of hippocampal reactivation during sleep memory consolidation." Curr Biol 34(13): 2801–2811 e2809.

Shin, J. D., W. Tang and S. P. Jadhav (2019). "Dynamics of Awake Hippocampal-Prefrontal Replay for Spatial Learning and Memory-Guided Decision Making." Neuron 104(6): 1110–1125 e1117.

Siapas, A. G. and M. A. Wilson (1998). "Coordinated interactions between hippocampal ripples and cortical spindles during slow-wave sleep." Neuron 21(5): 1123–1128.

Simor, P., G. van der Wijk, L. Nobili and P. Peigneux (2020). "The microstructure of REM sleep: Why phasic and tonic?" Sleep Med Rev 52: 101305.

Singer, A. C. and L. M. Frank (2009). "Rewarded outcomes enhance reactivation of experience in the hippocampus." Neuron 64(6): 910–921.

Sosa, M., H. R. Joo and L. M. Frank (2020). "Dorsal and Ventral Hippocampal Sharp-Wave Ripples Activate Distinct Nucleus Accumbens Networks." Neuron 105(4): 725–741 e728.

Sosa, M., M. H. Plitt and L. M. Giocomo (2025). "A flexible hippocampal population code for experience relative to reward." Nat Neurosci 28(7): 1497–1509.

Stark, E., L. Roux, R. Eichler and G. Buzsaki (2015). "Local generation of multineuronal spike sequences in the hippocampal CA1 region." Proc Natl Acad Sci U S A 112(33): 10521–10526.

Tang, W., J. D. Shin, L. M. Frank and S. P. Jadhav (2017). "Hippocampal-Prefrontal Reactivation during Learning Is Stronger in Awake Compared with Sleep States." J Neurosci 37(49): 11789–11805.

Tort, A. B., R. Scheffer-Teixeira, B. C. Souza, A. Draguhn and J. Brankack (2013). "Theta-associated high-frequency oscillations (110-160Hz) in the hippocampus and neocortex." Prog Neurobiol 100: 1–14.

Valero, M., T. J. Viney, R. Machold, S. Mederos, I. Zutshi, B. Schuman, Y. Senzai, B. Rudy and G. Buzsaki (2021). "Sleep down state-active ID2/Nkx2.1 interneurons in the neocortex." Nat Neurosci 24(3): 401–411.

van de Ven, G. M., S. Trouche, C. G. McNamara, K. Allen and D. Dupret (2016). "Hippocampal Offline Reactivation Consolidates Recently Formed Cell Assembly Patterns during Sharp Wave-Ripples." Neuron 92(5): 968–974.

van der Helm, E. and M. P. Walker (2011). "Sleep and Emotional Memory Processing." Sleep Med Clin 6(1): 31–43.

Vaz, A. P., S. K. Inati, N. Brunel and K. A. Zaghloul (2019). "Coupled ripple oscillations between the medial temporal lobe and neocortex retrieve human memory." Science 363(6430): 975–978.

Wilson, M. A. and B. L. McNaughton (1994). "Reactivation of hippocampal ensemble memories during sleep." Science 265(5172): 676–679.

Yang, S. R., H. Sun, Z. L. Huang, M. H. Yao and W. M. Qu (2012). "Repeated sleep restriction in adolescent rats altered sleep patterns and impaired spatial learning/memory ability." Sleep 35(6): 849–859.

Yu, J. Y., D. F. Liu, A. Loback, I. Grossrubatscher and L. M. Frank (2018). "Specific hippocampal representations are linked to generalized cortical representations in memory." Nat Commun

9(1): 2209.

Zhang, L. B., J. Zhang, M. J. Sun, H. Chen, J. Yan, F. L. Luo, Z. X. Yao, Y. M. Wu and B. Hu (2020). "Neuronal Activity in the Cerebellum During the Sleep-Wakefulness Transition in Mice." Neurosci Bull 36(8): 919– 931.

https://doi.org/10.7554/eLife.110795.2.sa0